NASA CR-135049
R76AEG218

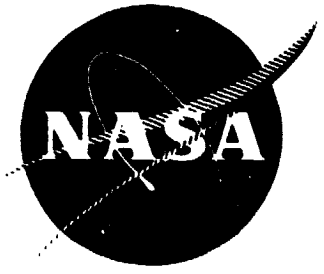

Quiet Clean Short-Haul Experimental Engine (QCSEE)

Over-the-Wing Engine and Control Simulation Results

October 1978

by

Advanced Engineering & Technology Programs Department

GENERAL ELECTRIC COMPANY

National Aeronautics and Space Administration

NASA Lewis Research Center

NAS3-18021

TABLE OF CONTENTS

TABLE OF CONTENTS (Concluded)

LIST OF ILLUSTRATIONS

LIST OF ILLUSTRATIONS (Continued)

LIST OF ILLUSTRATIONS (Concluded)

LIST OF TABLES

1.0 SUMMARY

This report describes the hybrid-computer simulation of the General Electric OTW (Over The Wing) QCSEE (Quiet, Clean, Short-haul, Experimental Engine) control system. The control system manipulates two variables: fuel flow and compressor stator angle. The system includes a full authority digital electronic control. The control system also contains a new Failure Identification and Corrective Action (FICA) scheme. The FICA logic is designed to recognize failures in the engine sensors of the digital control and to provide the corrective action for maintaining safe control of the engine. The digital control feeds a Fail-Fixed Servovalve (FFSV) contained in the hydromechanical fuel control portion of this system. The FFSV causes the fuel metering valve power piston to fail-in-position upon loss of electrical power or upon a hardover, electrical failure in either direction.

The primary purpose of the simulation has been to develop this control system design with the following objectives:

- Fast engine-thrust response for powered-lift operations.
- Accurate steady-state and fast-response control of the engine where thrust variations are maintained within acceptable limits.

Simulation results for throttle bursts from 62 to 100 percent net thrust predict that the experimental engine will meet the thrust requirement of 62 to 95 percent thrust in one second. Operation of the digital control with the fail-fixed servovalve can be designed to meet the accuracy and fast-response objectives. Furthermore, results indicate that the digital control FICA strategy will continue to provide thrust management when several sensors have failed.

2.0 INTRODUCTION

The major purpose of the QCSEE program is to develop and demonstrate the technology required for propulsion systems of quiet, clean, economical, STOL (Short Takeoff/Landing) aircraft. One element of this program is to provide the digital electronic engine control technology necessary for an over-the-wing (OTW) turbofan engine application.

Two key functions are to be performed by the digital electronic control. The first is to improve the thrust response of a conventional turbofan to meet the stringent requirements of a STOL aircraft. The second function is to provide sensor failure identification and corrective action (FICA) by using state-estimation techniques of modern control theory. In order to design this control and evaluate performance over the flight map, a hybrid simulation of the engine and control system was developed at the General Electric AEG (Aircraft Engine Group) Dynamic Analysis Simulation Center.

This report contains a general description of the analytical models for the engine and control components which have been used in the simulation. The simulation was implemented on the Simulation Center's two Electronic Associates, Inc. (EAI) Model 690 Hybrid Computing Systems. The engine and basic control system were constructed on one hybrid computing system to operate with or without FICA supervision from another hybrid computing system. This is possible because the FICA logic is designed to have no influence on the control unless there is a sensor failure.

Hybrid simulation data describing forward-thrust transients are presented for sea level, static, standard-day conditions. Simulation results for a fail-fixed servovalve and a failure identification and corrective action control are also included.

3.0 OTW EXPERIMENTAL PROPULSION SYSTEM

3.1 ENGINE

The OTW experimental propulsion system, shown in Figure 1, features a high Mach (accelerating) inlet, a gear-driven fan, a composite fan-vane frame, an acoustically treated fan duct with an acoustic splitter ring, a variable-geometry confluent exhaust nozzle, an advanced core and low pressure turbine, an acoustically treated core exhaust, engine-mounted accessories, and a digital electronic control system.

The fundamental design criterion which established the engine design approach was the fan engine cycle required to meet the noise objective. The fan and core exhaust pressure ratios were dictated by jet-flap noise constraints and by the powered-lift requirements of an over-the-wing installation. Analysis indicates that, when scaled in accordance with the specified ground rules, the engine will meet all of the program noise objectives.

The fan is a low pressure ratio (1.35), low tip speed (350.5 m/sec - 1150 ft/sec) configuration sized to provide 405.5 kg/sec (894 lb/sec) of corrected airflow at takeoff power setting. It contains 28 titanium fan blades having an aerodynamic contour capable of conversion to composite material in a flight system. The fan is driven by the low pressure turbine through a main reduction gear with a 2.0617 gear ratio.

The "D" shaped, confluent exhaust nozzle incorporates side doors to vary the area from takeoff to cruise. The experimental engine will not include a variable-exhaust-nozzle-actuation system; however, an actuation system for a flight-type engine can be extrapolated from current design technology.

3.2 CONTROL SYSTEM

The OTW engine control system manipulates fuel flow and core compressor stator angle to achieve an excellent balance between thrust, fuel consumption, noise, exhaust pollution, and transient response. New technology features to be demonstrated on the OTW experimental engine control system are: a Full Authority Digital Electronic Control (FADEC), a Failure Identification and Corrective Action (FICA) scheme, and a Fail-Fixed Servovalve (FFSV).

The OTW digital control is programmed to provide steady-state control, transient fuel schedules, core stator schedules, and limiting fuel-control functions. The transient fuel and core stator schedules on the OTW experimental engine were performed hydromechanically.

The FICA strategy uses a form of Kalman filtering to estimate the control system sensor outputs and replaces sensor values with estimated values when deviations between the two exceed the expected maximum.

Figure 1. OTW Experimental Engine Propulsion System.

The fail-fixed servovalve improves the reliability of the fuel delivery system. It causes the fuel metering valve power piston to fail-in-position upon loss of electrical power or upon a hard-over, electrical failure in either direction.

The primary design requirements for the overall control system are:

- Thrust control throughout the specified flight map with minimum pilot workload,
- Fast thrust response - from 62 to 95% takeoff thrust in one second,
- Specified noise and pollution goals.

The general structure of the control system is shown in Figure 2. The digital electronic control is the heart of the system, manipulating fuel flow and core stator angle in response to a power command representative of an aircraft propulsion system computer. Digital control of fuel flow is maintained through an electrohydraulic servovalve incorporated in a modified F101 hydromechanical fuel control. In addition, the hydromechanical control provides the following: a backup core speed control, a positive metering-valve feedback to the digital control, a separate electrically operated emergency-shutdown function, and a pressurized fuel output from the fuel pump to power the compressor stator servovalve and actuator assembly.

Selection of a control mode which will accurately regulate thrust was based primarily on a tolerance analysis (Reference 1). The effects of typical control and measurement tolerances, engine component tolerances, and engine component deterioration were determined for all potential control modes. The manipulated variables examined in this anlaysis were fuel flow and exhaust nozzle area, even though a variable exhaust nozzle is not included in the OTW experimental engine. Scheduling practicality, stability, and transient-response considerations were also factors in choosing the control mode. The control mode selected was one in which fuel flow controls corrected fan speed.

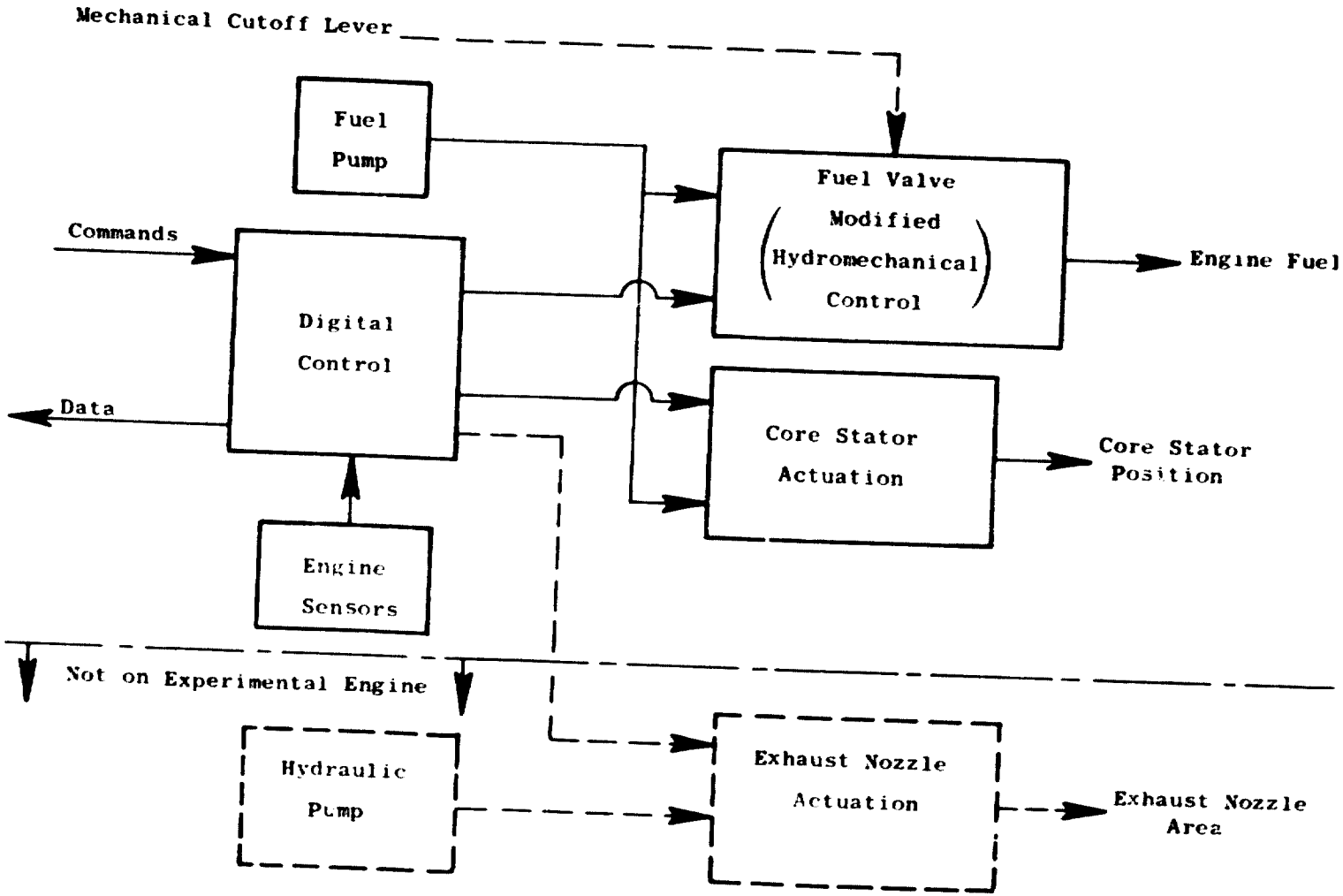

Figure 2. OTW Control System Schematic.

4.0 ANALYTICAL MODEL

The analytical model represents the functional relations that exist between the variables of the OTW QCSEE and control system. The engine portion of the simulation is based on the steady-state conservation equations, of the cycle deck, with the addition of significant dynamics. The model has detailed representations of the primary control system components: the fuel control and the compressor stator control.

4.1 ENGINE MODEL

4.1.1 General

The engine model is derived from the cycle deck which was used to generate the QCSEE preliminary technical requirements. Significant items represented are rotor dynamics, heat soak, and combustion delay. The effects of heat soak, combustion delay, and compressor stator error are based upon past experience with the F101 core engine. No distortion or reingestion effects are included; volume dynamic effects in the frequency range of consideration are insignificant and have been omitted.

The philosophy behind the model construction was to develop mathematical representations, for the components, to duplicate the thermodynamics used in the cycle deck. Memory limitations in the hybrid computer require linear table-interpolations; whereas, some cycle deck maps use polynomial interpolation.

Due to the computation time and memory involved, the iteration procedure of the cycle deck was considered undesirable. To keep cycle time at a minimum on the hybrid (maximum sampling rate), no actual iterative process involving tolerances is used; instead, all variables requiring an iteration are computed using values based on the previous time sample. This results in two types of iterative process: one internal to the component and one between components. Since the latter cannot be evaluated without the components, the first step was to develop the component representations and internal "iterations." The choice of input and output variables was based on past experience. With the exception of the fan and compressor map input variables, all of the component internal iterations can be considered as direct-substitution iterations under steady-state conditions. The component representations were considered adequate if, with inputs held constant, the iteration variables were stable and the outputs within two percent of the cycle deck.

Based on past experience, it was recognized that some iteration variables might require filtering due to the iterative process between components. For this reason, a digital filter routine was constructed to produce a lag in the input variable based on an Euler integration using the average sampling rate. This changes the effective iteration process from direct substitution to weighted averaging under steady-state conditions. Variables requiring this treatment are fan front-face total flow used in the installed

inlet, combustor discharge pressure in the HP (high pressure) turbine, and LP (low pressure) turbine vane inlet total pressure. Based on 16.67 samples/sec and a 20:1 time scale, the respective time constant are 30, 12, and 48 milliseconds.

Figure 3 illustrates the information flow between components.

4.1.2 Inlet

The inlet simulation receives flight altitude, (ALT), Mach number (XM), and temperature increment (DTAMB) from the standard day ambient temperature as determined by the desired flight condition. Fan front-face total flow (W2A) is received from the fan when the inlet is in the installed mode. Outputs are free-stream pressure (PO) and temperature (TO), inlet throat static (PS11) and total pressure (P11), and fan front-face total temperature (T11) and pressure (P12). A constant specific heat ratio of 1.4 is used in the inlet simulation. No distortion or reingestion effects are considered. The only dynamic effect is a lag of 30 milliseconds in fan front-face total flow. This lag is necessary to provide model iteration stability between components in the installed mode which produces a total pressure drop between the inlet throat and fan front face.

4.1.3 Fan Tip

The fan tip simulation receives front-face total temperature (T11) and pressure (P12) from the inlet, physical speed from the LP rotor (XNL), and tip discharge total pressure (P13) from the bypass duct. Outputs are tip discharge specific heat (CP13), tip inlet (H12) and discharge enthalpies, percent fan corrected speed (PCNLR), tip inlet entropy function (PHI12), tip inlet gas constant (R12), tip discharge total temperature (T13), and front face total flow (W2A). No dynamics are used. To conserve memory, the polynomial, fan-tip maps used in the cycle deck have been converted to use linear interpolation. The general-parameter map input is an internal iteration variable; the value depends on the previous-pass value, discharge total pressure input, and the discharge total pressure computed from the map on the previous pass.

4.1.4 Fan Hub

The fan hub simulation receives front face total temperature (T12) and pressure (P12) from the inlet; fan tip inlet (H12) and discharge enthalpies (H13), inlet entropy function (PHI12), inlet gas constant (R12), percent fan corrected speed (PCNLR), and front-face total flow (W2A) from the fan tip; and compressor inlet airflow (W25) from the compressor. Outputs are fan hub (PW2) and tip (PW12) power, fan tip inlet airflow (W12), and compressor inlet total temperature (T25) and pressure (P25). No dynamics are involved with the fan hub simulation. Reynolds number effects are the same as in the cycle deck. Because of memory limitations, the polynomial, fan-hub maps used in

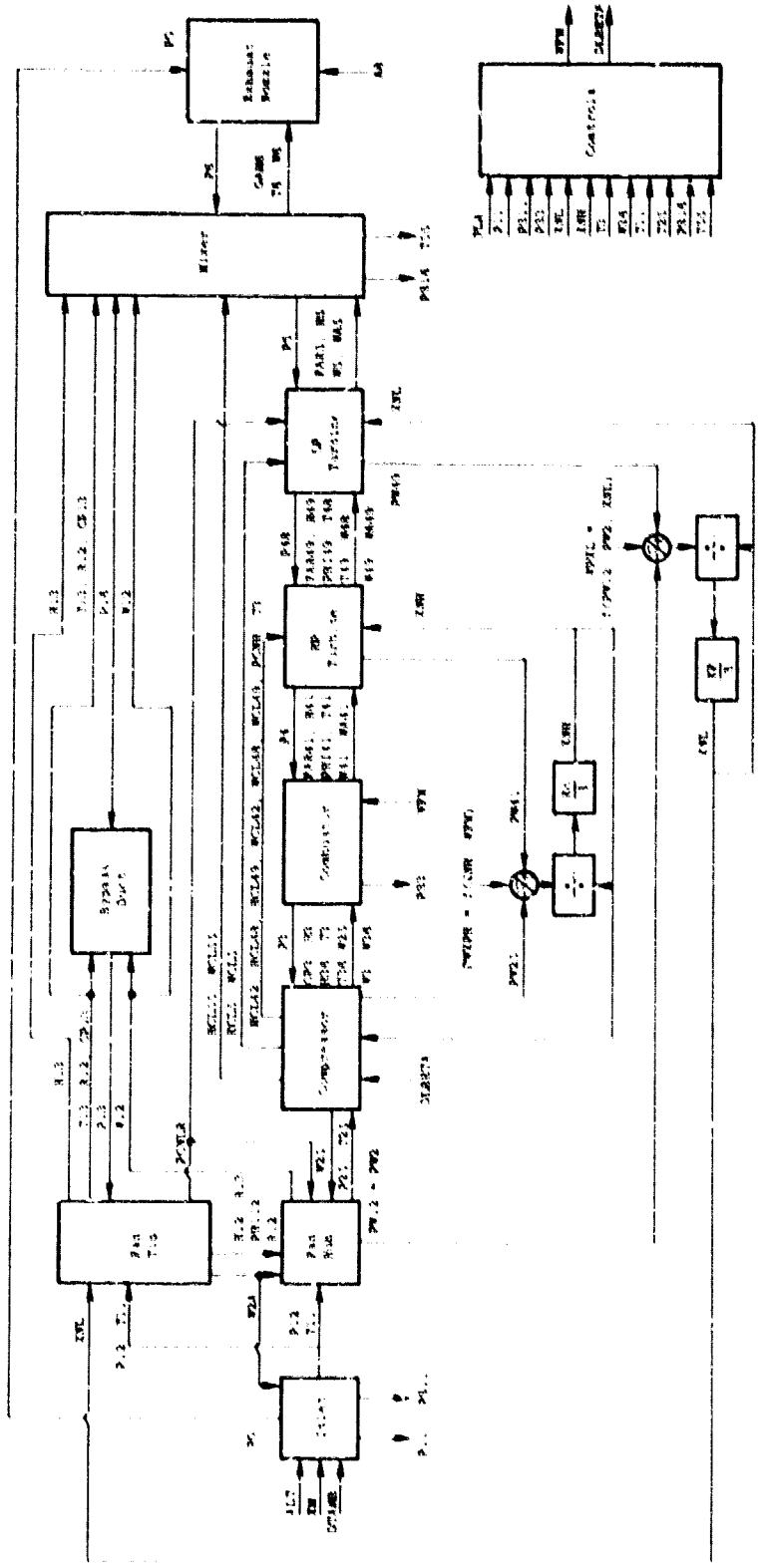

Figure 3. GTW Simulation Information Flow Diagram.

the cycle deck have been converted to use linear interpolation in the hybrid model. The general-parameter map input is an internal iteration variable whose value depends on the past value and the difference between [hub inlet airflow (W12)]/[hub pressure ratio (P23Q2)] input and the previous map value; this uses the cycle deck assumption that all hub flow goes into the compressor. The total pressure drop between the fan hub discharge and the compressor inlet is calculated as in the cycle deck.

4.1.5 Bypass Duct

The bypass duct simulation receives fan tip discharge specific heat (CP13) and total temperature (T13), and inlet gas constant (R12) from the fan tip; fan tip discharge flow (W12) from the fan hub; and bypass duct discharge total pressure (P16) from the mixier. Output is bypass duct inlet total pressure (P13). No dynamics are involved in the simulation. Since the cycle deck variation in the fan tip discharge and the bypass duct inlet total pressure ratio is less than 0.00003, this pressure ratio is assumed constant. The total pressure drop between the bypass duct inlet and discharge is calculated as in the cycle deck.

4.1.6 HP Compressor

The HP compressor simulation receives compressor inlet total pressure (P25) and temperature (T25) from the fan hub, compressor discharge total pressure (P3) from the combustor, HP compressor physical speed (XNH) from the HP rotor, and off-stator error (DLBLA) from the control. Produced are compressor discharge (W3) and inlet (W25) airflows, combustor inlet gas flow (W36), all cooling flows and enthalpies, compressor discharge (H3) and combustor inlet enthalpies (H36), compressor discharge specific heat (CP3), compressor discharge (T3) and combustor inlet total temperature (T36), and compressor power (PW25). The simulation uses the same base compressor maps used on the UTW simulation. Changes were made to agree with cycle deck modifiers and to be compatible with the new hybrid software. Reynolds number effects are assumed negligible and are omitted. The UTW simulation of off-schedule stator effects on airflow and efficiency was modified to provide an accurate representation for the large, off-schedule positions associated with reset of stators for OTW approach power transients. This modification was based on recent compressor test data.

The only dynamics are due to heat soak producing an effective lag in compressor discharge total temperature.

4.1.7 Combustor

The combustor simulation receives compressor discharge specific heat (CP3), enthalpy (H3), total temperature (T3), and flow (W3) from the compressor; combustor inlet enthalpy (H36), total temperature, (T36) and flow (W36) from the compressor; compressor inlet airflow (W25) from the compressor; fuel

flow (WFM) from the control; and combustor discharge total pressure (P4) from the HP turbine. Outputs produced are HP turbine rotor inlet fuel/air ratio (FAR41), enthalpy (H41), total temperature (T41), airflow (WA41), gas flow (W41) and entropy function (PHI41); and compressor discharge static (PS3) and total pressures (P3). The total pressure drop between the compressor discharge (P3) and the combustor disharge (P4) is represented as in the cycle deck. The efficiency map is identical to the cycle deck. Two dynamic effects are included in the combustor; one is a 25-millisecond combustor delay between the fuel flow produced by the control and the fuel flow that is burned in the engine. The second is a heat soak calculation which produces an effective lag in HP turbine rotor inlet total temperature (T41). Both effects are based on previous experience with the F101 core engine. Mixing of primary gas flow and a cooling flow is accomplished for the HP turbine rotor inlet using steady-state conservation of energy. There is no effect on total pressure.

4.1.8 HP Turbine

The HP turbine receives HP turbine rotor inlet fuel/air ratio(FAR41), entropy function (PHI41), total temperature (T41), enthalpy (H41), gas flow (W41), and airflow (WA41) from the combustor; compressor discharge total temperature (T3) and percent compressor physical speed (XNH) from the compressor; cooling flows and enthalpies for the HP turbine discharge (WCL42), LP turbine vane inlet (WCL48), and LP turbine rotor inlet (WCL49) from the compressor; LP turbine vane inlet total pressure (P48) from the LP turbine; and HP compressor physical speed (XNH) from the HP rotor. Outputs are combustor discharge total pressure (P4); HP turbine power (PW41); LP turbine rotor inlet fuel/air ratio (FAR49), enthalpy (H49), entropy function (PHI49), total temperature (T49), gas flow (W49), and airflow (WA49); LP turbine vane inlet total temperature (T48) and gas flow (W48). The component maps used are identical to those of the cycle deck. Mixing of primary gas flow and cooling flow is accomplished using steady-state conservation of energy at the HP turbine discharge, the LP turbine vane inlet, and the LP turbine rotor inlet. There is no effect on total pressure. The only dynamic effect is a 12-millisecond lag on combustor discharge total pressure, which is necessary for model iteration stability between components.

4.1.9 LP Turbine

The LP turbine receives LP turbine vane inlet total temperature (T48) and gas flow (W48) from the HP turbine; LP turbine rotor inlet fuel/air ratio (FAR49), enthalpy (H49), entropy function (PHI49), total temperature (T49), gas flow (W49), and airflow (WA49) from the HP turbine; LP turbine discharge cooling flow (WCL5) and enthalpy (HCL5) from the compressor; percent fan corrected speed (PCNLR) from the fan tip; fan physical speed (XNL) from the LP rotor; and LP turbine discharge total pressure (P5) from the mixer. Produced are LP turbine power (PW49); LP turbine discharge fuel/air ratio (FAR5), enthalpy (H5), gas flow (W5), and airflow (WA5); and LP turbine vane inlet total pressure (P48). The component maps used are identical to those of the

cycle deck. Mixing of primary gas flow and cooling flow at the LP turbine discharge is accomplished using steady-state conservation of energy. There is no effect on total pressure. As in the cycle deck, LP turbine rotor and vane inlet total pressures are equal. The only dynamic effect is a 48-millisecond lag on LP turbine rotor inlet total pressure which is necessary for model iteration stability between components.

4.1.10 Mixer

The mixer simulation receives fan tip discharge specific heat (CP13), enthalpy (H13), and total temperature (T13) from the fan tip; fan tip inlet gas constant (R12) from the fan tip; fan tip inlet airflow (W12) from the fan hub; LP turbine discharge fuel/air ratio (FAR5), enthalpy (H5), gas flow (W5), and airflow (WA5) from the LP turbine; LP turbine frame discharge cooling flow (WCL55) and enthalpy (HCL55) from the compressor; and mixer discharge total pressure from the exhaust nozzle. Outputs are mixer discharge fuel/air ratio (FAR6), specific heat ratio (GAM6), enthalpy (H6), total temperature (T55), and gas flow (W6); bypass duct discharge total (P16) and static pressures (PS16); LP turbine discharge total pressure (P5); and LP turbine frame discharge total temperature (T55). Mixing of primary gas flow and cooling flow at the LP turbine frame discharge is accomplished using steady-state conservation of energy. LP turbine swirl effect is represented as a constant (LP turbine frame discharge total pressure)/(LP turbine discharge total pressure). Mixing of the bypass and core flow is performed using steady-state conservation of mass, energy, and momentum. This also uses the cycle deck assumption that core duct discharge static pressure equals bypass duct discharge static pressure. No dynamics are involved. Total pressure drops from mixer discharge to mixing plane and core duct discharge to LP turbine frame discharge are represented as in the cycle deck.

4.1.11 Exhaust Nozzle

The exhaust nozzle simulation receives mixer discharge specific heat ratio (GAM6), total temperature (T6), and gas flow (W6) from the mixer; exhaust nozzle throat actual area from the control (A8); and free-stream pressure (P0) from the inlet. Produced are exhaust nozzle throat effective area (AE8), static pressure (PS8), and velocity head; and mixer discharge total pressure (P6). No dynamics are used. Nozzle flow coefficient maps are identical with those of the cycle deck.

4.1.12 Rotor Dynamics

Rotor speeds are computed using conservation of angular momentum. The LP rotor receives fan tip (PW12) and hub powers (PW2) from the fan hub, LP turbine power from the LP turbine (PW49), and a power-loss term that is a function, derived empirically, based on cycle deck data. All moments of inertia for the LP rotor have been reflected to the fan side of the gearbox. Using this inertia, a dynamic value for fan physical speed (XNL) is calculated.

For the HP rotor, a dynamic HP compressor physical speed (XNH) is calculated using the core inertia and powers from the compressor (PN25), HP turbine (PW41), HP rotor loss calculation (PWPXH), and desired customer power takeoff. The HP rotor power-loss calculation is based on an empirical fit of cycle deck data.

4.2 CONTROL SYSTEM MODEL

4.2.1 General

In order to develop the control independent of FICA logic, the control system is simulated on the same EAI hybrid computing system as the engine. For the purpose of discussion, the control system model is divided into two sections: that which manipulates core engine fuel flow and that which positions the HP compressor stators. Both are primarily contained on the analog portion of the hybrid computer. As a consequence, the simulation does not account for round-off errors associated with the 12-bit words in the digital control computer. It has been assumed that the software program for the digital control computer will be designed to prevent deteriorating effects of round-off errors on control performance.

Both simulations include an analog approximation for the effect of the digital computer time delay. Using the estimated cycle time of 10 milliseconds for the digital control, the effect of the digital-to-analog conversion may be approximated by a 5-millisecond delay in the frequency domain (Reference 2). Therefore, the analog of the digital control computer time delay is represented by a total of 15 milliseconds. Due to equipment limitations, this time delay is further approximated by a first-order lag with a 15-millisecond constant. This lag provides a reasonable approximation for phase shift, in the range of the control loop crossover frequencies, which is important for stability considerations. The lag does provide some effect of time delay during large transients, but is not precise. In the simulations, the lag is located just prior to the torque motor driver amplifier simulations.

4.2.2 Fuel Control

A schematic of the engine fuel control model is shown in Figure 4. The model includes representations for the digital electronic and the hydromechanical portions of the fuel control. The model for the digital electronic portion is based on the detailed block diagrams contained in Appendix A. Appendix A also contains the specifications for the gains, time constants, and limits which were developed from the hybrid simulations of the engine and control system. Currently, these diagrams and specifications are being used to program the digital fuel control for the first build of the QTW experimental engine. It should be noted that the actual hybrid simulation of the digital fuel control is not a one-to-one representation of all details in the Appendix A block diagrams and specifications. For example, it does not include the polynomial equation curve-fits for the acceleration fuel schedule;

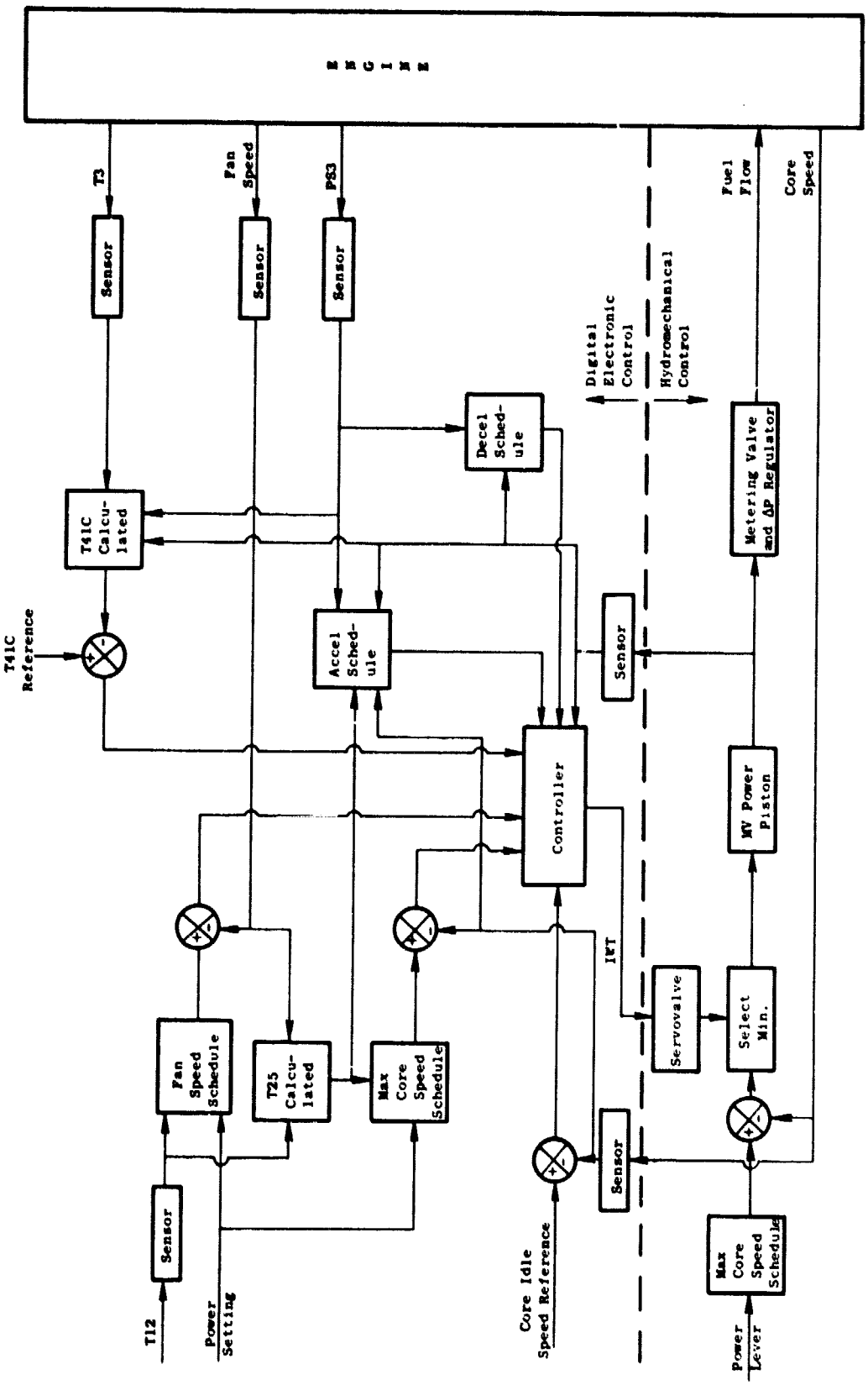

Figure 4. OTW Core Engine Fuel Control Model Schematic.

the hybrid simulation contains the base functions for this schedule, from which the polynomial equation fits were derived. In summary, the hybrid simulation includes those details which were necessary to develop and evaluate steady-state and transient performance of the engine and digital fuel control.

The model for the hydromechanical portion of the fuel control is defined by Figure 5. The hydromechanical portion is a modified F101 fuel control. The model includes representations for the backup core-speed-limit control, two servovalve designs, the metering valve power piston, the metering valve port shape, and an effective 0.02-second lag for the delta pressure regulator that functions to maintain a constant pressure drop across the metering valve port. The two servovalve designs contained in the model are the fail-fixed servovalve and the linear servovalve normally used in the F101 fuel control. The details of the fail-fixed servovalve are discussed in the next section of this report. The following transfer function for the linear servovalve is used in the model;

$$\frac{\Delta \text{ Servovalve Flow}}{\Delta \text{ Torque Motor Current}} = \frac{0.0191}{0.03\ S + 1} \qquad \frac{\text{in.}^3/\text{sec}}{\text{mA}}$$

where torque motor current is limited to the -80 to +80 mA range.

As indicated by Figure 4, several control modes are accommodated by the fuel control. In the power setting range from approach to takeoff, the primary control mode is the manipulation of fuel flow (WF) to control corrected fan speed, which is a variable related to thrust. The control mode is changed to either maximum core speed, maximum core turbine inlet temperature (T41C), accel schedule (WF/PS3), or the decel schedule (WF/PS3) when the engine tries to operate beyond the scheduled limit of one of these variables. In addition, an inlet duct Mach number limit controller would be used in the digital fuel control design for a flight-type OTW engine. It is not included for the experimental engine in order to reduce digital memory requirements. The actual hybrid simulations of the fuel control contains this controller for analytical purposes; however, it is not defined in the Appendix A block diagram and specifications.

When the engine operates within the above scheduled limits, a fan speed error term is generated based on sensed fan speed and an uncorrected fan speed from the corrected fan speed schedule. The fan speed error and the lagged rate of change of sensed, metering-valve position are used to determine the torque motor current output (IWT) from the digital control. This current positions an electrohydromechanical servovalve which is ported to the metering-valve, power piston. The magnitude and polarity of the current determine the rate and direction of metering-valve, power-piston position (XMV). The metering-valve area is proportional to the square of the power-piston position. A pressure regulator maintains a constant pressure drop across the metering valve; thus, the metered fuel flow to the engine is proportional to the square of the power-piston position.

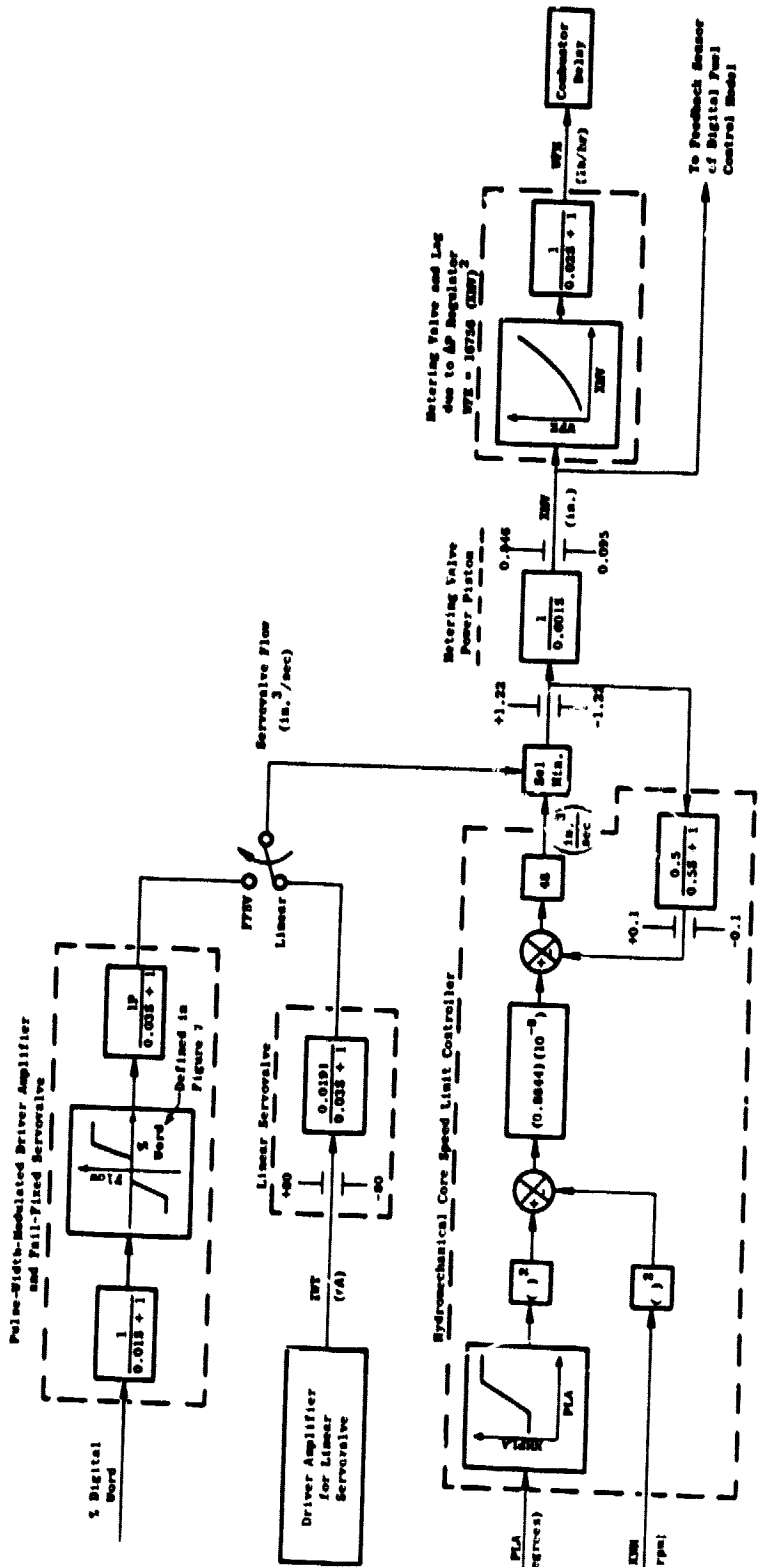

Figure 5. OTW Hydromechanical Fuel Control Model.

For small perturbations, the transfer function from fan speed error to fuel flow is approximated by:

$$\frac{\Delta \text{ Fuel Flow}}{\Delta \text{ Fan Speed rpm}} \approx \frac{K\ (0.5\ S+1)}{S}$$

The gain "K" varies with respect to the square-law shape of the metering-valve area. The lead-time constant in this transfer function is due to, and thus equal to, the time constant of the lag on the rate of change of sensed, metering-valve position. The valve of the lead-time constant is chosen to compensate for the engine lag from fuel flow to fan speed. In summary, the fan-speed/fuel-flow control is an integrating (i.e., Type 1) control with lead compensation and is designed to provide accurate control of corrected fan speed.

The dynamic designs of the limit controls for core speed, core turbine inlet temperature, and inlet Mach number are similar to those of the fan speed control; each is an integrating control with lead compensation. To compensate for engine and sensor lags, lead-time constants are 0.5 seconds for the core speed and inlet Mach number controls, and 0.1 second for the core turbine inlet temperature control.

During engine accelerations, fuel flow is limited by the WF/PS3 accel schedule which is a function of HP compressor (core) speed and HP compressor inlet temperature (T25). HP compressor inlet temperature is calculated based on sensed fan speed and sensed fan inlet temperature (T12). The accel schedule is designed to provide adequate HP compressor stall margin and to be a backup for the core turbine inlet temperature control. During engine decelerations, fuel flow is limited by a constant WF/PS3 decel schedule to prevent combustor blow out.

4.2.3 Fail-Fixed Servovalve

The model of the fail-fixed servovalve used in the simulation studies included representations for two types of pulse-width-modulated, torque-motor-driver amplifiers. The unipolar-pulse-driver amplifier uses current pulses of only one polarity chosen by the sign of the digital word. The bipolar-pulse-driver amplifier uses a train of positive and negative pulses; pulse-width is determined by the sign and magnitude of the digital word. Both operate at a frequency of 500 hertz. Operation of the servovalve with the unipolar amplifier was felt to have better resolution from percent digital-word-to-flow, but poorer null shift and dead-zone characteristics than operation with the bipolar amplifier. Figure 6 illustrates the difference between servovalve operation with the unipolar and the bipolar amplifiers.

Since the primary concern was the effect of the dead-zone and null shift, the digital-word-to-servovalve flow characteristics were linearized

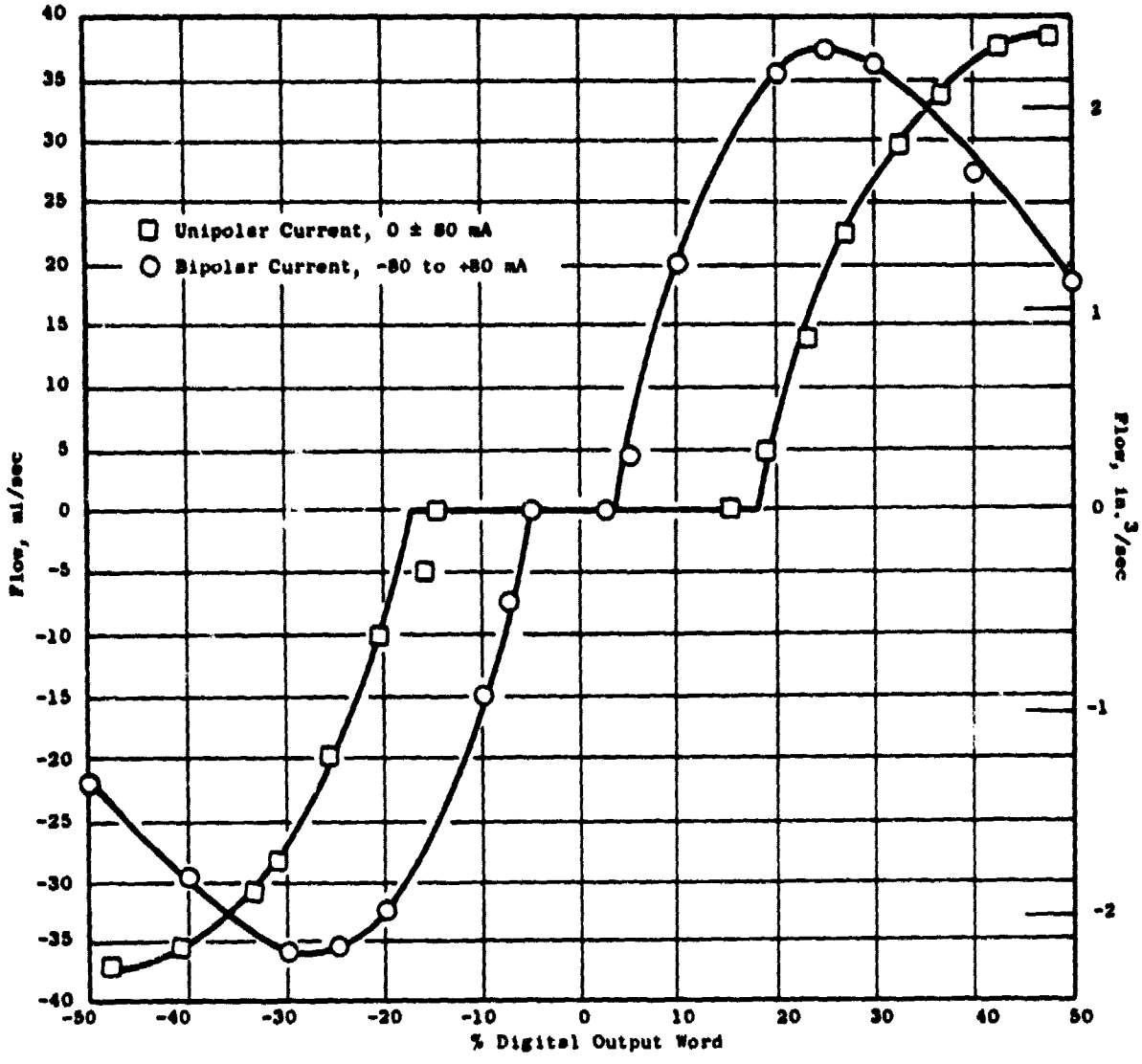

Figure 6. Fail-Fixed Servovalve Characteristics; Digital Amplifier and Servovalve, 500 Hz, Pulse-Width Modulation.

and limited as shown in Figure 7. Tolerances on the dead-zone size and amount of null shift were estimated based on past experience with similar valves. The pulse-driver amplifiers and the servovalve were assumed to respond like first-order lags with time constants of 0.01 and 0.03 seconds respectively. The same time constants were assumed for the torque-motor-driver amplifier and linear servovalve discussed in the preceding section of this report.

4.2.4 Core Compressor Stator Control

The model for the core compressor stator control is described in Figure 8. It includes representations for the digital electronic and hydromechanical portions of the stator control. The model for the digital electronic portion is based on the detailed block diagram in Appendix B (Note: See Appendix A for procedure to calculate T25 and corrected core speed which are used in both the fuel and the stator controls). Appendix B also contains the specifications for the gains, time constants, schedules, and limits which were developed from design studies on the engine and control system. Currently, these diagrams and specifications are being used to program the digital core compressor stator control for the first build of the OTW experimental engine. It should be noted that the actual hybrid simulation of the digital stator control is not a one-to-one representation of all details in the block diagram and specifications. For example, it does not include the logic associated with detecting a failure in one of the position-feedback sensors. However, the hybrid simulation does include those details which are necessary for proper evaluation of steady-state and transient performance.

The model for the hydromechanical portion of the core stator control is defined in Figure 9. The velocity of the stator actuators, in units of cm (inches) ZBETA feedback stroke to the LVDT (linearly variable, differential transformer), is represented by the product of servovalve current (IB) times a linear function of fuel flow. This linear function is used to approximate the effect of the varying fuel-pump-discharge pressure which is the supply source for the core stator servovalve. For example, an increase in fuel flow causes an increase in pump-discharge pressure and, thus, an increase in gain from servovalve current to flow output. The net result is a larger velocity gain from servovalve current to actuator position. The model also includes the nonlinear linkage relation between actuator position and actual core stator angle.

The combined operation of the digital and hydromechanical portions of the core stator control in Figure 8 is as follows. When the digital control logic is set for the "reset off" mode, the output of the reset control is zero. Therefore, the position of the stator vanes is scheduled as a function of core corrected speed. The error between the scheduled and sensed stator positions determines the magnitude of torque motor current (IB) from the digital control. This current determines the servovalve flow to the two ram actuators which position the stator angle.

When the digital control logic is set for the "reset on" mode, the reset control adds a scheduled amount of degrees to the nominal core stator sched-

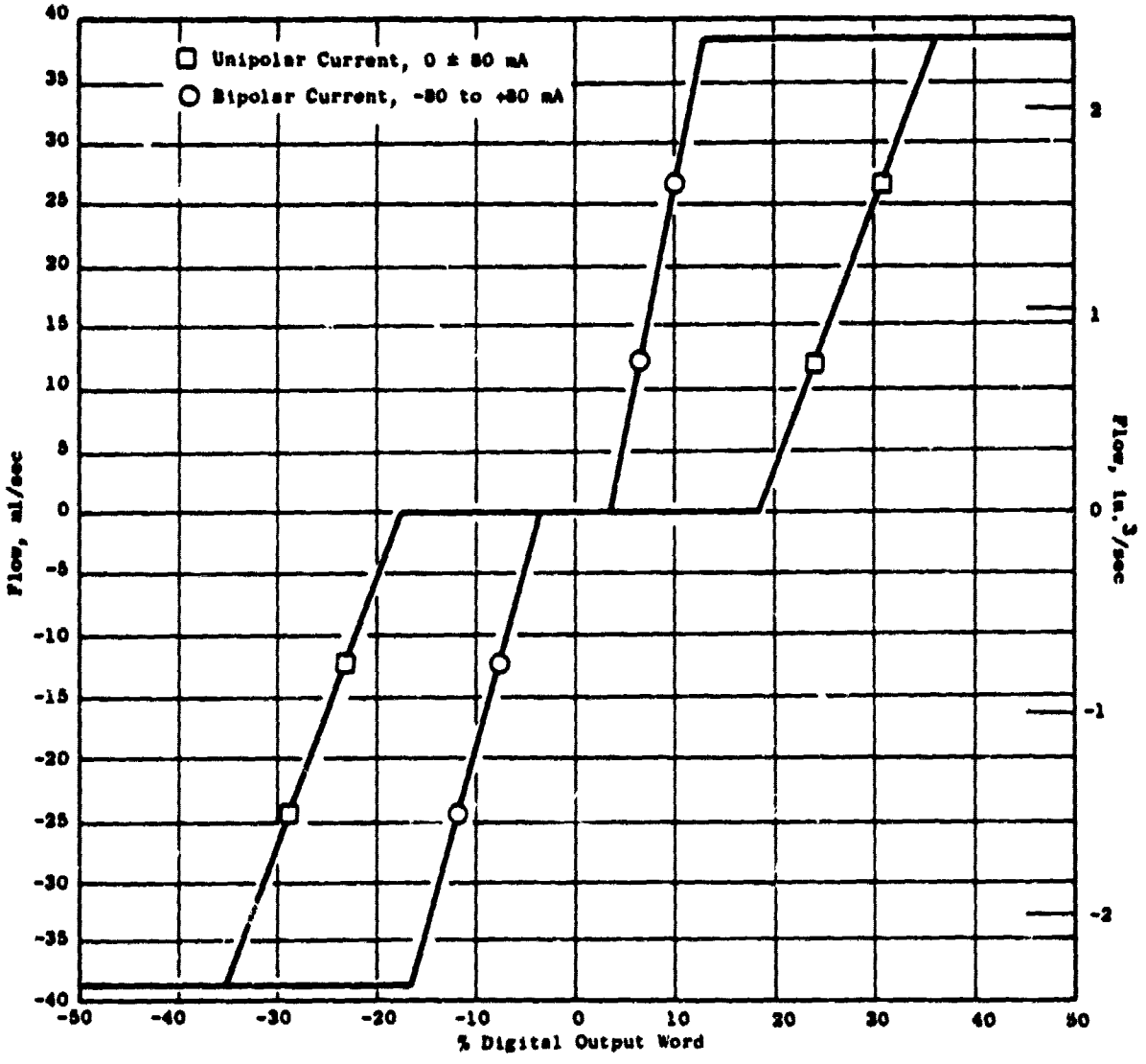

Figure 7. Simulation of Fail-Fixed Servovalve Characteristics.

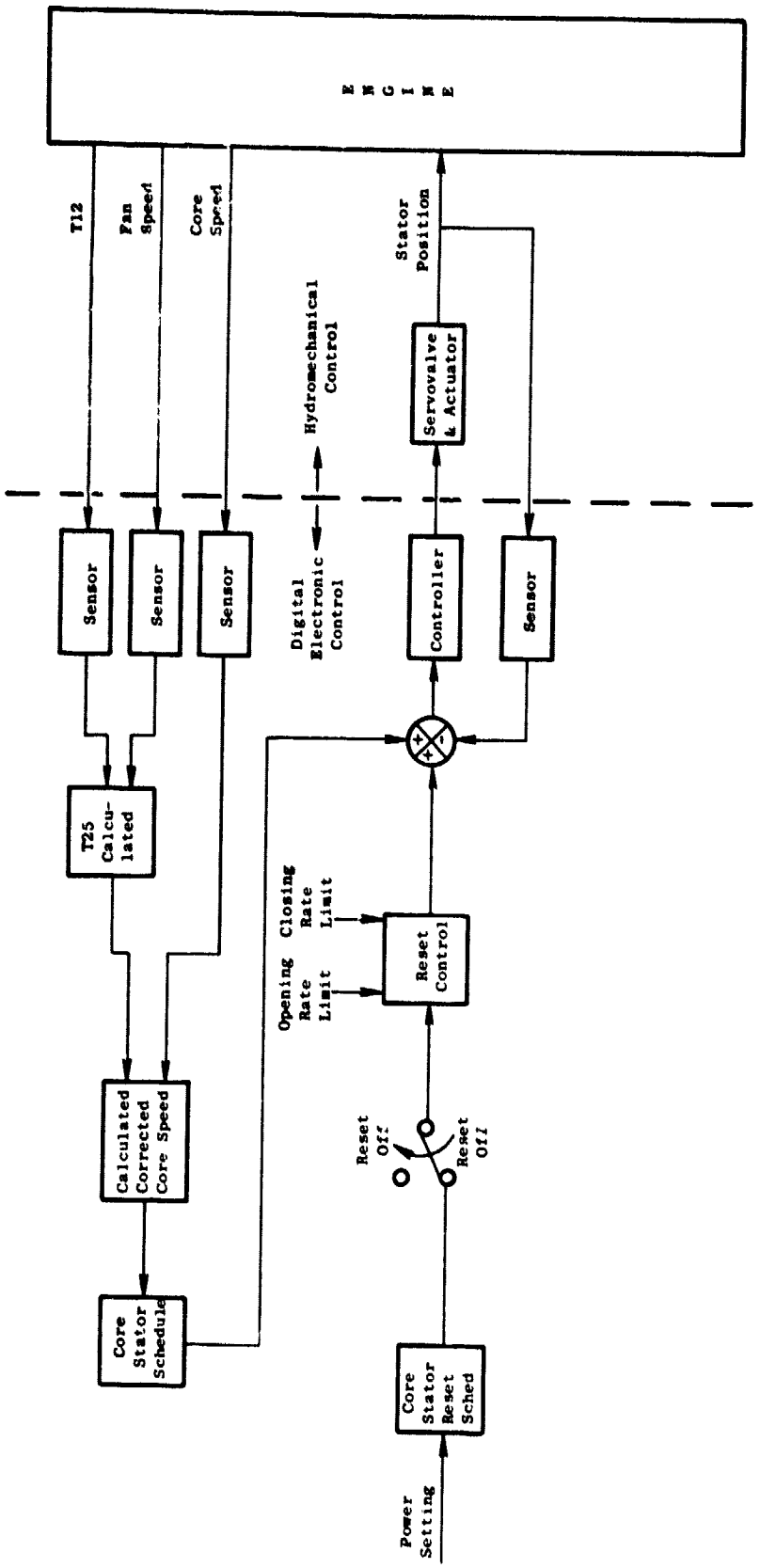

Figure 8. OTW Core Compressor Stator Control Model Schematic.

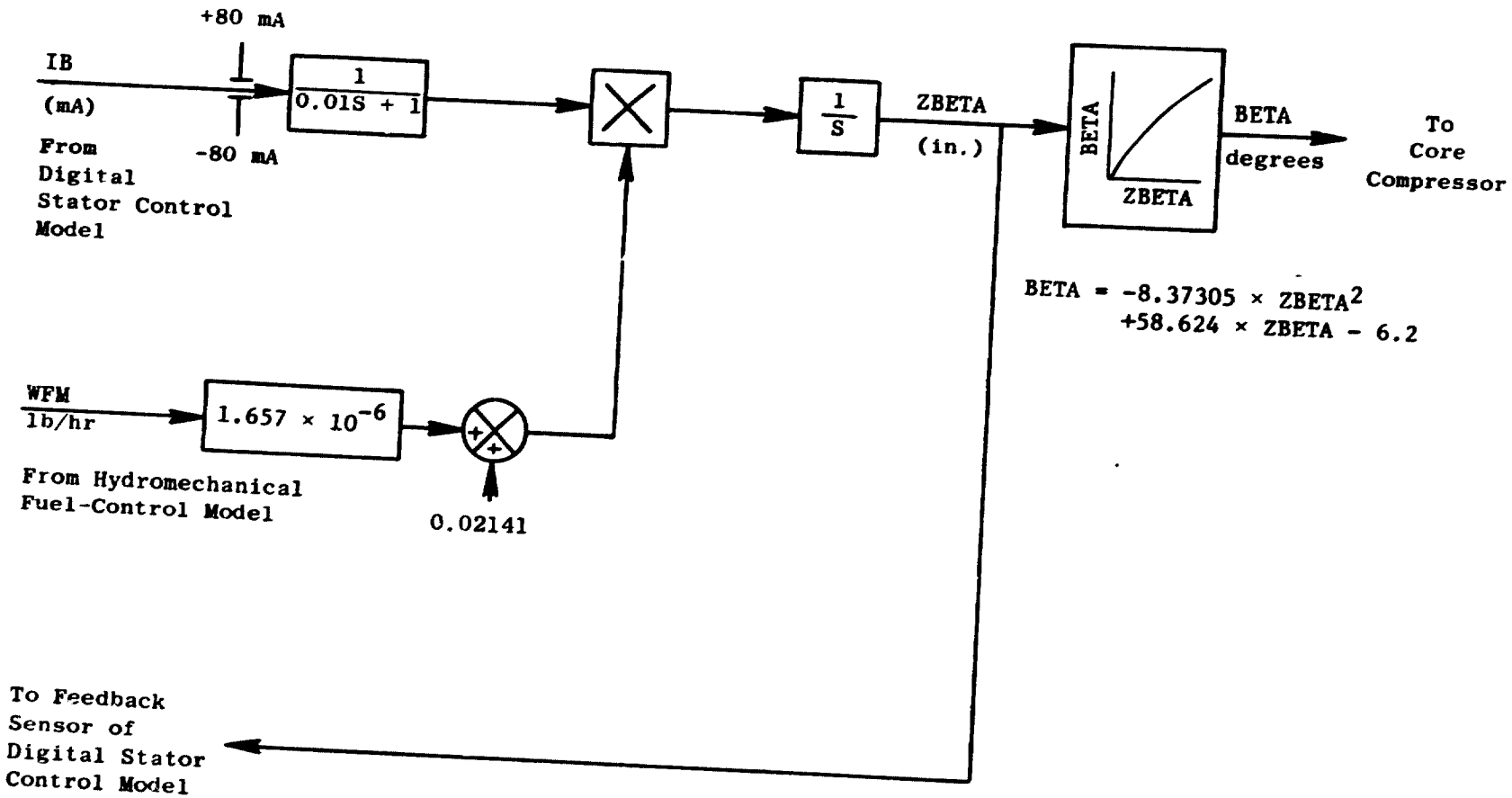

Figure 9. OTW Hydromechanical Core Stator Actuation System Model.

ule. The net effect is to set the stators at a more closed position. For the OTW experimental engine, the core stator reset schedule is an adjustable function of power setting. The rate of adding reset is limited by the reset control. The rate of removing reset (i.e., opening stators) is also limited. The details of the reset control are described by the block diagram in Appendix B.

4.3 FAILURE IDENTIFICATION AND CORRECTIVE ACTION SIMULATION

Failure Identification and Corrective Action (FICA) is an integral part of the digital control. The FICA will replace the output of a sensor in the event of failure. The FICA has no effect on unfailed-sensor output, so it can be separate from the rest of the control system. The inputs to the FICA are the sensors and the control outputs. The outputs from the FICA are the estimated values of the failed sensors and the values of the unfailed sensors.

The FICA strategy has been developed and has first application in the OTW QCSEE full authority digital control. It is based on an extended Kalman filter incorporating a nonlinear model of the engine to provide a best estimate of the state and expected sensor outputs of the engine controls.

Since the FICA acts only in the event of a sensor failure, it has no effect on the normal control action. The logic, schedules, and dynamics of the control were designed independently of the FICA, and the FICA was designed with the control in place. The simulation of the FICA was run on the Number 2 hybrid computer while the engine and control of the QCSEE was simulated on the Number 1 hybrid computer. The connections between the two computers were analog trunk lines. In adding the FICA, the simulated sensor outputs were reconnected to the FICA, and the FICA supplied the sensor outputs to the controls simulation. For unfailed-sensor operation the FICA does not alter the sensor output signals.

The control inputs and sensed output variables for the QCSEE are shown in Figure 10. The inputs are current to the fuel flow valve, IWF, and current to the compressor stator blade torque motor, IB. The actual fuel flow and actual compressor stator angle are sensed output variables. Also sensed are the high and low rotor speeds, compressor discharge pressure and temperature, and turbine discharge temperatures for a total of seven sensed output variables. In addition, the three environmental variables P2, T2, and PO are sensed and used for model inputs.

An overall block diagram of the failure detection and correction strategy is shown in Figure 11. The strategy consists of three parts: a nonlinear model of the engine, decision logic to determine when a failure has occurred and to take corrective action when a failure is detected, and a feedback-gain matrix to update the model and keep it in close agreement with the actual engine. The engine control logic is unaffected by the failure detection and correction logic. The same control signals are applied to the model as well as to the engine. The outputs of the models, which are the

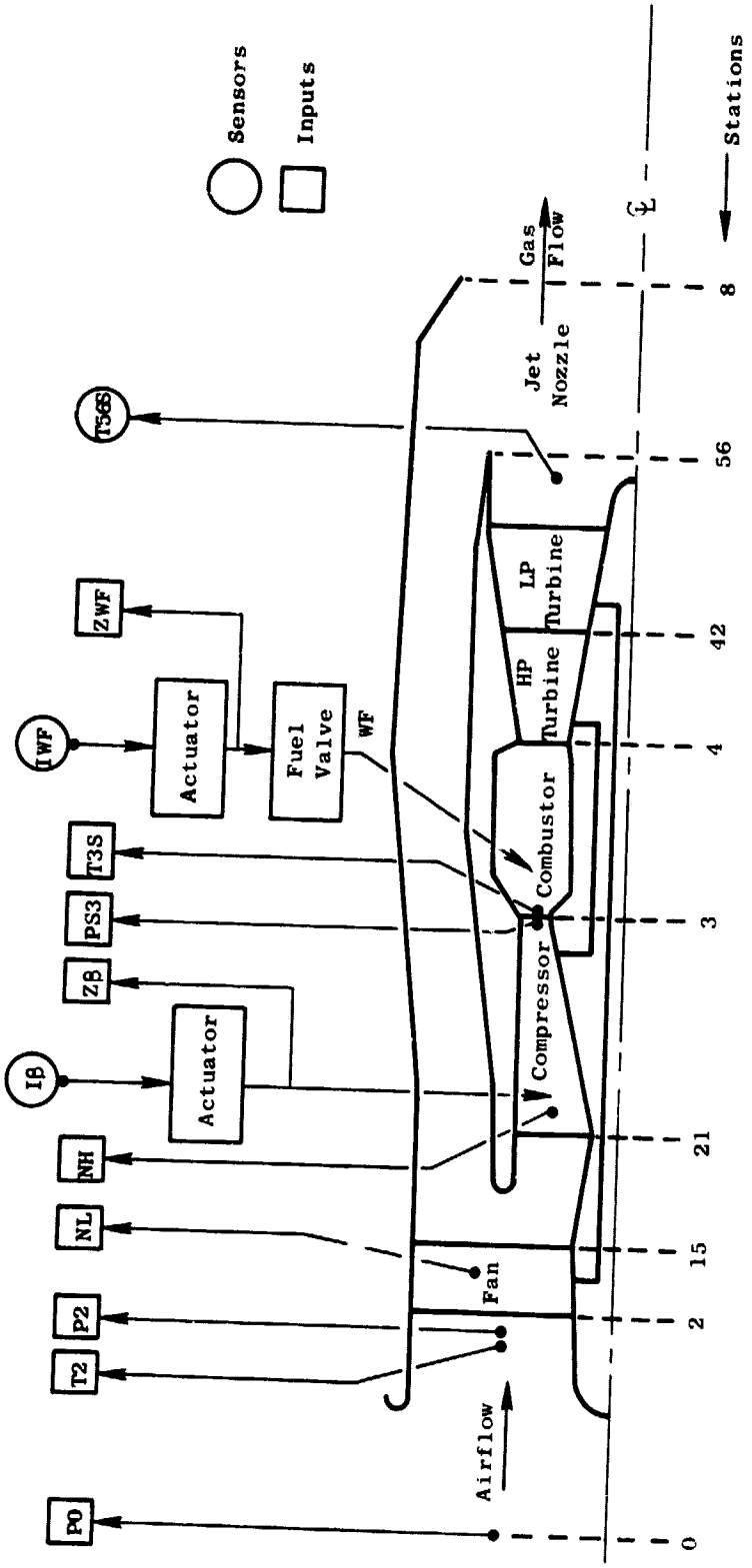

Figure 10. QCSEE Schematic - Stations, Inputs, and Sensors.

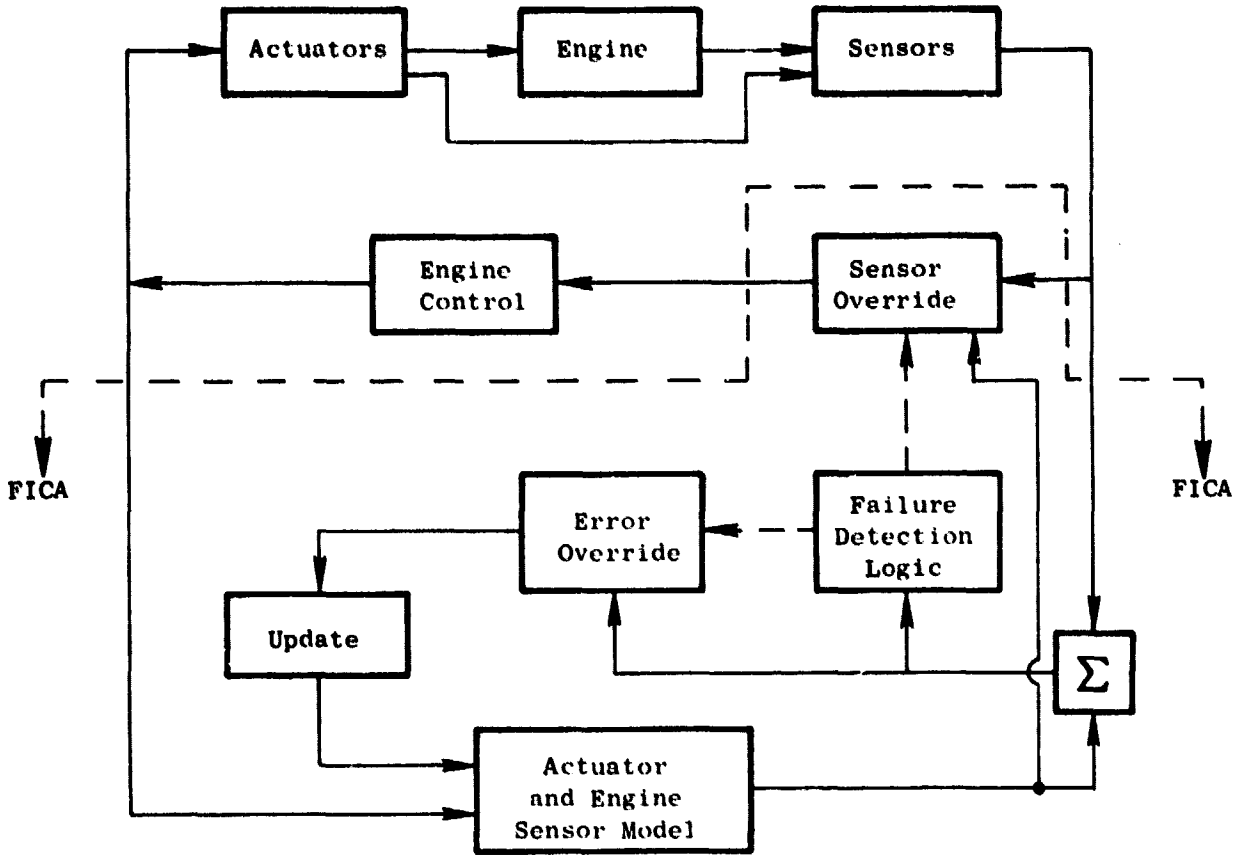

Figure 11. Block Diagram of the FICA Strategy.

expected outputs of the engine, are compared with the actual outputs of the engine. If the difference between the actual and expected outputs is too large, it is assumed that the sensor has failed. In that case, the sensor output is replaced by the expected output from the model for control purposes. The difference between the actual and expected output for an unfailed sensor is fed-back through a gain matrix to correct the model.

Obviously, this strategy relies heavily on the nonlinear model. This will be discussed in more detail below. The theory behind the feedback gain and decision logic is also given below. Since the strategy is to be implemented with an on-engine digital computer, the feedback matrix could not be computed in an on-line basis. This matrix is constant and is not changed for any combination of sensor failures or engine-operating conditions. the strategy has been extensively tested using an accurate, hybrid simulation of the engine. Some results of these tests are shown under Simulation Results, Section 6.

4.3.1 Model

The model is designed to have good dynamic and static accuracy and yet be simple enough to be solved by an on-engine, digital computer. The high accuracy is necessary to allow good, tight control even though a sensor has failed. The engine model for the subsonic transport is designed to be accurate for a power range from flight idle to maximum, over an inlet temperature range from about -54 to 54° C (-65 to 130° F) and an inlet pressure range from about 20 to 132 kN/m^2 (0.2 to 1.3 atm) to accommodate a sensor failure at any condition in flight.

The engine model has the same inputs and outputs as the actual engine, as indicated by Figure 10, plus the inlet air pressure and temperature and the ambient air pressure that determine the external operating environment.

The form of the model follows the engine cycle schematically shown in Figure 10. It consists of a low pressure ratio fan driven by the low pressure turbine that gets the exhaust gasses from the high pressure turbine. A small fraction of the fan discharge air enters the high pressure compressor that is driven by the high pressure turbine. Fuel is burned in a combustor, using air from the high pressure compressor, exhausting into the high pressure turbine. Most of the fan discharge air bypasses the compressor, combustor, and turbines and is mixed with the low pressure turbine exhaust gasses. The mixed gasses are accelerated in the jet nozzle and exhausted.

The model must account for the steady-state and transient performance of the engine. This is done in a simplified accounting for the mass flows, pressures, and temperatures in the engine and for the power in the fan, compressor, and turbines. The representation of the fans, compressors, and turbines is designed to approximate the operating line for steady-state and the off-operating line for transient response. These representations are in the form of polynomials and tables, and the choice in each case was made to get the simplest calculation with the desired accuracy. Rather than present

the detailed polynomials and tables, which will vary from engine to engine, the basic engine relationships will be presented in functional form indicating the interrelationships between variables. The block diagram shown in Figure 12 shows how these relationships follow from the engine cycle of Figure 10. The nomenclature is: W - gas flow, P - stagnation pressure, T - stagnation temperature, and the following characters, numbers, or subscripts provide identification (see Figure 12 and Appendix C). Since there is a significant lag in the temperature sensors, the output of these sensors is a state and is indicated by a terminal S in the nomenclature.

For the fan, the airflow is of the form

$$W2 = (P2/\sqrt{T2}) \times f_{FW} (NL/\sqrt{T2}, P15/P2) \quad (1)$$

and the temperature rise across the fan is

$$T15 = T2 \times f_{FT} (NL/\sqrt{T2}, P15/P2) \quad (2)$$

where NL is the fan speed, rpm.

The core inlet pressure and temperature are affected by the flow split and core inlet ducts.

$$T21 = f_{IT} (T15, T2) \quad (3)$$

$$P21 = P15 \times f_{IP} (NL/\sqrt{T2}) \quad (4)$$

The high pressure compressor airflow is

$$W21 = (P21/\sqrt{T21}) \times f_{CW} (NH/\sqrt{T2}, PS3/P21, Z\beta) \quad (5)$$

where NH is the high pressure rotor speed, $Z\beta$ is the stator position, and the temperature rise is:

$$T3 = T21 \times f_{CT} (NH/\sqrt{T2}, PS3/P21 \quad (6)$$

The combustor inlet airflow is

$$W3 = C_W \times W21 \quad (7)$$

where C_W is a constant.

The combustor temperature rise depends on fuel/air ratio

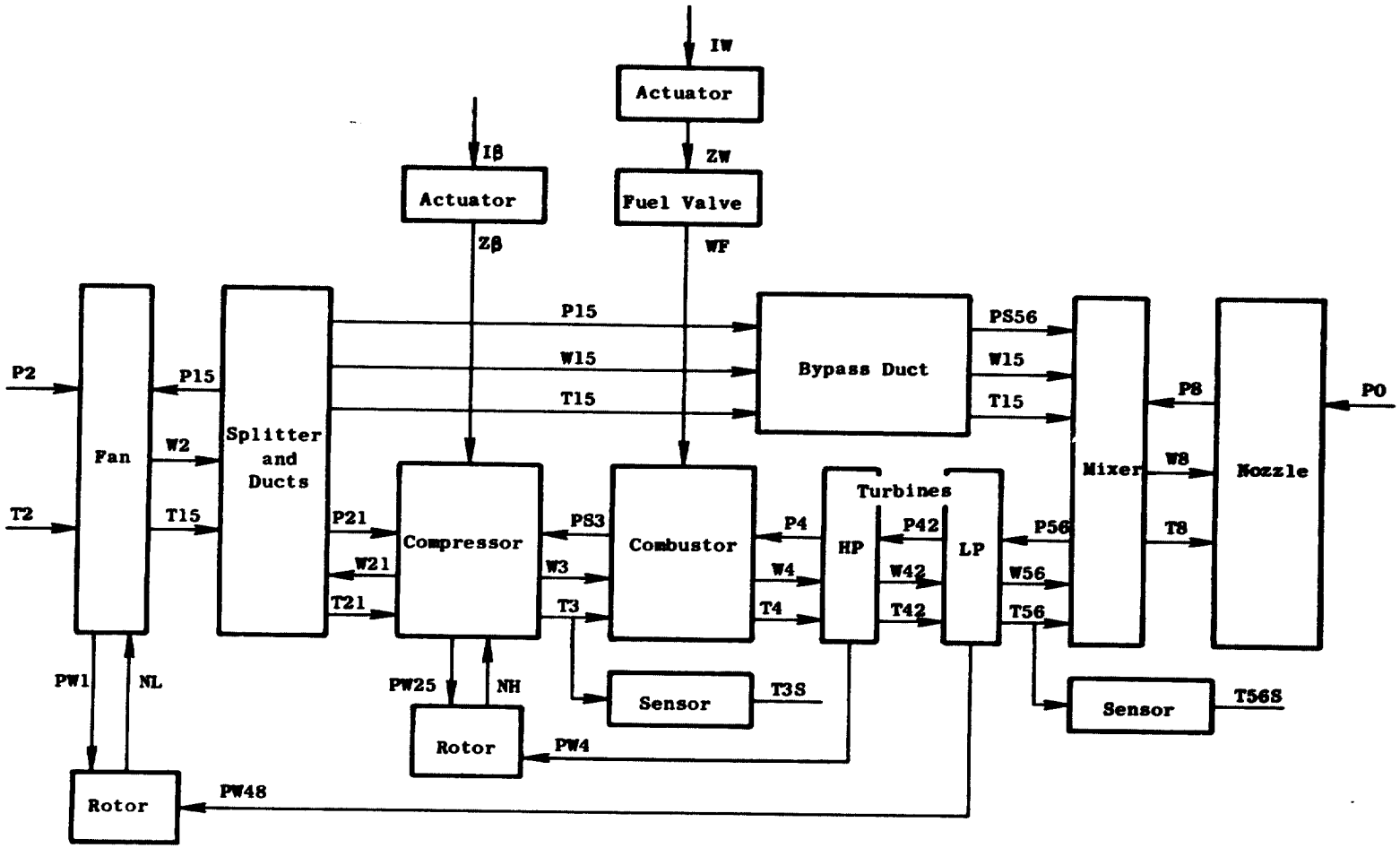

Figure 12. Block Diagram of Engine Model Computation.

$$T4 = T3 + f_C\,(WF/W3) \tag{8}$$

where WF is the fuel flow rate and discharge airflow is:

$$W4 = W3 + WF \tag{9}$$

The high pressure turbine inlet pressure is based on a fixed-area nozzle.

$$P4 = C_{TN} \times W4 \times \sqrt{T4} \tag{10}$$

The combustor inlet static pressure is related to the turbine inlet pressure.

$$PS3 = C_{BL} \times P4 \tag{11}$$

The fuel flow is a function of the metering valve position.

$$WF = f_{MV}\,(Z_{WF}) \tag{12}$$

The bypass duct airflow is the fan flow less the compressor airflow.

$$W15 = W2 - W21 \tag{13}$$

The turbine discharge pressure is computed from the bypass duct pressure loss. At the mixing plane between the core gas flow and bypass airflow, the approximation that the static pressures of the two streams are equal is used.

$$PS56 = P15 - f_{BL}\,(W15,\ P15,\ T15) \tag{14}$$

$$W56 = W21 + WF \tag{15}$$

The stagnation pressure at the turbine discharge is:

$$P56 = PS56 + f_{DL}\,(W56,\ PS56,\ T56) \tag{16}$$

The interturbine pressure and temperature are:

$$P42 = P56 \times f_{LP}(P4/P56) \tag{17}$$

$$T42 = T4 \times f_{NT}\,(P4/P56) \tag{18}$$

The low pressure turbine exit temperature is:

$$T56 = T42 \times f_{LT}(P56/P42) \tag{19}$$

The total gas flow leaving the mixer and entering the nozzle is the fan flow plus the fuel flow.

$$W8 = W2 + WF \tag{20}$$

The gas temperature leaving the mixer is:

$$T8 = [W56 \times f_M(T56) + W15 \times T15]/W8 \tag{21}$$

The nozzle pressure is:

$$P8 = f_N(W8, T8, P0) \tag{22}$$

The mixer inlet static pressure is:

$$PS56 = C_M \times P8 - C_{MH} \times W8^2 \times T8/P8 \tag{23}$$

The fan power is

$$PW1 = T2 \times W2 \times f_{FP}(P15/P2) \tag{24}$$

and the compressor power is:

$$PW25 = C \times W21 \times (T3 - T21) \tag{25}$$

The high and low pressure turbine powers are:

$$PW4 = f_{HP}(T4, P4/P42, W3, WF) \tag{26}$$

$$PW48 = f_{LP}(T42, P42/P56, W3, WF) \tag{27}$$

The above equations describe the static relationships within the engine. The dynamic states of the engine within the frequency range of the controls are primarily the rotor accelerations, metering valve and compressor variable stator actuators, and the thermal inertia of the temperature sensors.

The rotor accelerations are proportional to the unbalanced power and inversly proportional to the polar moment of inertia and speed.

$$\dot{NL} = C_R \times (PW48 - PW1)/(J_L \times NL) \tag{28}$$

$$\dot{NH} = C_R \times (PW4 - PW25)/(J_H \times NH) \tag{29}$$

The metering valve and compressor variable stator actuator velocities are proportional to the respective electrical currents from the control logic.

$$\dot{Z}_W = C_W \times I_W \tag{30}$$

$$\dot{Z}\beta = C_B \times I\beta \tag{31}$$

The rate of change of the temperature sensors is proportional to the weight flow of the gas past the sensor and the difference between the gas temperature and the sensor temperature.

$$\dot{T3S} = C_{T3} \times W3 \times (T3 - T3S) \tag{32}$$

$$\dot{T56S} = C_{T56} \times W56 \times (T56 - T56S) \tag{33}$$

The overall accuracy of the model cannot be simply stated because the accuracy as operated depends on which states are input. However, the accuracy of individual functions can be given. For example, on the operating line the accuracy of the fan and high pressure compressor airflow are within two percent. Many of the fits are within one percent.

4.3.2 Feedback Gain and Decision Logic

One can recognize that the nonlinear model and the feedback-gain matrix are actually the well-known extended Kalman filter (Reference 3). Thus the feedback gain can be chosen to minimize the mean square error between the actual and estimated outputs. The engine can be represented in compact form as:

$$x_{n+1} = x_n + f(x_n, u_n) \tag{34}$$

$$y_n = g(x_n, u_n) + \epsilon'_n \tag{35}$$

where, at $t = n\tau$, x_n = state of the engine

u_n = input to the engine

y_n = measured output

The measurement noise is ϵ_n' with $E(\epsilon_n') = 0$ and $E(\epsilon_n' \epsilon_n'^T) = R_2'$

The "best" estimate of the measured output, $\hat{y}$, can be represented by:

$$\hat{x}_{n+1} = \hat{x}_n + f_M(\hat{x}_n, u_n) + K(y_n - \hat{y}_n) - v_n \tag{36}$$

$$\hat{y}_n = g_M(\hat{x}_n, u_n) - \epsilon_n'' \tag{37}$$

where, at $t = n\tau$, f_M and g_M represent the nonlinearities in the model.

$\hat{x}_n$ = estimated state of the engine given the past measurements

$\hat{y}_n$ = expected measured output of the engine

u_n = error in the model which is assumed Gaussian $[0, R_1]$

ϵ_n'' = error in the measurement model which is assumed Gaussian $[0, R_2'']$

To obtain the best feedback gain, we look at the error, e_n, between the states of the engine and the model.

$$e_{n+1} = e_n + f(x_n, u_n) - f_m(\hat{x}_n, u_n) + v_n - K_n(y_n - \hat{y}_n) \tag{38}$$

$$y_n - \hat{y}_n = g(x_n, u_n) - g_m(\hat{x}_n, u_n) + \epsilon_n \tag{39}$$

For small errors:

$$e_{n+1} = \Phi e_n + v_n - K_n(y_n - \hat{y}_n) \tag{40}$$

$$y_n - \hat{y}_n = C e_n + \epsilon_n \tag{41}$$

where $\epsilon_n = \epsilon_n' + \epsilon_n''$ is Gaussian $[0, R_2]$, $R_2 = R_2' + R_2''$. The gain K which minimizes this error is well known (Reference 3) and is given by the equations:

$$K_n = \Phi P_n C^T [R_2 + C P_n C^T]^{-1} \tag{42}$$

$$P_{n+1} = [\Phi - K_n C] P_n [\Phi - K_n C]^T + R_1 + K_n R_2 K_n^T \tag{43}$$

$$P_o = E[e_o e_o^T]$$

where

$$P_n = E[x_n - \hat{x}_n)(x_n - \hat{x}_n)^T] \tag{44}$$

Obviously, the gain matrix given by equation 42 depends on the operating point of the engine.

Under the assumption of Gaussian noise and modeling errors, the error between the actual and estimated outputs will also be Gaussian with zero mean and covariance.

$$R_y = R_2 + C P_n C^T \tag{45}$$

The expected variance of the error for the i-th individual sensed variable is

$$E[(y_{i,n} - \hat{y}_{i,n})(y_{i,n} - \hat{y}_{i,n})^T] = R_{yii} \tag{46}$$

where R_{yii} is the i-th diagonal element of R_y. Thus, the optimum detector for failure (Reference 4) is:

$$|y_{i,n} - \hat{y}_{i,n}| \leq k_i \sqrt{R_{yii}} \quad \text{No Failure} \tag{47}$$

$$|y_{i,n} - \hat{y}_{i,n}| > k_i \sqrt{R_{yii}} \quad \text{Failure} \tag{48}$$

The threshold constant is k.

When a sensor failure is detected, the output of that sensor is ignored until it is again within the tolerance. In the computation of the feedback gain, this is equivalent to setting to zero the corresponding row of the matrix C and the row and column of R_2 in equations 42 and 43. This implies that the gain K should be computed, at each time step, taking into account the available sensors and changes in flight conditions. However, the on-board calculation of the Riccati equation requires considerably more memory and computational speed than is conveniently available. An analysis of the

eigenvalues for the open and closed loops has shown that a constant-feedback matrix can be found which will yield a stable system for the range of power at sea level and for various sensor failures and combinations of sensor failures. The hybrid-computer simulation also confirms the realizability of of this simplification. This permits the K matrix to be computed off-engine and still maintain satisfactory performance.

5.0 HYBRID SIMULATION

The hybrid simulation of the QCSEE OTW model was constructed at the General Electric AEG Dynamic Analysis Simulation Center using two Electronic Associates, Inc. (EAI) 690 Hybrid Computing Systems. The engine and basic control system were implemented on an EAI 690 Hybrid Computing System which consisted of two EAI 680 Analog Computers with a total of 224 amplifiers, an EAI 693 Hybrid Interface Unit (Model 1) with 64 channels for A/D (analog/digital) and D/A (digital/analog) conversion, and an EAI 640 Digital Computer puter with a 16,000-word core memory. The FICA portion of the model was implemented on a smaller EAI 690 Hybrid Computing System which consisted of one EAI 680 Analog Computer with a total of 70 amplifiers, an EAI 693 Hybrid Interface Unit (Model 3) with 32 A/D channels and 24 D/A channels, and an EAI 640 Digital Computer with a 15,000-word core memory. Peripheral equipment includes three EAI 8875 eight-channel strip-chart recorders, two EAI 600 high-speed line printers, two EAI 500 card readers, an EAI 1700 cartridge tape unit, and X-Y recorders.

5.1 TECHNIQUES

The two computing systems are linked through trunks between the analog consoles. The computing system containing the engine and basic control system is programmed to operate with or without the FICA logic of the second computing system. This permitted the design of the basic control system to proceed independently of the FICA development. All engine calculations except for noniteration dynamics are performed on the digital computer. Basic control calculations are split between the digital and the analog computers with all dynamics on the analog and most function generation on the digital. Transient data is output from the analog computer to the strip-chart and X-Y recorders.

The split of the computational load for the engine and basic control system is shown in Figure 13.

The digital program for simulating the OTW engine and basic control system requires approximately 15,300 words of core memory. The resulting digital sampling interval (with steady analog inputs) is approximately 60 milliseconds. As a consequence, the simulation is run at a time base which is twenty times slower than real time. Thus, the digital delay is an effective 3 milliseconds in simulation time.

The FICA portion of the model is primarily a digital simulation requiring 9,637 words of core memory. The only analog calculations are the temperature sensor dynamics and the logic which control the sampling rate and printout intervals. The high speed line printer and paper-tape punch are used to provide transient output data from the FICA simulation.

EAI 690 Hybrid	
EAI 640 Digital	**EAI 680 Analog**
Calculations For	**Calculations For**
Inlet	
Fan Tip	
Fan Hub	
Bypass Duct	
Compressor	Compressor Heat Soak
Combustor	Combustion Delay
	Turbine Heat Soak
HP Turbine	
LP Turbine	
Mixer	
Exhaust Nozzle	
Thrust	
Main Engine Control	Control Dynamics
	Rotor Dynamics

Figure 13. Split of QCSEE OTW Simulation Computation Load.

5.2 SIMULATION VERIFICATION

The simulation of the engine was compared to the cycle deck at several operating points which were felt to be of primary importance for control studies. These points were at sea level, static, standard-day conditions for the following thrust levels: takeoff, 85% of takeoff, 75% of takeoff, 65% of takeoff, 50% of takeoff, and 30% of takeoff. The comparison data were generated by setting simulation fuel flow and exhaust nozzle area at the cycle deck values. The cycle deck data, simulation data, and percent error are shown in Table I.

The simulation data in Table I show good agreement with the cycle deck at the power settings from 65 to 100% takeoff thrust. All percent errors are less than 2% except for fan stall margin at 65% takeoff thrust. At this point, the percent error in fan stall margin is -3.4%; however, since the value of stall margin is 14.91%, the actual difference in terms of stall margin is less than 0.5%. Below 65% takeoff thrust, agreement deteriorates to a maximum of 4.81% in net thrust. This deterioration can be attributed to several factors: round-off errors, truncation errors, and map inaccuracies due to linear interpolation. The deviation of the model at the lower power levels was not considered significant because the primary goal was to produce a tool which could be used to design a control system which would meet the required 1.0-sec accel time from approach to 95% of takeoff thrust.

Since no other source of transient data was available, it was not possible to verify the model transiently against an independent data source. However, several model transients were run at a time base one-hundred times slower than real time with no observable differences from the 20:1 time scale. Thus, the effects due to hybrid simulation (iteration dynamics, A/D multiplexer slewing, digital time delay, etc.) were assumed to be negligible.

Table I. Steady-State Verification Data for QCSEE OTW Simulation.

Parameter	Takeoff			85% of Takeoff		
	Cycle Deck	Simulation	Percent Error	Cycle Deck	Simulation	Percent Error
ALT	0	0		0	0	
XM	0	0		0	0	
FN, kN	90.29	90.58	0.32	76.75	76.25	-0.65
(lbf)	(20300)	(20364)		(17255)	(17143)	
DTAMB	0	0		0	0	
XM11	0.7778	0.7741	-0.48	0.6635	0.6555	-1.20
XNL, rpm	3751	3758	0.18	3456	3442	-0.40
W2A, kg/sec	398.3	397.8	-0.14	371.6	369.1	-0.67
(lb/sec)	(878.1)	(876.9)		(819.3)	(813.8)	
SM12	17.97	17.81	-0.87	17.26	16.93	-1.92
XNH, rpm	13553	13654	0.74	13086	13137	0.37
W25, kg/sec	35.68	35.93	0.70	32.36	32.65	0.83
lb/sec)	(78.67)	(79.22)		(71.39)	(71.98)	
T25, K	327.2	327.3	0.03	321.8	321.6	-0.09
(° R)	(589.0)	(589.2)		(579.3)	(578.8)	
SM25	20.24	19.90	-1.66	25.20	25.08	-0.46
T3, K	726	728	0.23	686.1	686.4	0.04
(° R)	(1307)	(1310)		(1235)	(1235.5)	
P3, MN/m^2	1.72	1.73	0.62	1.50	1.51	0.63
(psia)	(249.7)	(251.2)		(217.1)	(218.5)	
PS3, MN/m^2	1.63	1.64	0.52	1.41	1.42	0.47
(psia)	(236.3)	(237.5)		(205.2)	(206.2)	
WFM, kg/hr	3160	3162	0.05	2525	2526	0.05
(lb/hr)	(6967)	(6970)		(5566	(5569)	
W8, kg/sec	399.2	398.6	-0.15	372.3	369.9	-0.66
(lb/sec)	(880.1)	(878.8)		(820.8)	(815.4)	
T8, K	399.9	379.9	-0.02	366.9	367.1	0.06
(° R)	(683.9)	(683.8)		(660.4)	(660.8)	

Table I. Steady-State Verification Data for QCSEE OTW Simulation (Continued).

Parameter	75% of Takeoff			65% of Takeoff		
	Cycle Deck	Simulation	Percent Error	Cycle Deck	Simulation	Percent Error
ALT	0	0		0	0	
XM	0	0		0	0	
FN, kN	67.72	67.09	-0.93	58.69	57.92	-1.32
(lbf)	(15225)	(15083)		(13195)	(13021)	
DTAMB	0	0		0	0	
XM11	0.5990	0.5922	-1.14	0.5400	0.5315	-1.57
XNL, rpm	3262	3237	-0.78	3044	3011	-1.07
W2A, kg/sec	351.0	348.8	-0.64	328.7	325.2	-1.05
(lb/sec)	(773.9)	(768.9)		(724.6)	(717.0)	
SM12	16.15	15.99	-0.98	14.91	14.46	-3.04
XNH, rpm	12821	12861	0.31	12535	12565	0.24
W25, kg/sec	30.17	30.42	0.84	27.94	28.15	0.73
(lb/sec)	(66.51)	(67.07)		(61.60)	(62.05)	
T25, K	318.2	317.9	-0.09	314.2	313.7	-0.13
(° R)	(572.7)	(572.2)		(565.5)	(564.7)	
SM25	27.75	27.87	0.45	30.28	30.10	-0.59
T3, K	665.0	665.4	0.06	643	642	-0.15
(° R)	(1197.0)	(1197.7)		(1158)	(1156)	
P3, MN/m^2	1.36	1.37	0.58	1.23	1.23	0.43
(psia)	(197.4)	(198.6)		(177.9)	(178.7)	
PS3, MN/m^2	1.28	1.29	0.47	1.16	1.16	0.29
(psia)	(186.3)	(187.2)		(167.7)	(168.2)	
WFM, kg/hr	2181	2180	-0.02	1854	1854	0.00
(lb/hr)	(4808)	(4807)		(4087	(4087)	
W8, kg/sec	351.6	349.6	-0.64	329.2	325.7	-1.05
(lb/sec)	(775.2)	(770.3)		(725.7)	(718.1)	
T8, K	365.7	365.9	0.05	353.6	353.9	0.10
(° R)	(648.3)	(648.6)		(636.4)	(637.0)	

Table I. Steady-State Verification Data for OTW Simulation (Concluded).

Parameter	50% of Takeoff			30% of Takeoff		
	Cycle Deck	Simulation	Percent Error	Cycle Deck	Simulation	Percent Error
ALT	0	0		0	0	
XM	0	0		0	0	
FN, kN	45.15	43.78	-3.02	27.09	25.79	-4.81
(rpm)	(10150)	(9843)		(6090)	(5797)	
DTAMB	0	0		0	0	
XM11	0.4552	0.4454	-2.16	0.3375	0.3289	-2.56
XNL, rpm	2682	2643	-1.44	2081	2029	-2.48
W2A, kg/sec	295.2	285.8	-1.68	227.6	222.5	-2.23
(lb/sec)	(640.9)	(630.1)		(501.8)	(490.6)	
SM12	12.38	11.86	-4.18	8.94	8.67	-3.05
XNH, rpm	12080	12038	-0.35	11318	11289	-0.26
W25, kg/sec	24.44	24.22	-0.90	18.93	18.72	-1.08
(lb/sec)	(53.87)	(53.39)		(41.73)	(41.28)	
T25, K	308.3	307.8	0.16	299.9	299.6	-0.14
(° R)	(554.9)	(554.0)		(539.9)	(539.2)	
SM25	33.85	33.18	-1.97	36.91	36.25	-1.78
T3, K	608	609	-0.16	554.2	554.6	0.07
(° R)	(1095)	(1097)		(997.5)	(998.2)	
P3, MN/m^2	1.02	1.02	-0.77	0.74	0.73	-0.78
(psia)	(148.5)	(147.4)		(107.0)	(106.2)	
PS3, MN/m^2	0.96	0.95	-0.82	0.69	0.69	-0.86
(psia)	(139.6)	(147.4)		(100.3)	(99.44)	
WFM, kg/hr	1398	1397	-0.07	862	861	-0.10
(lb/hr)	(3082)	(3080)		(1900)	(1898)	
W8, kg/sec	291.1	286.2	-1.68	227.8	222.7	-2.24
(lb/sec)	(641.8)	(631.0)		(502.3)	(491.0)	
T8, K	344.0	344.6	0.18	332.1	332.7	0.17
(° R)	(619.2)	(620.3)		(597.8)	(598.8)	

6.0 SIMULATION RESULTS

The QCSEE OTW hybrid simulation has been used to develop the control system design for the experimental engine. The control system manipulates two variables: fuel flow and core compressor stator angle. The system includes a full authority digital electronic control; the design includes three key functions.

- Reset of the core compressor stator to achieve acceleration-thrust-response characteristics required for powered-lift operation,
- Fail-fixed servovalve which causes the fuel-metering-valve, power piston to fail-in-position if there is a loss in electrical power to the digital control or if there is a digital control failure resulting in a hard-over, electrical output in either direction.
- Failure identification and corrective action logic which recognizes failures in sensor feedbacks to the digital control and provides corrective action for maintaining safe control of the engine.

Simulation results on each of the above control functions are described in the following sections.

6.1 TRANSIENT THRUST RESPONSE

The thrust-response requirement for the QCSEE OTW propulsion system at altitudes up to 1.8 km (6000 ft) is defined in Figure 14. To simplify the discussion of transient response, the overall requirement defined in Figure 14 has been interpreted as a response time from 62 to 95 percent of takeoff thrust in 1.0-second maximum. This thrust-response requirement is aimed primarily at the landing approach condition where rapid thrust recovery capability is required.

The UTW experimental engine has a variable-pitch fan, variable fan bypass duct exhaust nozzle area, and variable core engine compressor stators. The variable-pitch fan and variable nozzle area were utilized in the UTW control design to achieve the above-cited, thrust-response requirement. However, the OTW experimental engine has a fixed-pitch fan and does not have a variable exhaust nozzle area-actuation system. (Note: A variable nozzle area-actuation system is planned for an OTW flight-type engine.) Early simulation studies on the OTW experimental engine predicted thrust-response times greater than the 1.0-second requirement. As a consequence, attention was directed to more effective utilization of the core compressor stators to achieve acceptable thrust-response times with the OTW experimental engine. It was determined that the required 1.0-second acceleration time from 62 to 95 percent net thrust could be achieved with the following control action.

- Reset the core stators 30 degrees further closed than the normal stator schedule at the 62 percent net thrust operating condition.

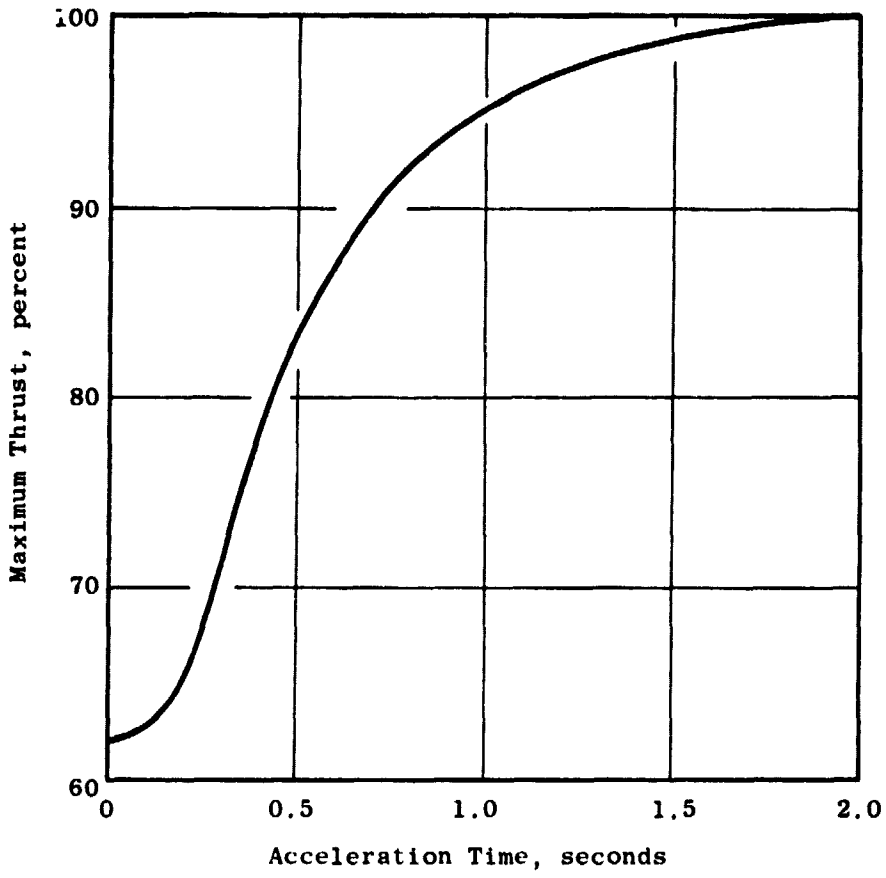

Figure 14. Engine Dynamic Thrust-Response Requirement.

- Rapidly open the core stators to the normal stator schedule during the acceleration to 100 percent net thrust.

Figure 15 illustrates the potential advantage of using the above core stator reset operation. The transient with core stator reset shows that acceleration time from 62 to 95% net thrust is less than 1.0 second; whereas, the acceleration time with no core stator reset is greater than 1.6 seconds.

6.1.1 Effect of Core Stator Reset

Fan speed, and thus engine thrust, during an aircraft approach will be controlled by manipulating fuel flow. If the pilot desires the capability for fast recovery from approach to takeoff thrust, the proposed procedure is to activate the digital control core stator reset mode. The control logic causes the core stators to slew in a closed direction. The final stator position is determined by the summation of the core stator reset schedule and the normal core stator schedule. (The reset schedule is a function of power setting, and the normal schedule is a function of core engine corrected speed.) Closing the core stators reduces the compressor airflow for a given core corrected speed. If fuel flow is held constant, the engine cycle will balance at a lower fan speed. The fan speed control senses the deceleration tendency and increases fuel flow to maintain the scheduled fan speed. As a consequence, the core engine rotor settles out at a higher speed when steady-state operation is achieved. The basic objective of the core stator reset at the approach power setting is for the core engine rotor to settle at a speed close to the takeoff power setting. Thus, when the pilot demands a fast recovery from approach to takeoff thrust, the core engine rotor is already near the final speed, and only the fan rotor needs to be accelerated to takeoff speed condition. Such operation removes the dynamic effect of the core rotor inertia on engine acceleration and achieves fast response from approach to takeoff thrust.

Figure 16 shows the effect of core stator reset on pertinent engine variables at 62% of takeoff thrust for the sea level, static, standard day, zero-bleed condition. When the stator schedule is reset 30 degrees closed, core speed increases to about 13,800 rpm, which is some 150 rpm above the speed at the takeoff power setting. As the stator schedule is reset from 0 to 30 degrees closed, fuel flow increases from 1785 to 2010 kg/hr (3940 to 4440 lb/hr), i.e., an increase of 225 kg/hr (500 lb/hr); specific fuel consumption (sfc) increases from 0.313 to 0.354. In effect, a trade off is being made between the specific fuel consumption and the capability to meet the 1.0-second acceleration requirement when 30 degrees of stator reset is used. The simulation data indicates that this transient response capability can be achieved at the cost of 3.77 kg (8.33 lb) more fuel for every minute at the 62% thrust approach condition.

Using 30 degrees of stator reset results in an actual core stator position of 24 degrees at 90.4% corrected core speed (see Figure 16). At 90.4% corrected speed, the nominal stator schedule as a function of corrected

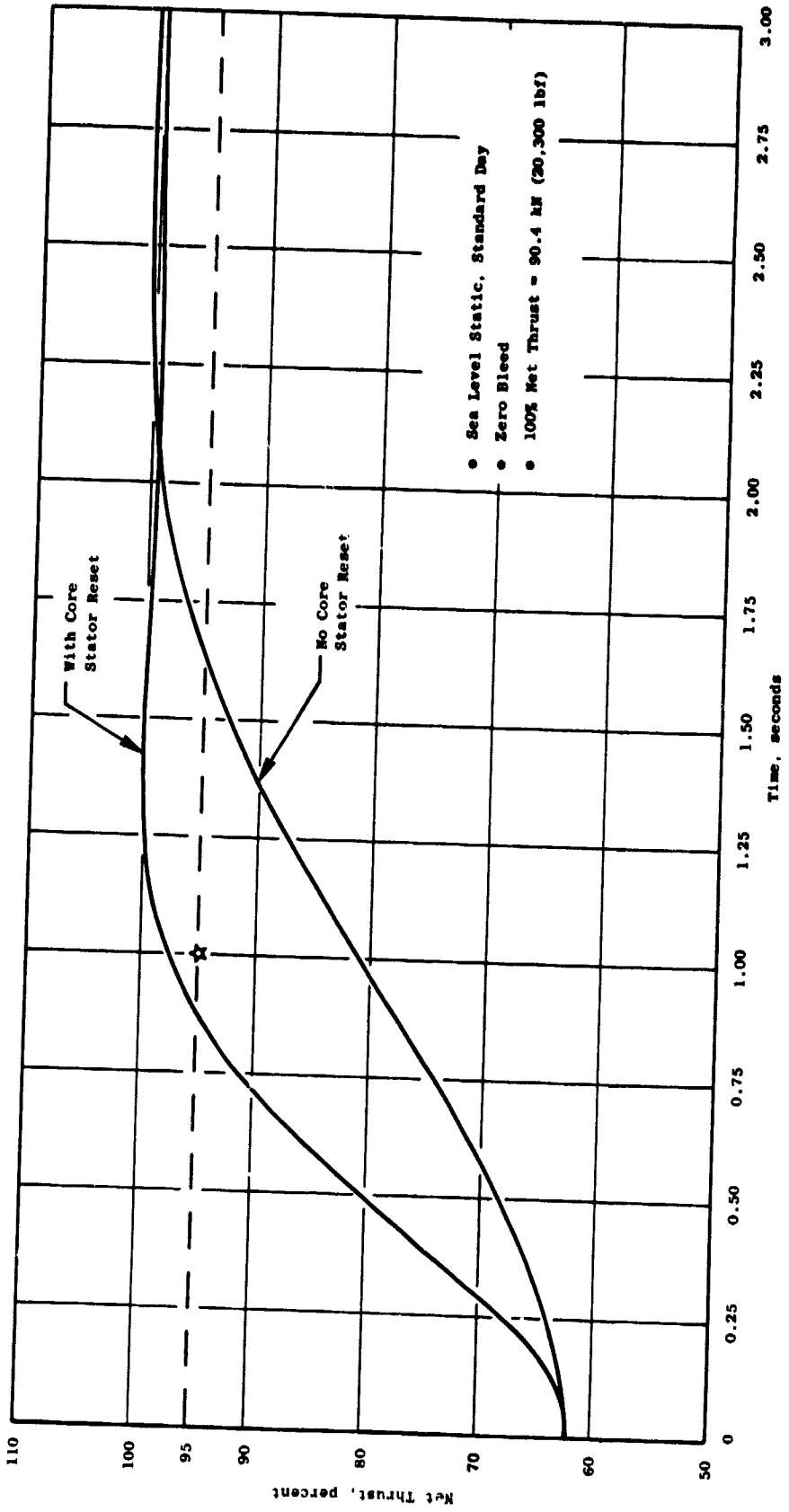

Figure 15. Initial Predictions of QCSEE Transient Response; Throttle Burst from 62 to 100% Net Thrust.

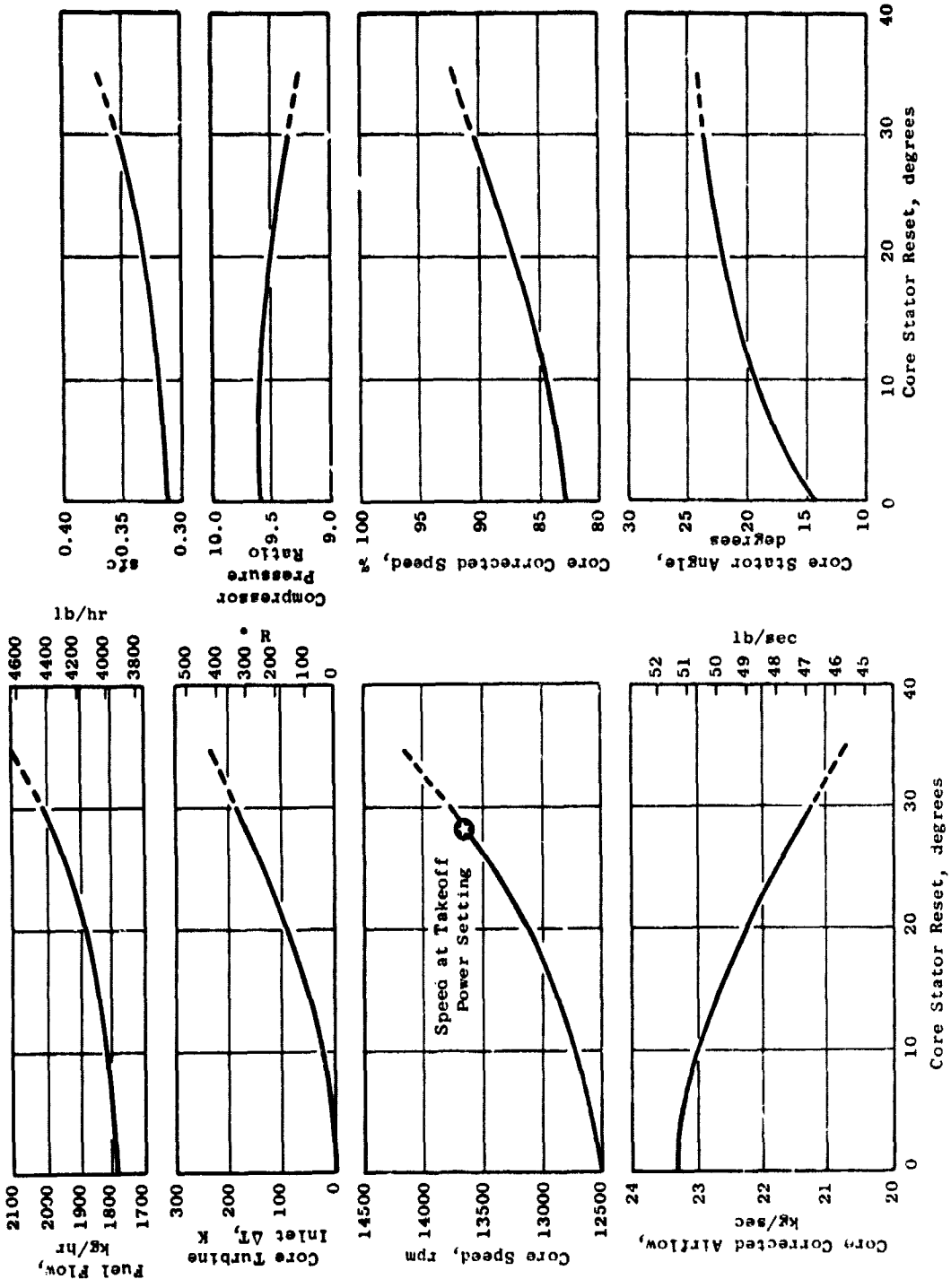

Figure 16. Engine Variables at 62% Net Thrust Versus Core Stator Reset; Sea Level, Static, Standard Day, Zero Bleed.

core speed calls for the stators to operate on the full-open stop; that is, -6 degrees. Thus -6 degrees, plus the 30 degrees reset, results in the above +24 degree position.

6.1.2 Simulated Go-Around Maneuver

The QCSEE control system is designed to meet the required transient response for a go-around maneuver while maintaining safe engine operation. Simulation results for an acceleration from 62 to 100% net thrust are shown in Figure 17. The left-hand portion of Figure 17 shows the specific values of selected engine and control variables at the 62% net thrust condition. After the step increase in power setting, the figure shows:

- The response time from 62 to 95% of takeoff thrust is 0.73 seconds, which is well within the 1.0-second requirement.
- The core stators start opening within the first 0.05 seconds and slew to the full-open stop (-6 degrees) at a rate of 60 degrees per second, producing a rapid increase in compressor airflow. The full-open stop is reached in approximately 0.55 seconds.
- Fuel flow increases due to the step in corrected fan speed demand (scheduled as a function of power setting). During the first 0.45 seconds, fuel flow is limited by the WF/PS3 acceleration fuel schedule.
- During the interval from 0.45 to 0.85 seconds, the rate of fuel flow increase is limited by the calculated core turbine temperature control. This control has anticipated that turbine inlet temperature is approaching, but still below, the reference limit for temperature. In this time interval, turbine temperature overshoots the steady-state temperature at takeoff by some 122 K (220° R). Minimum compressor stall margin is 14.9%.
- After 0.85 seconds, the fan speed has accelerated to the point where it again controls fuel flow. Core speed peaks at 14,200 rpm. Both rotor speeds, the core stators, and fuel flow settle out at the final takeoff operating levels within the next 1.75 seconds.

6.1.3 Acceleration Study

Several factors were evaluated to establish the transient control design for the OTW engine. The design process started with the development of the WF/PS3 acceleration fuel schedule. This schedule was designed to use 5% of the available core compressor stall margin during accelerations with no core stator reset. Results from initial simulation studies on transient core stall margin are plotted versus corrected core speed in Figure 18. The figure contains typical stall margin transients for a

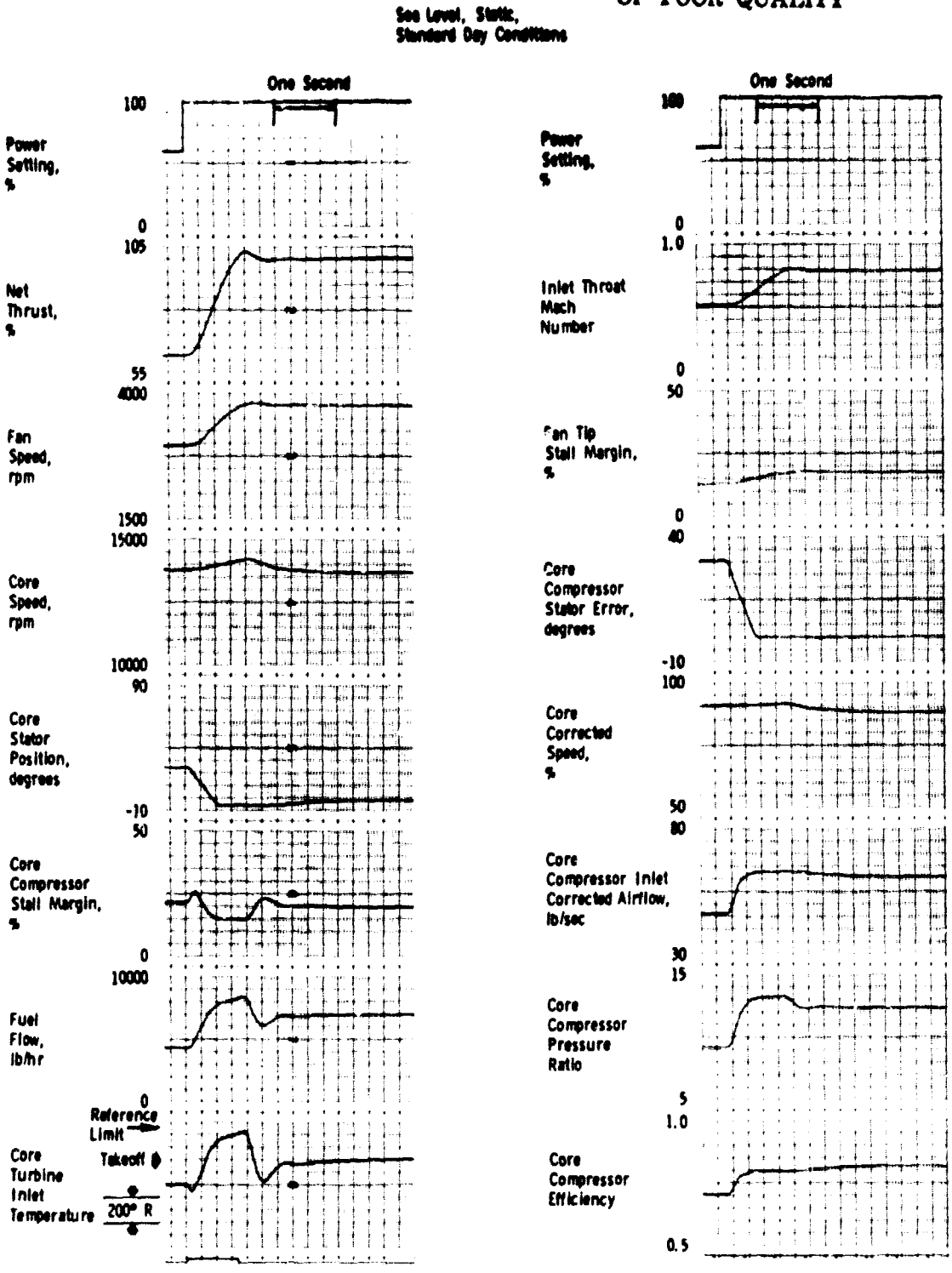

Figure 17. Throttle Burst from 62 to 100% Thrust using Linear Servovalve and Core Stator Reset.

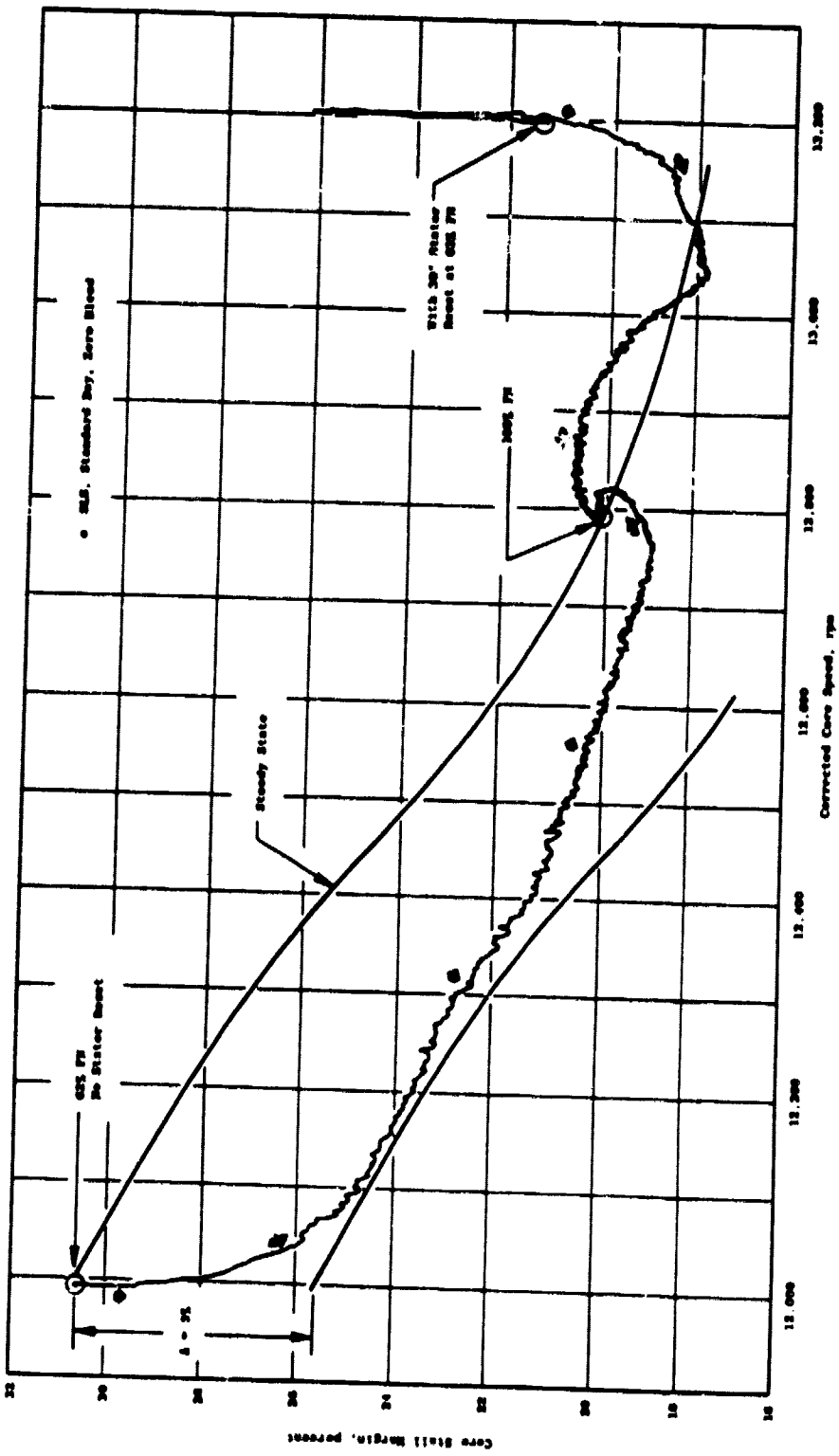

Figure 18. Initial Predictions of Core Stall Margin for Throttle Burst from 62 to 100% PW.

control with no stator reset and for a control with stator reset; satisfactory performance is indicated in both cases.

The rate of removing core stator reset (i.e., the opening rate of the compressor stators) was also investigated in the initial design studies. As shown in Figure 19, rates greater than 60 degrees per second do not provide a significant reduction in acceleration time. The adequacy of the fuel pump to supply stator actuator flow for the 60 degrees per second rate was checked out by the component engineer; his assessment was that this rate could be achieved with the current pump design. This 60 degrees per second opening rate was chosen for the control design and maintained throughout the remainder of the simulation studies.

Initial design studies also considered how core turbine inlet temperature overshoot affects acceleration time from 62 to 95% net thrust. The simulation results in Figure 20 show the acceleration time as a function of the delta between peak-temperature overshoot and the steady-state temperature of 100% net thrust for control designs with and without core stator reset. Based on the results in Figure 20, the following conclusions were reached at this stage in the control design effort:

- Unrealistic turbine overtemperatures would be required to meet the one-second acceleration requirement when the control design does not include core stator reset.

- Temperature overhsoots of 28 to 33 kelvins (50 to 60° R) will produce acceleration times in the 0.9-second range for a nominal control design (using 30 degrees stator reset at 62% thrust). Therefore, the control design should allow for more temperature overshoot to provide more margin with respect to the 1.0-second requirement. The judgement was that the above-indicated, 0.1-second margin was not sufficient to account for control component tolerances.

The above study was limited to the 33-kelvin (60° R) overtemperature range because further refinements to engine simulation scale factors were needed. These refinements were accomplished prior to the final simulation studies discussed below.

The OTW experimental engine has a titanium fan; however, a lower inertia, composite fan is planned for a flight-type engine. The initial study predictions in Figure 21 indicate an 0.2-second reduction in acceleration time when the composite fan is used and when the control design includes 30 degrees core stator reset at 62% net thrust.

In the final acceleration design studies, the core turbine inlet temperature control loop was refined so that the fuel control would remain in the acceleration fuel schedule mode for a longer period of time during the transient. Rate feedback limits were "tuned" to provide the desired anticipation for the different control loops. The final simulation predictions for the experimental engine acceleration times as a function of initial

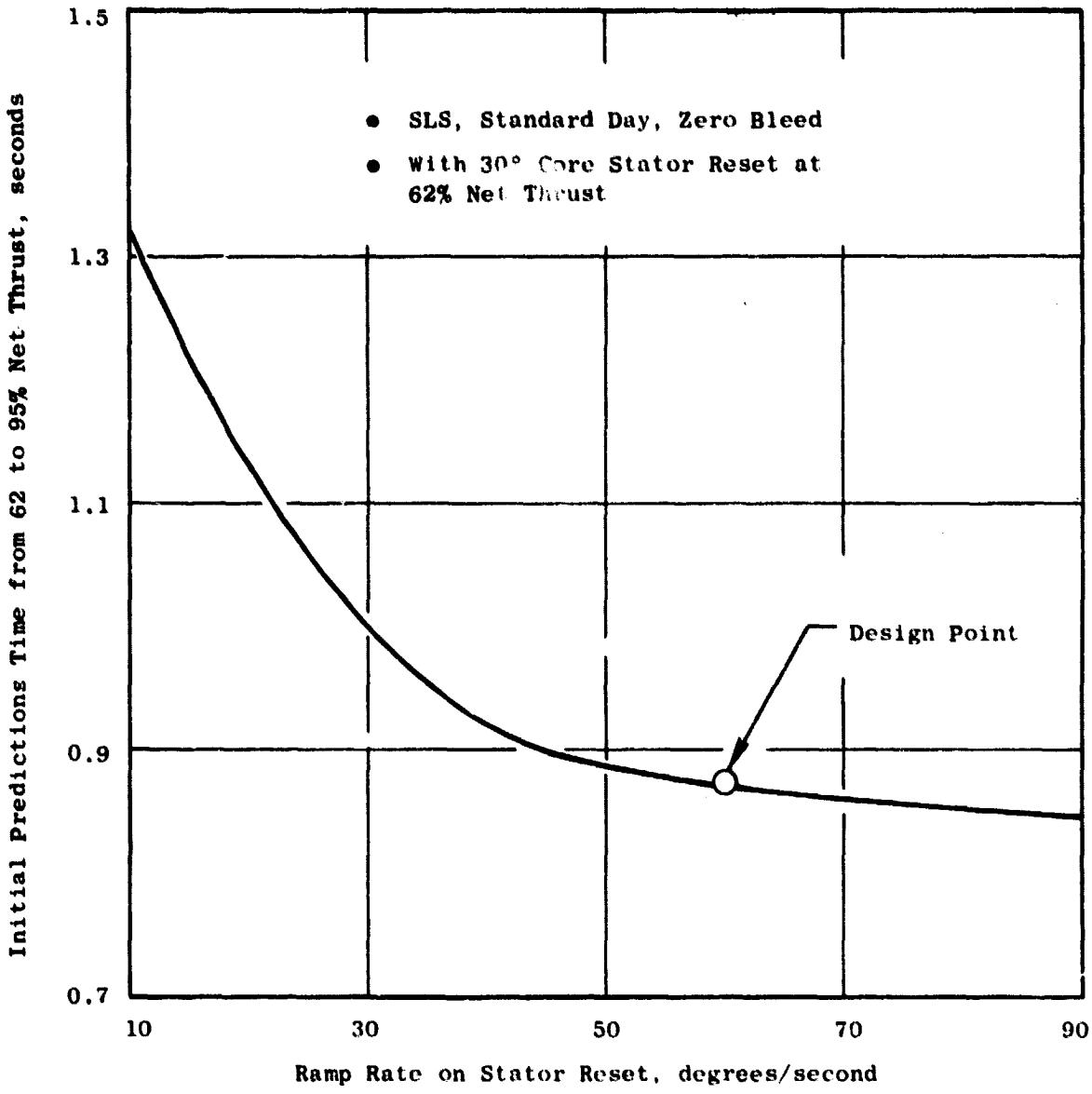

Figure 19. Transient Response; Accel Time Versus Rate of Removing Core Stator Reset.

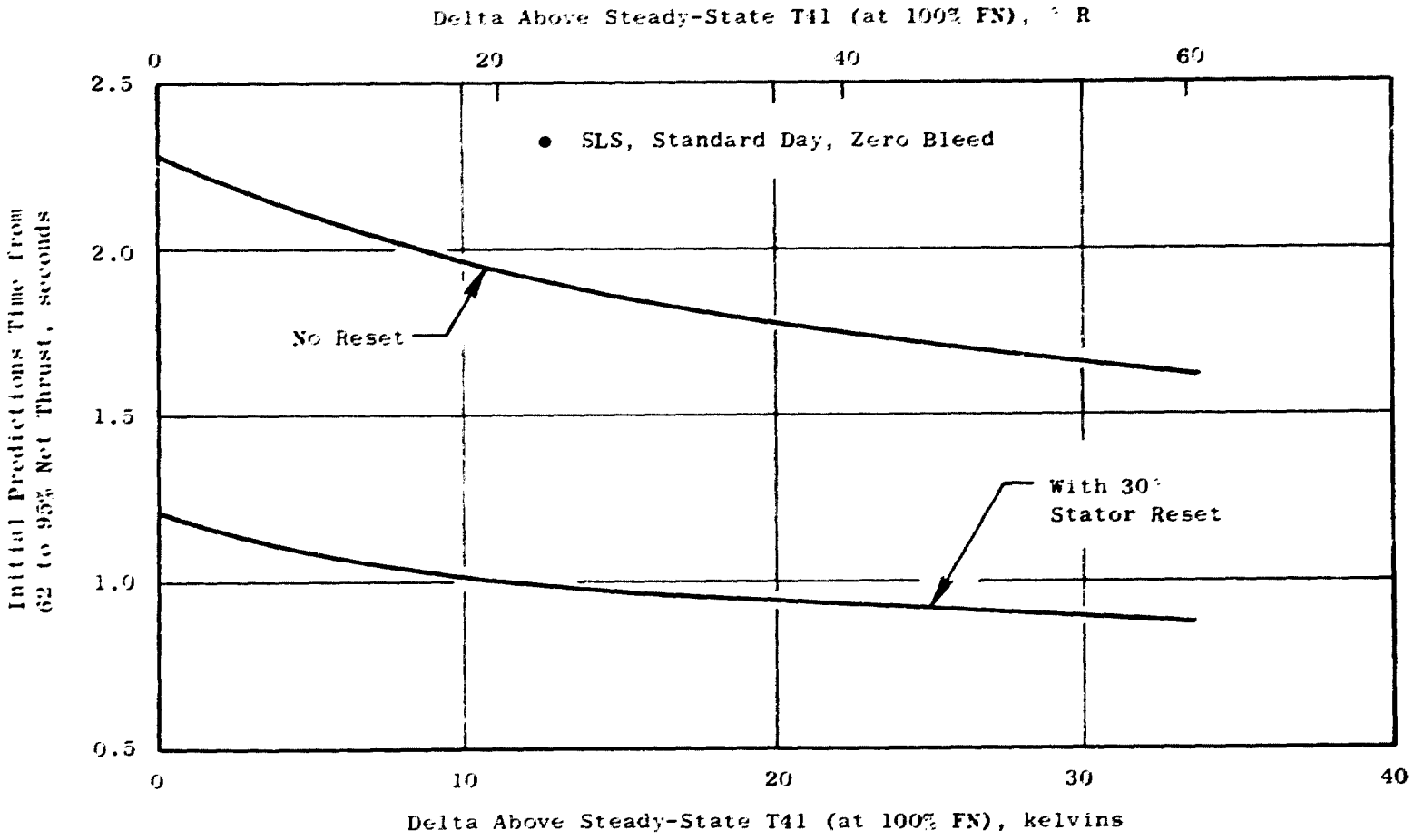

Figure 20. Transient Response; Accel Time Versus Peak T41.

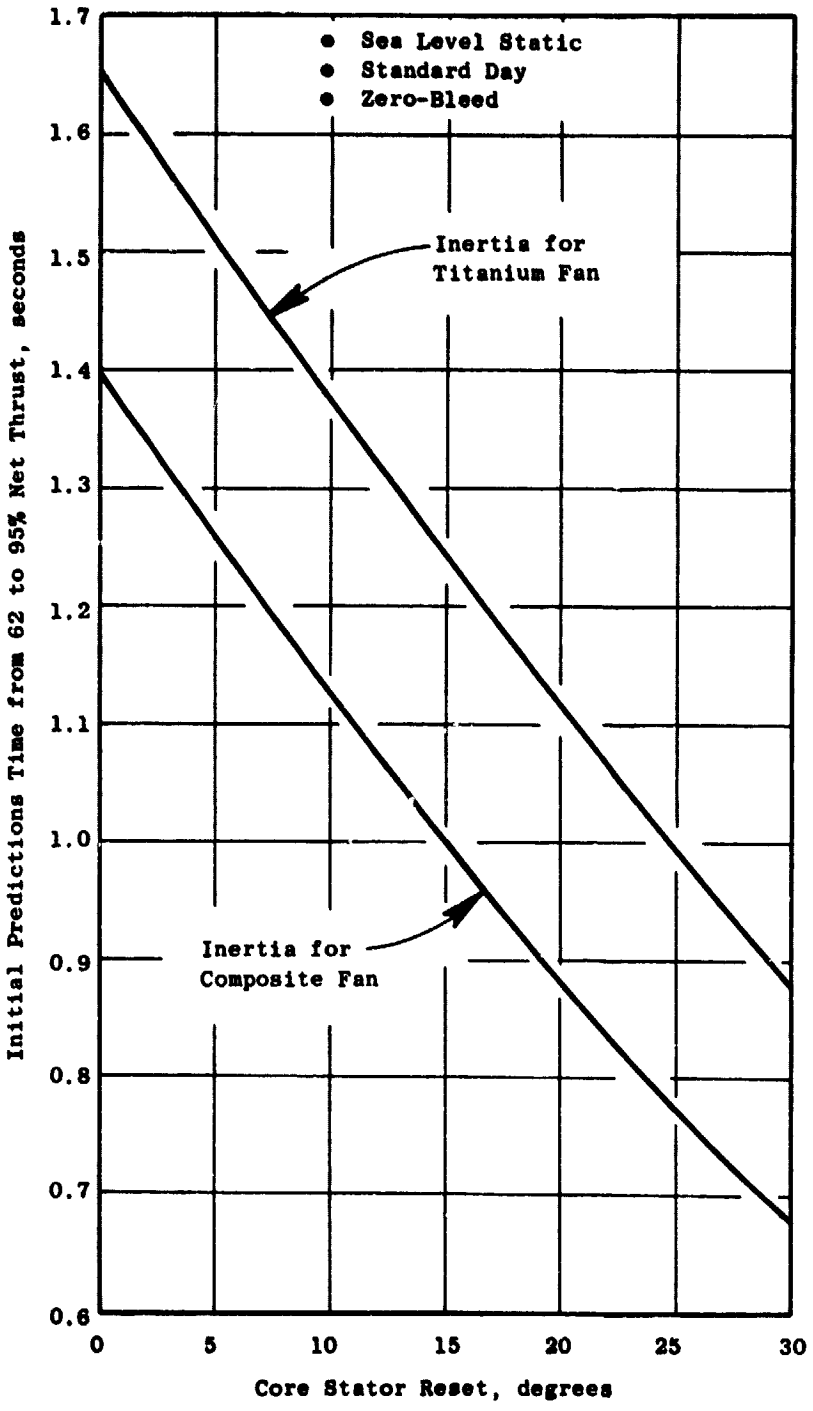

Figure 21. Initial Predictions of Transient Response for Accel Time Versus Core Stator Reset and Fan Rotor Inertia.

thrust level are shown in Figure 22. The predicted time from 62 to 95% net thrust is 0.73 seconds for the nominal control design.

6.1.4 Deceleration Study

Since there is no transient requirement for decelerations to approach power, the primary concern of the deceleration study was safe engine operation. The WF/PS3 deceleration schedule was checked out on the model to ensure that combustor blowout conditions will not occur.

A transient for a deceleration from 100 to 62% of takeoff power at sea level, static, standard day conditions is shown in Figure 23. For this transient, the core stator control logic is set in the "reset on" mode. The response time from 100 to 62% thrust is less than 1.0 second. Thrust and fan speed both settle close to the final values within 2.5 seconds after the step decrease in power setting. The core stator control limits the rate at which reset is added to the normal core stator schedule. This rate limit is approximately 4 degrees per second; thus, it takes approximately 7.5 seconds to reset the stators 30 degrees closed as shown by the core compressor stator error recording in Figure 23. This closing rate limit is significantly lower than the 60 degree per second opening rate limit used during accelerations. The slow closing rate prevents the simulation from operating in a region where the fan hub characteristics are undefined.

6.2 FAIL-FIXED SERVOVALVE STUDY

The purpose of this study was to design the control logic when the digital electronic control is connected to a fail-fixed servovalve. The hybrid-computer simulation of the engine and control system was used to determine the logic. Results from this simulation study indicated that the digital control logic should perform the following functions:

- An inverse function which compensates for both the servovalve dead zone and the nonlinear gain of the pulse-width-modulated (PWM) driver amplifier.
- A dynamic method which compensates for servovalve null shift.

The schematic in Figure 24 describes the location of these functions in relation to other digital control logic and also to the PWM driver amplifier which is connected to the torque motor of the fail-fixed servovalve. The left-most block in Figure 24 represents all schedules, dynamics, and selection logic for the several controllers which are contained in the digital control. The output of this block represents the controller selected to regulate engine fuel flow. This output is connected to the blocks representing the null-shift compensation and the inverse function. The digital output word from the inverse function is the signal to the PWM driver amplifier, whose output is connected to the fail-fixed servovalve assembly. Subsequent paragraphs in this section discuss simulation study

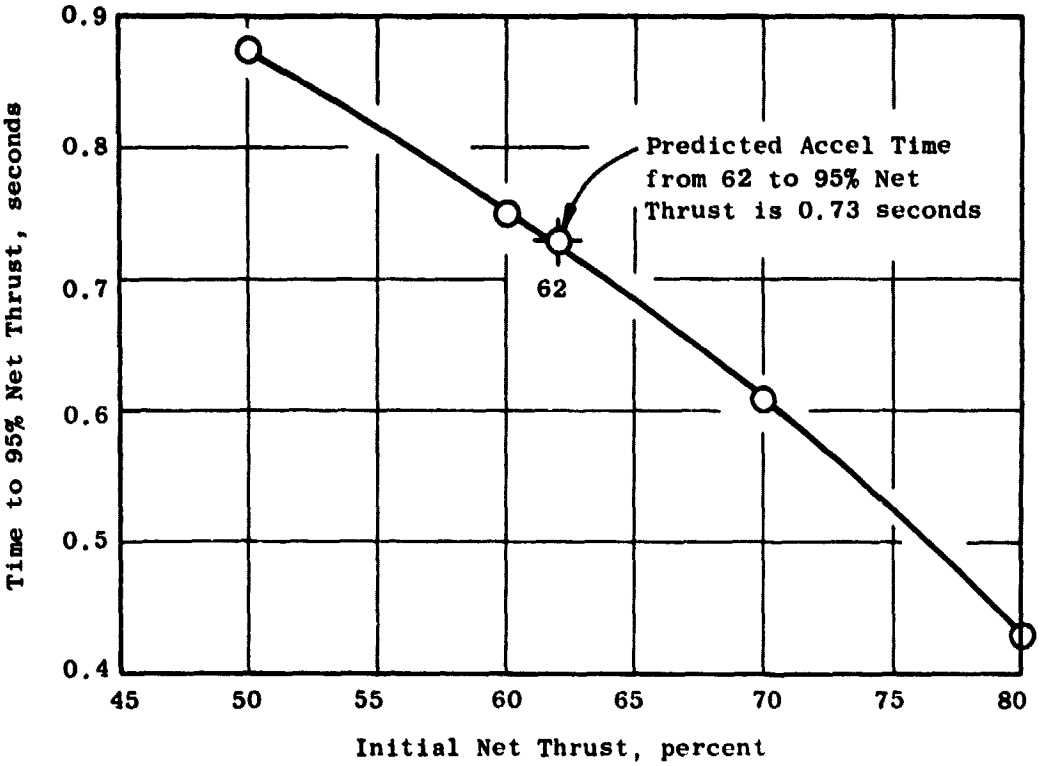

Figure 22. Final Prediction of Transient Response for Throttle Bursts to 100% Net Thrust at Sea Level, Static, Standard Day, Zero-Bleed Conditions.

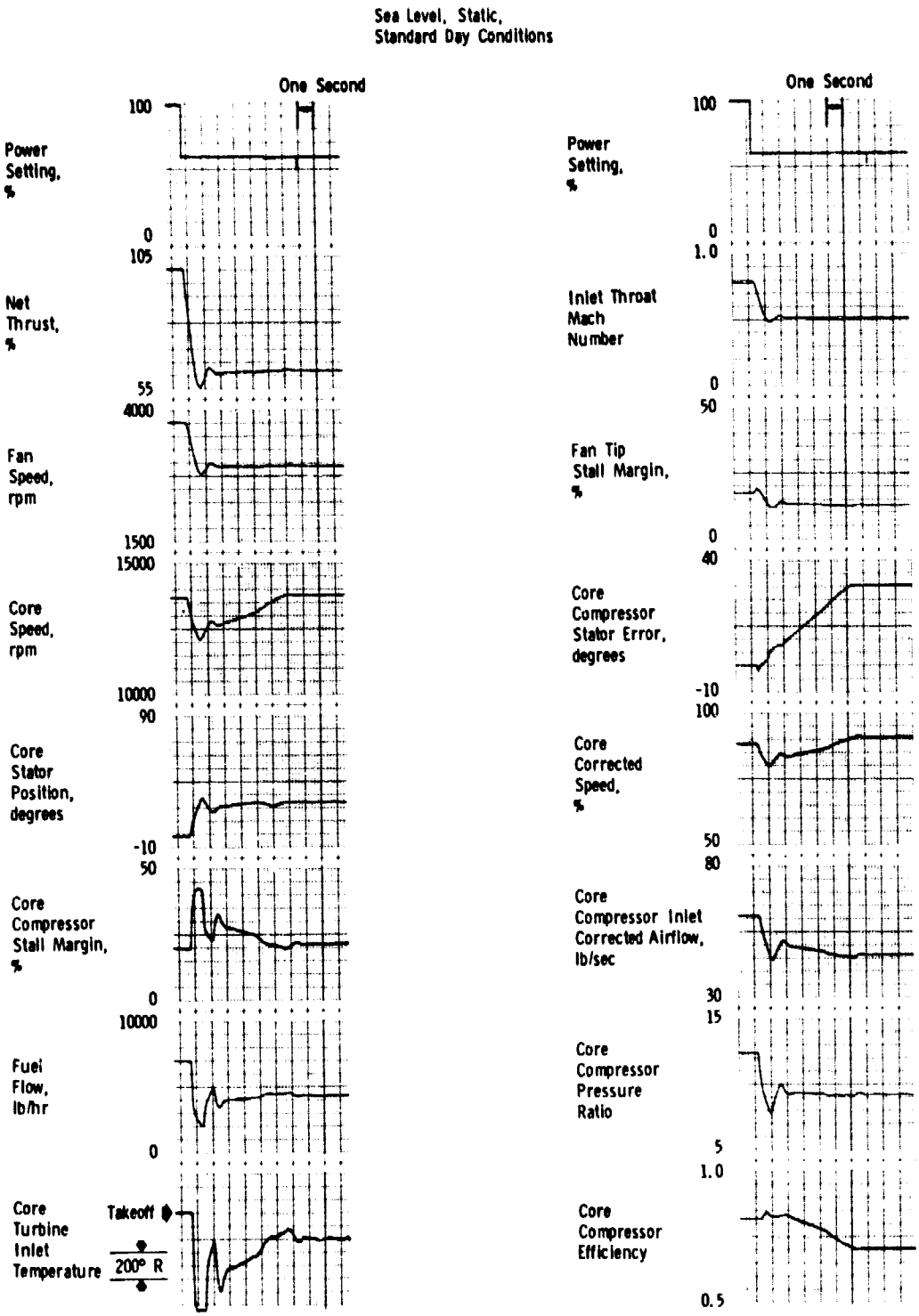

Figure 23. Throttle Chop from 100 to 62% Thrust using Linear Servovalve and Core Stator Reset.

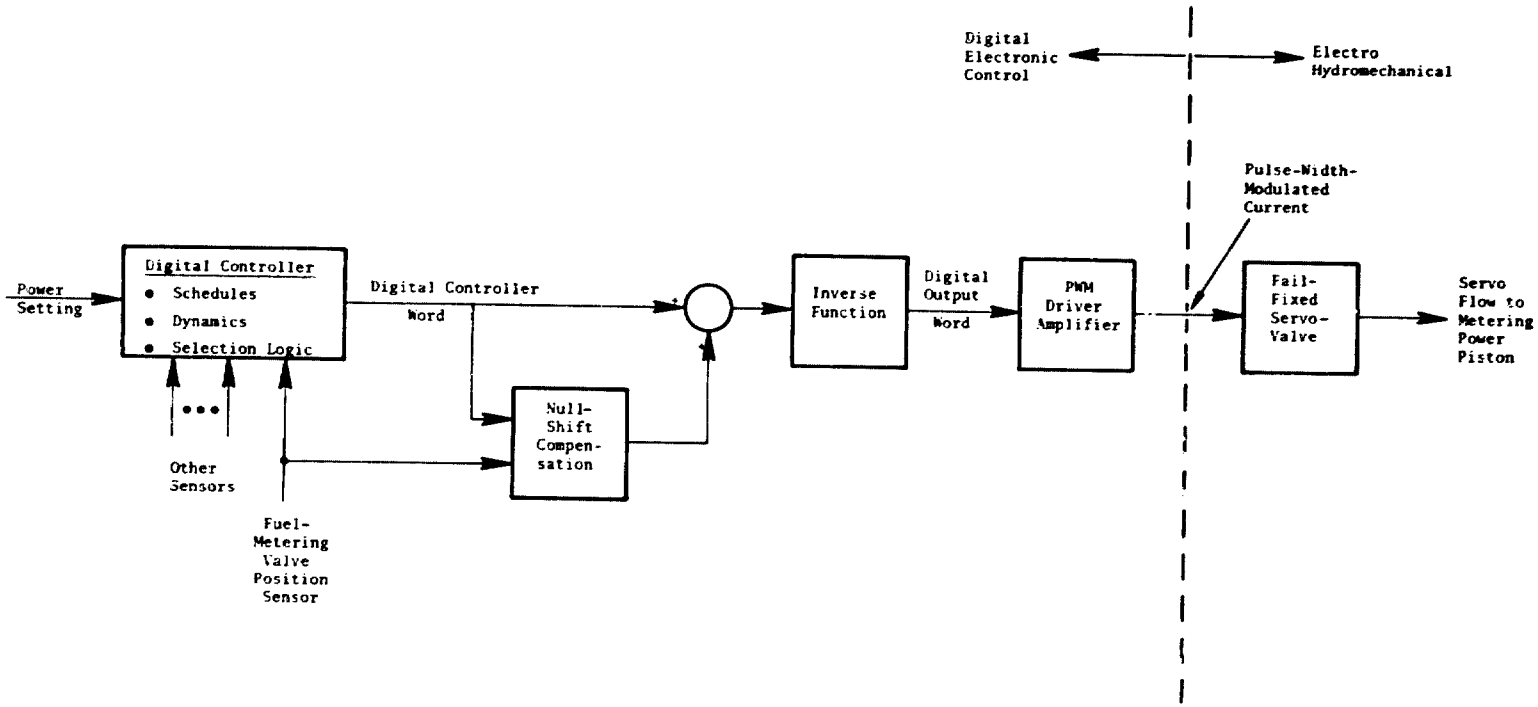

Figure 24. Functional Schematic Showing Location of Inverse Function and Null-Shift Compensation for Fail-Fixed Servovalve.

results which ultimately led to the above compensation logic design. Both unipolar and bipolar PWM driver amplifiers were considered in this study.

The initial study of the fail-fixed servovalve used the characteristics of the unipolar-pulse-driver amplifier because it yields better resolution from percent digital word to servoflow. An inverse function was developed to compensate for the dead zone and to provide characteristics equivalent to a linear servovalve from percent digital control word to servovalve flow. The control will not perform properly without this compensation because of the large dead zone and the use of rate feedback to provide the control-loop integration. For example, at steady-state conditions, the rate feedback could be zero and the fan-speed error too small to overcome the dead zone.

The effect of perfect compensation for the dead zone on a throttle chop to approach power and a burst back to takeoff power is shown in Figures 25 and 26. The effect of having the inverse overcompensated for the dead zone is shown in Figure 27 where the compensation is 10% greater than the dead zone. This produces a step in the digital-control-word/servoflow relationship resulting in a very high gain at null and sustained fuel flow oscillations at takeoff. Thus, any dead-zone compensation must be sized for the minimum expected dead zone.

When the maximum null shift (±5% of digital output word) for a unipolar pulse was used with the dead-zone compensation, the control would not perform approach-power transients. Depending on the polarity of the null shift, the control could either decelerate to 62% takeoff thrust or accelerate back to takeoff thrust, but not both. This was due to the effect of the dead-zone compensation which created a dead zone on one side of null and a vertical step on the other side of null. This is illustrated in Figure 28 for a maximum, positive, null shift. Because of the dead zone, the vertical step does not produce an oscillatory system. However, the dead zone prevents transients requiring the same polarity of servoflow as the dead zone.

To improve the performance with null shift, the unipolar-pulse-driver amplifier was replaced with the bipolar-pulse-driver amplifier which has a maximum null shift of ±1% of the digital output word. The effect of no dead-zone compensation on a chop to approach power and a burst back to takeoff power is shown in Figures 29 and 30. Note the large inaccuracy in thrust at approach, 41% instead of 62% of takeoff thrust. This is due to the large dead zone and the use of rate feedback to provide the integration of the control. Since the system has reached steady state, the rate feedback is zero and the error in fan speed is not large enough to overcome the dead zone. A similar result is seen when an attempt is made to accelerate back to takeoff power with the engine stopping at 62% of takeoff thrust.

To provide better accuracy with null shift, a compensation method was developed which should not appreciably affect transient operation. The method uses the difference of expected and sensed metering-valve rates to drive a low-gain integrator; the output is added with the digital control

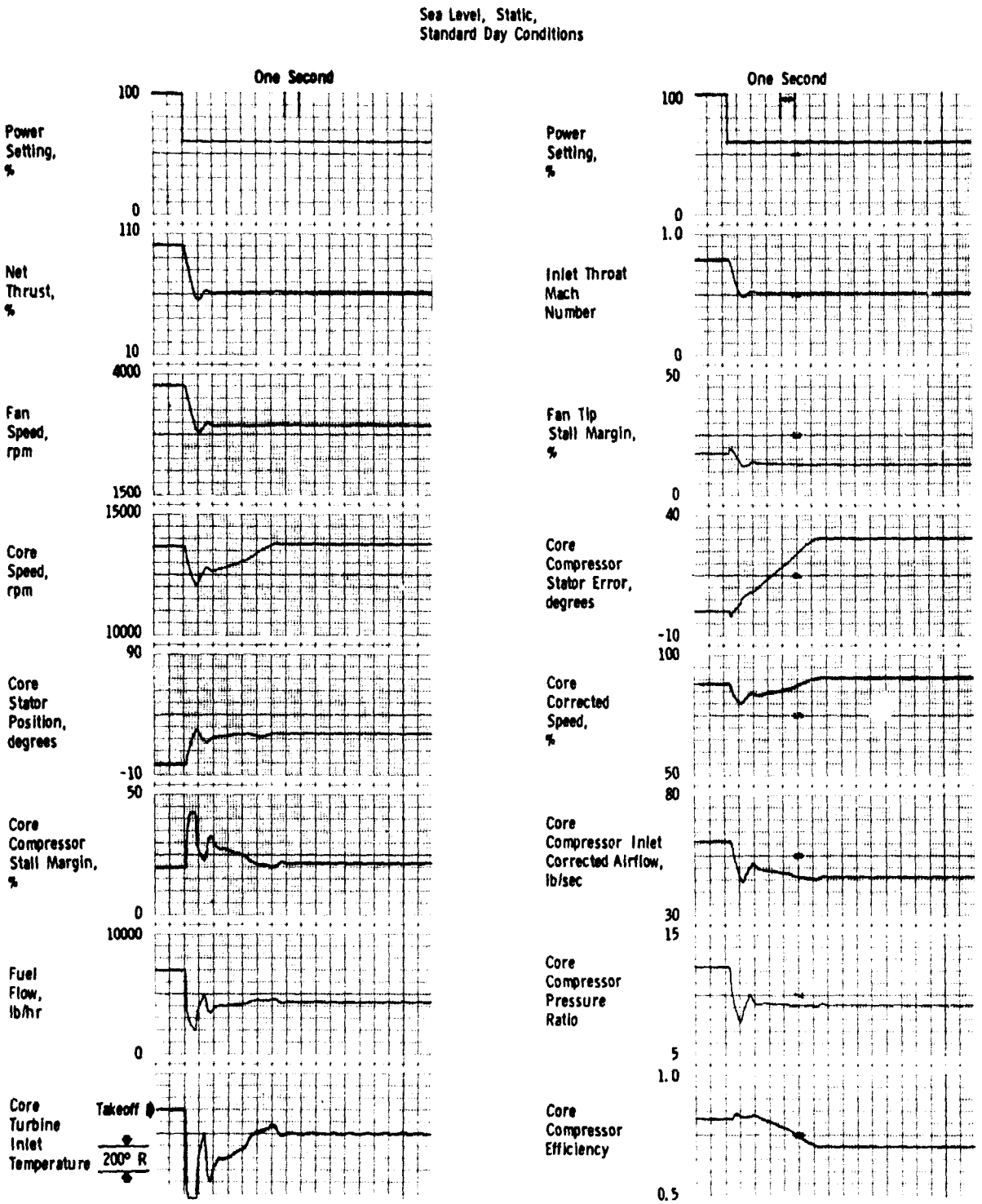

Figure 25. Throttle Chop from 100 to 62% Thrust using Fail-Fixed Servovalve with Perfect Dead-Zone Compensation.

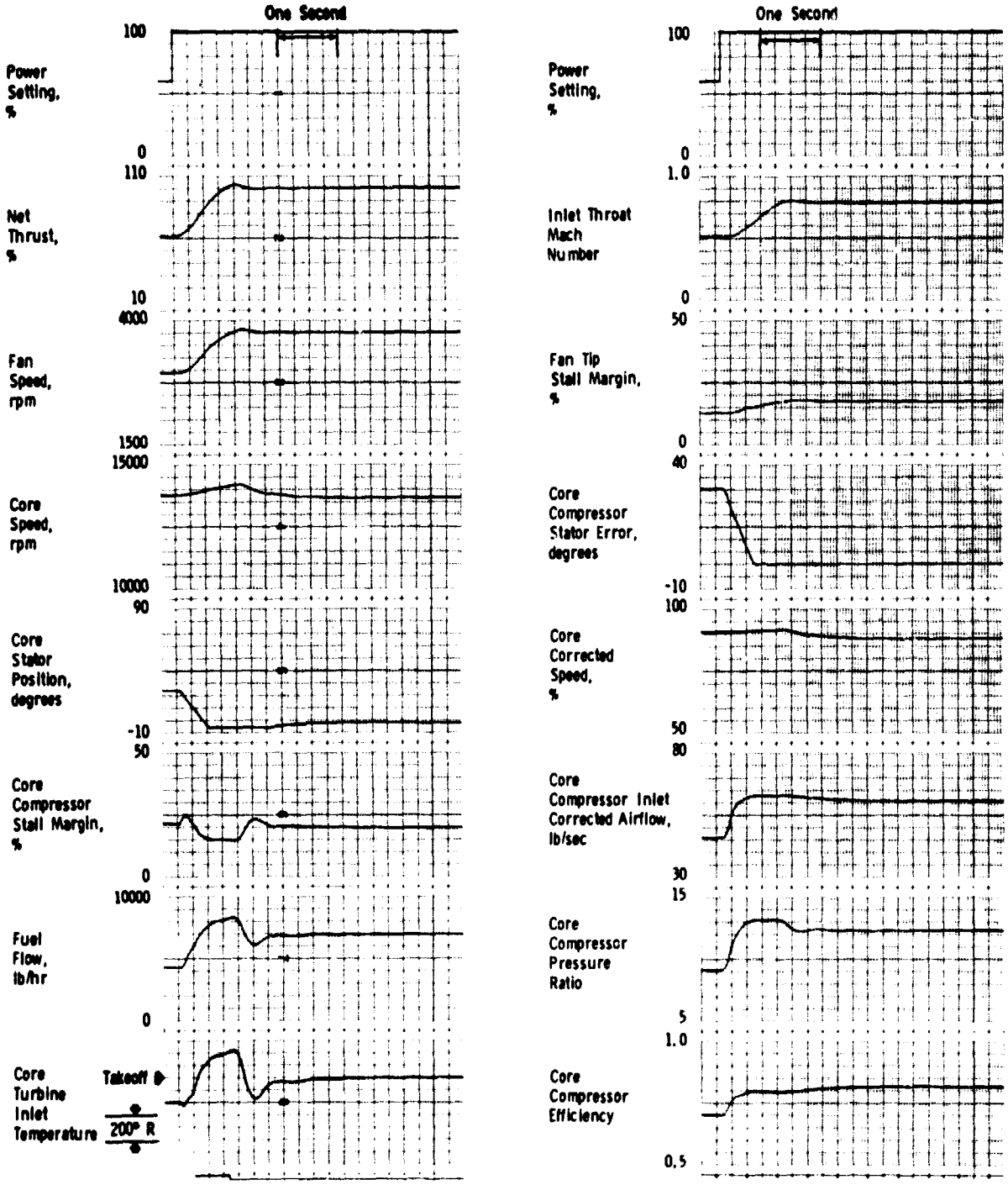

Figure 26. Throttle Burst from 62 to 100% Thrust using Fail-Fixed Servovalve with Perfect Dead-Zone Compensation.

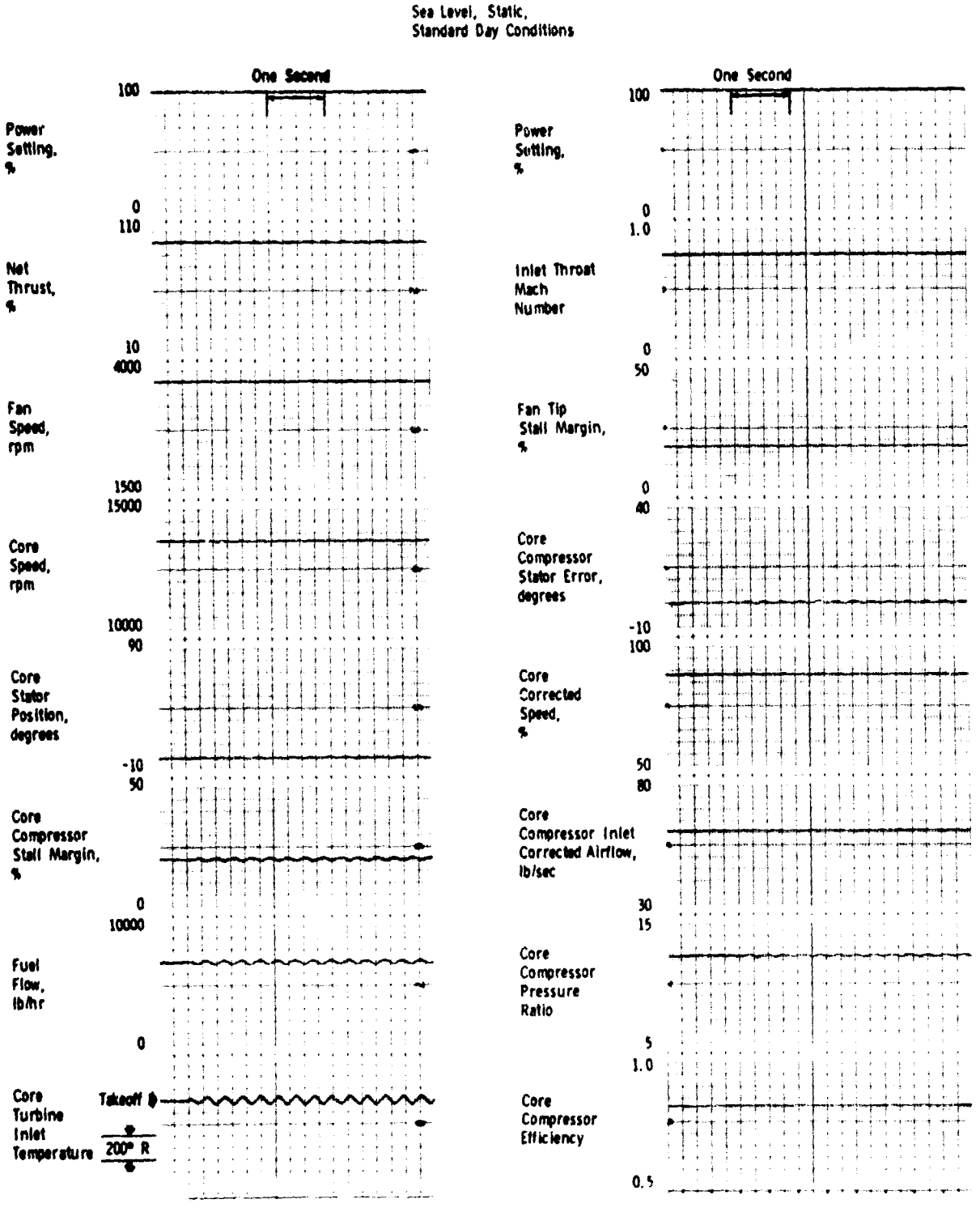

Figure 27. Takeoff Thrust using Fail-Fixed Servovalve with Dead-Zone Compensation 10% High.

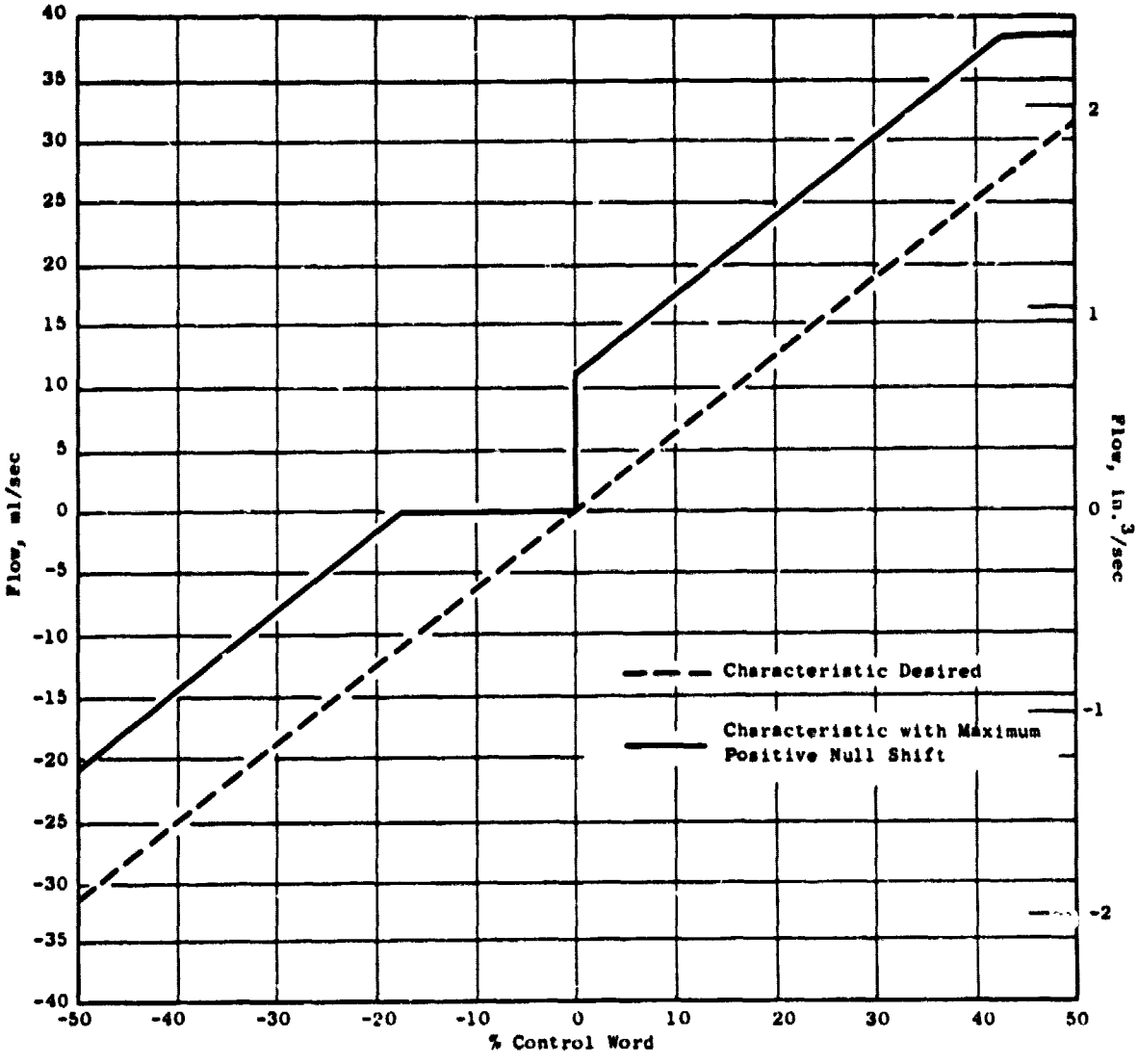

Figure 28. Effect of Null Shift on Simulation of Overall Fail-Fixed Servovalve Characteristics.

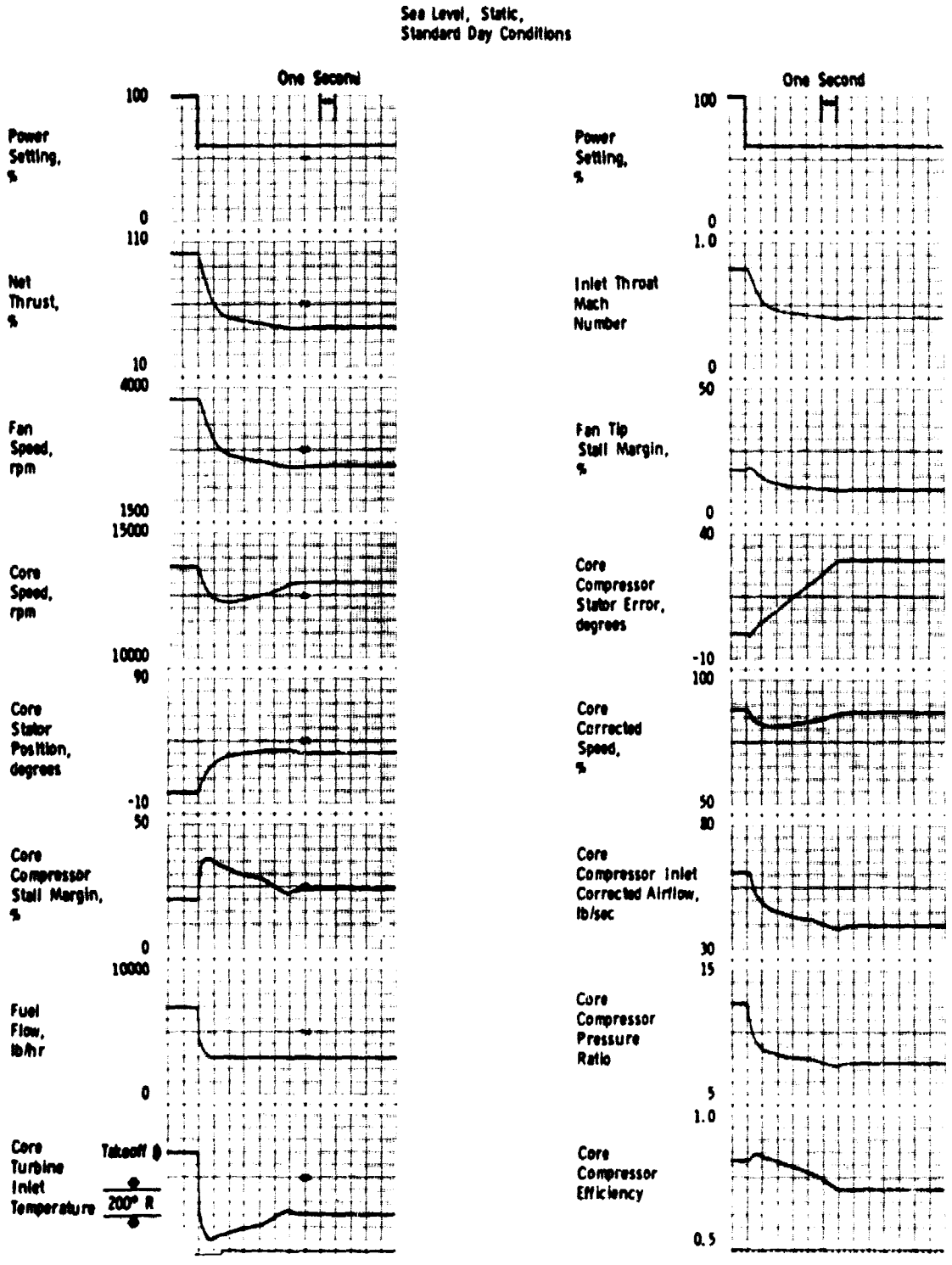

Figure 29. Throttle Chop to 62% Power Setting using Bipolar-Pulse, Fail-Fixed Servovalve with No Dead-Zone Compensation.

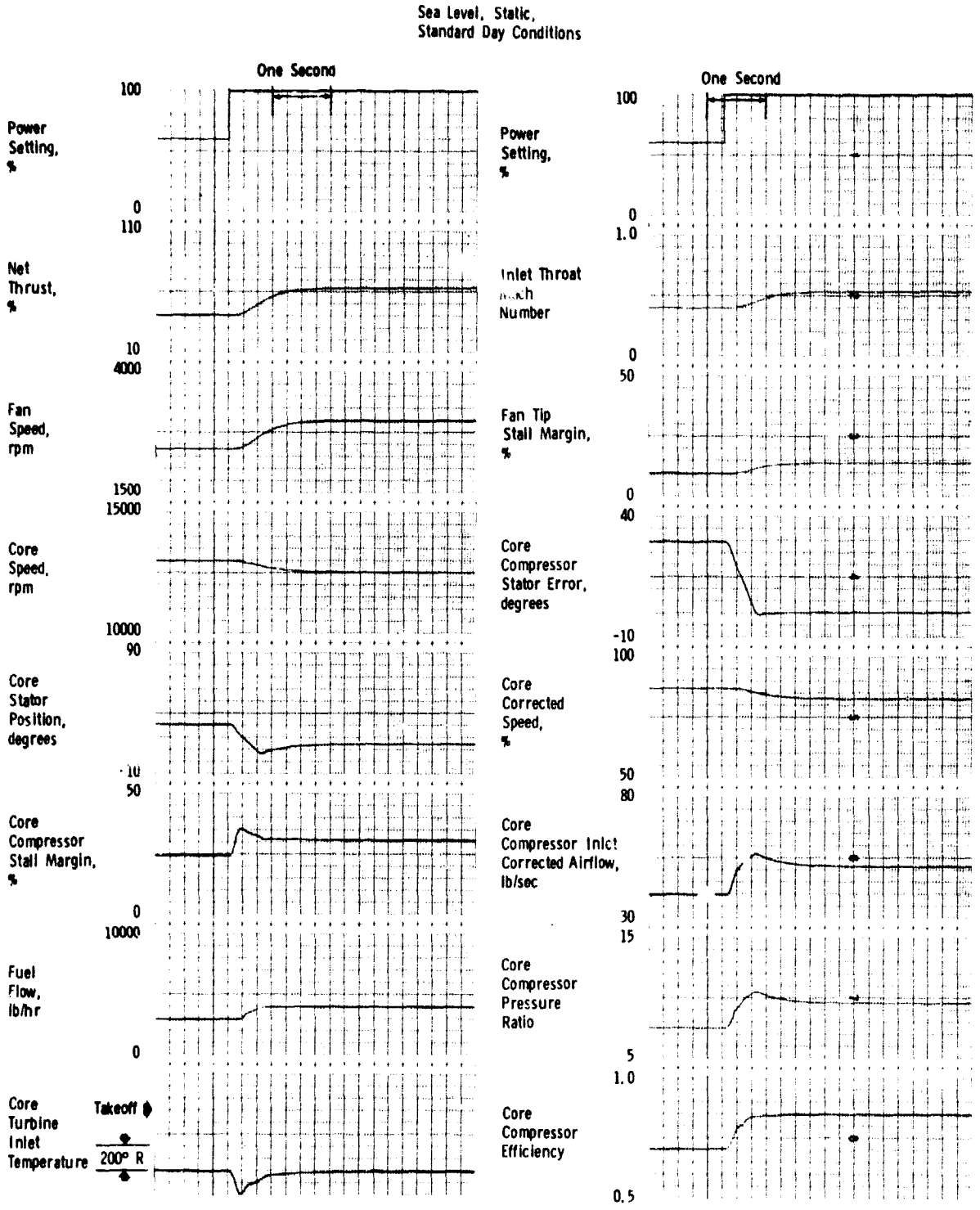

Figure 30. Throttle Burst to Takeoff Power Setting using Bipolar-Pulse, Fail-Fixed Servovalve with No Dead-Zone Compensation.

word to counteract the null shift. If the expected rate gain (KER) and expected rate lag (τER) exactly match the hardware, there will be no transient effect once the null-shift compensation has settled out. The low integrator gain (KDC) reduces the transient effect of the compensation if transients are initiated before it has settled or if the hardware is not perfectly matched. If the dynamics used to generate the expected rate are well tuned to the hardware, the compensation will respond to a null shift as a lag with time constant approximately equal to KFF/(KER × KDC). See block diagrams in Appendix A which contain the above gain- and time-constant symbols.

The specification for the fail-fixed servovalve portion of the control was developed from the above results. This specification includes an adjustment for dead-zone compensation; the adjustment (see Appendix A) will be used to "tune out" any dead zone during the control system bench tests prior to control delivery to the engine. Since the servovalve characteristics are symmetric and linear with respect to effective current in the operating range, the inverse function, referred to as f(DIFFS) in Appendix A, will be used to linearize effective current with respect to the digital control word. This should make the servovalve characteristic linear with respect to the digital control word in the operating range.

The block diagram in Appendix A shows that the digital control logic has been designed to connect either to a fail-fixed servovalve or to a linear servovalve. The capability to test the digital electronic control with each of these two valve types was a control system requirement. Thus, when the servovalve type is changed from fail fixed to linear or vice versa, a rebuild of the digital control memory is not required, and testing can proceed with little or no delay.

6.3 FICA SIMULATION RESULTS

To evaluate the stability and response of failure detection and correction, it has been simulated on one hybrid computer; an accurate, nonlinear, cycle-balance simulation of the QCSEE and nonlinear control system was on a second hybrid computer. The failure detection and correction was connected between the sensor simulation and the controls simulation. In this manner the performance of the system, as it would operate the actual engine, could be predicted.

The development work on the hybrid simulation showed that the model could be simplified to eliminate the states representing heat soak. Also, the work showed that sensors not otherwise needed could be eliminated; that is, no extra sensors are needed for the system.

The typical results obtained are shown in Figures 31, 32, and 33 in which the power demand to the controls is stepped between 70 percent of takeoff and takeoff power. The response shown in Figure 31 is for the system with all sensors functioning and with the failure detection and correction functioning. The simulation showed the Kalman filter tracked

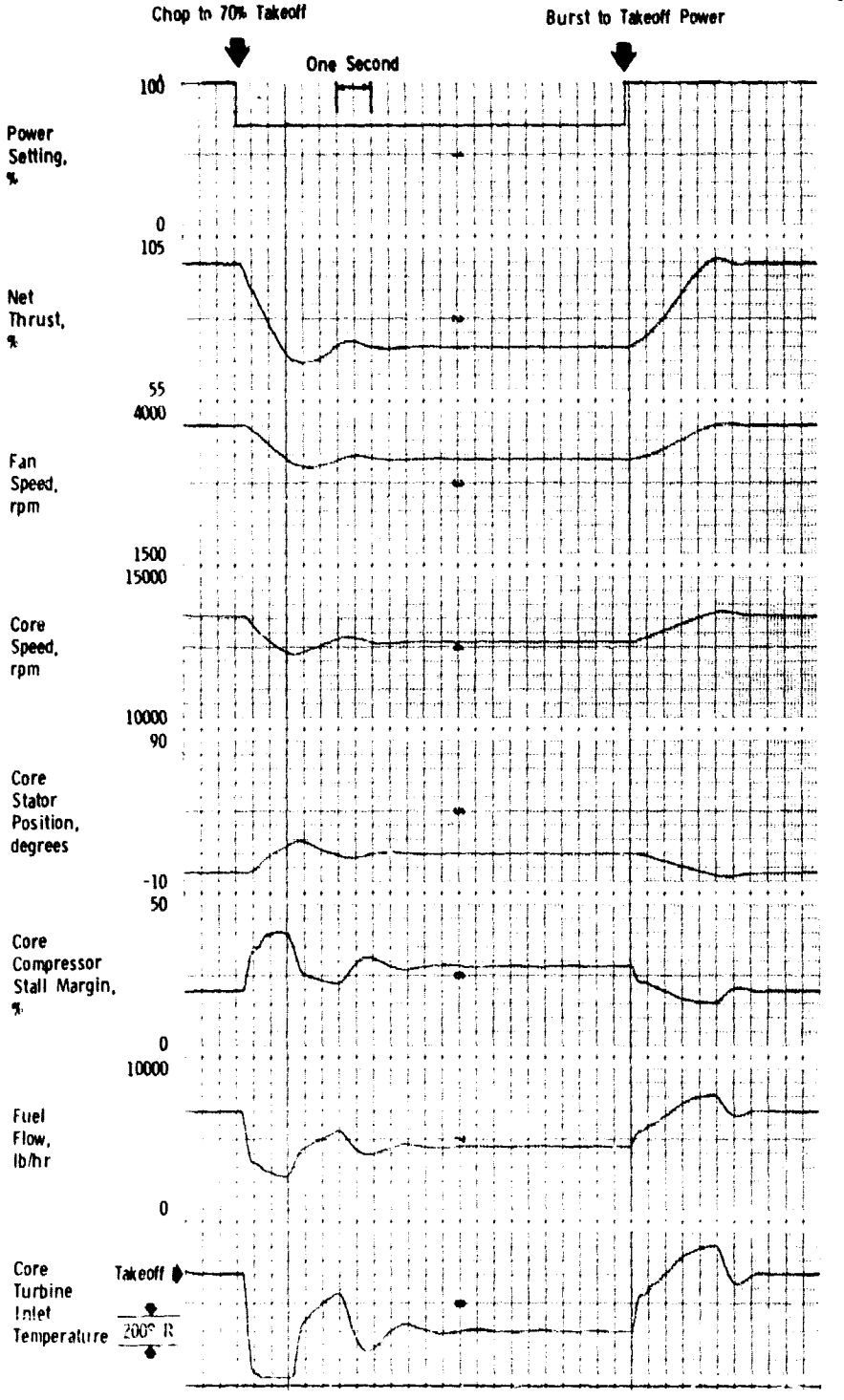

Figure 31. Computer Trace with All Sensors Functioning.

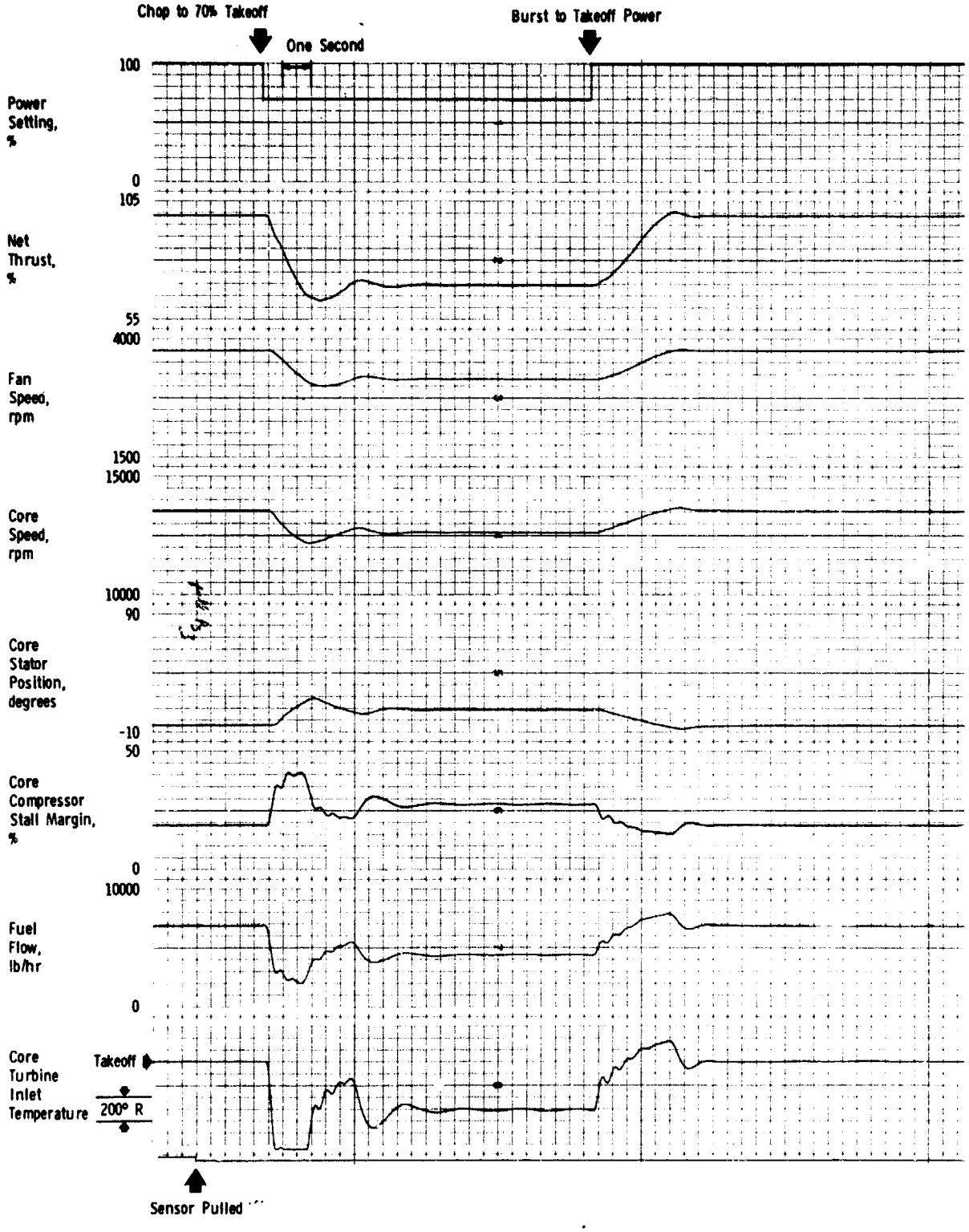

Figure 32. Computer Trace with PS3 Sensor Pulled.

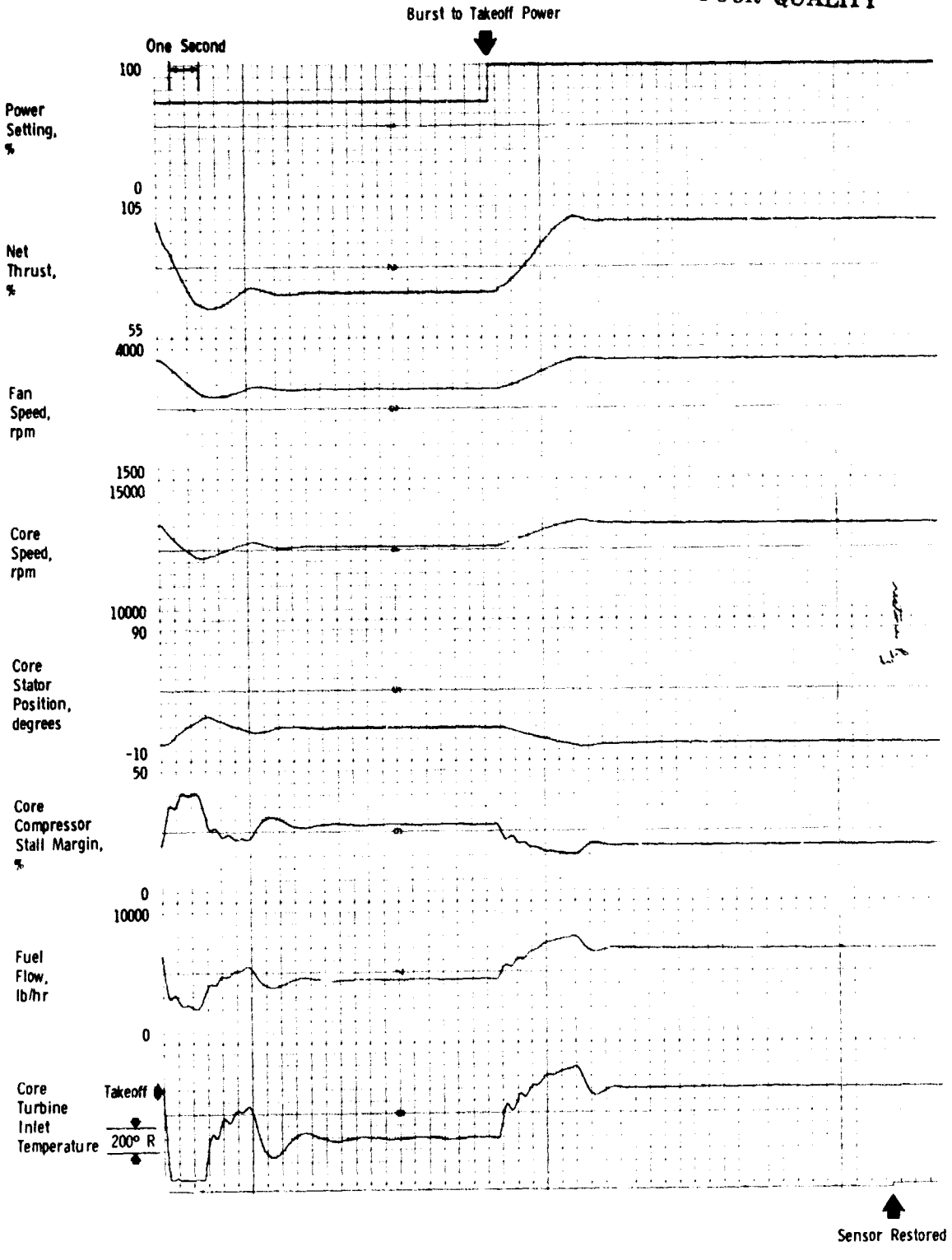

Figure 32. Computer Trace with PS3 Sensor Pulled (Concluded).

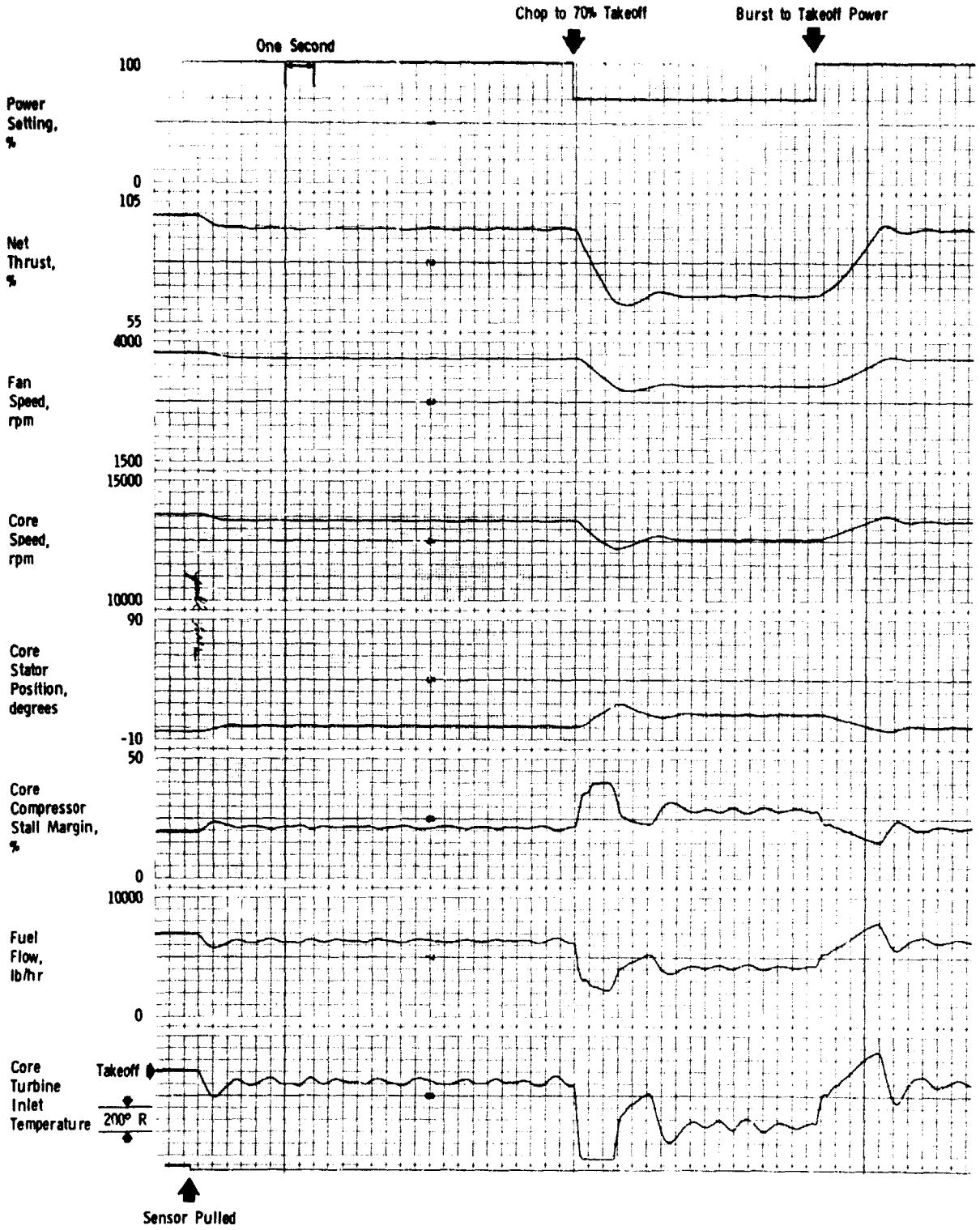

Figure 33. Computer Trace with XNL Sensor Pulled.

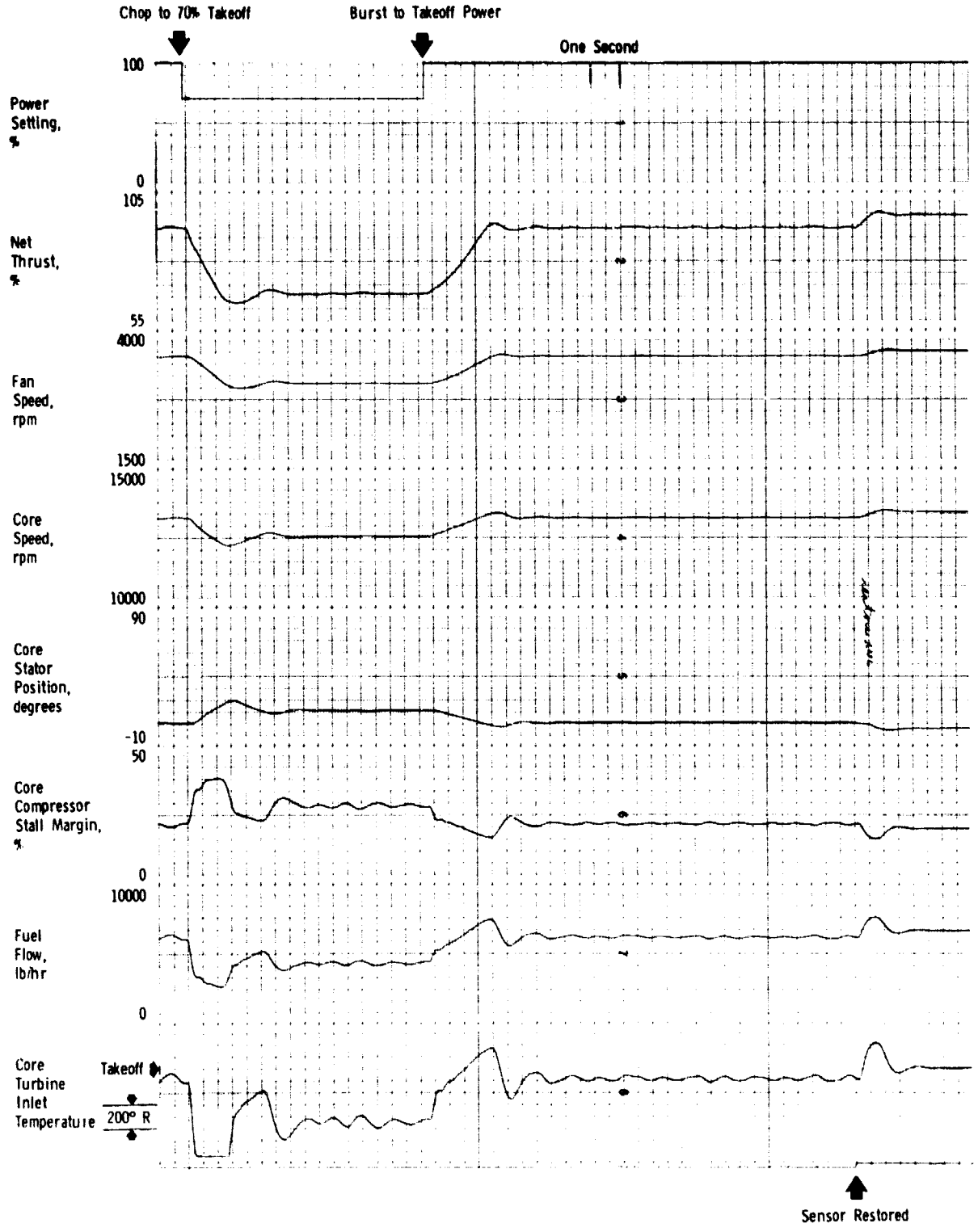

Figure 33. Computer Trace with XNL Sensor Pulled (Concluded).

the accurate simulation so that at no point in the transient did any sensor errors exceed the tolerances. This latter is indicated by the event trace in the margin next to the core turbine inlet temperature. When this trace steps outward, one or more sensors are indicated as failed.

The traces in Figures 32, 33, and 34 show PS3, NL, and NH pulled (failed) separately. When PS3 is pulled at takeoff power there is no shift in the operating point, but there is a change in the transient response. The explanation for this is: PS3 is the primary variable for transient fuel flow scheduling, but it is not used for steady-state control. With NL pulled there is a slight shift in the operating point, and the settling transient is changed because this is a controlled variable at takeoff power and 70 percent of takeoff power. With NH pulled the speed input to the transient fuel scheduling and the compressor variable stator control are estimated. As a result there is a small shift in the core stator position.

The on-engine digital control computer has a 12-bit word with double-precision capability. The hybrid computer has a 16-bit word with double-precision capability, but software is used to mask the least significant bits to simulate the digital computer controller 12-bit word. Comparisons have been made of the accuracy (as indicated by the shift set point with a sensor pulled) and steady-state hunting with a sensor pulled. The results indicate that there is a substantial improvement in the hunting with a 16-bit computation. This hunting is shown most strongly in the core turbine inlet temperature channel as is shown in Figures 33 and 35. The former is with a simulated 12-bit control computer and the latter is with a 16-bit control computer, and both are with the XNL sensor pulled. These two traces indicate that there is no significant difference in accuracy or stability to disturbances.

It can be seen from the figures that good engine control is maintained while the transient is altered for failed sensors. A fixed-gain feedback matrix has been used which shows that it is not necessary to supply a separate feedback matrix for each sensor failure and each power range for the engine. Although not shown in the computer traces included herein, multiple sensor failures have been demonstrated in which chop and burst transients have been controlled adequately. This further demonstrates the advantage of the extended Kalman-filter technique in which a fixed-gain-feedback matrix is satisfactory for a wide range of conditions.

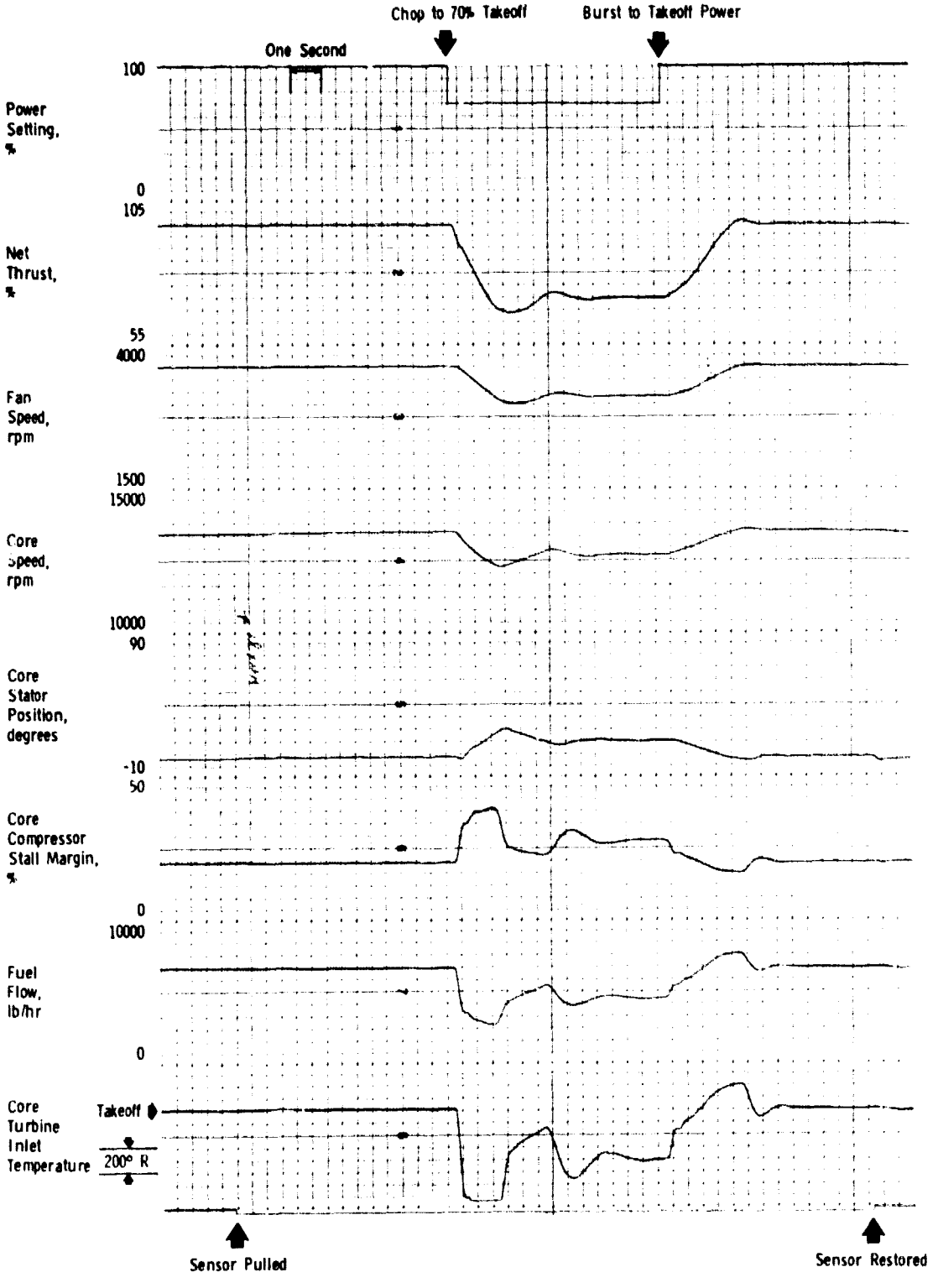

Figure 34. Computer Trace with XNH Sensor Pulled.

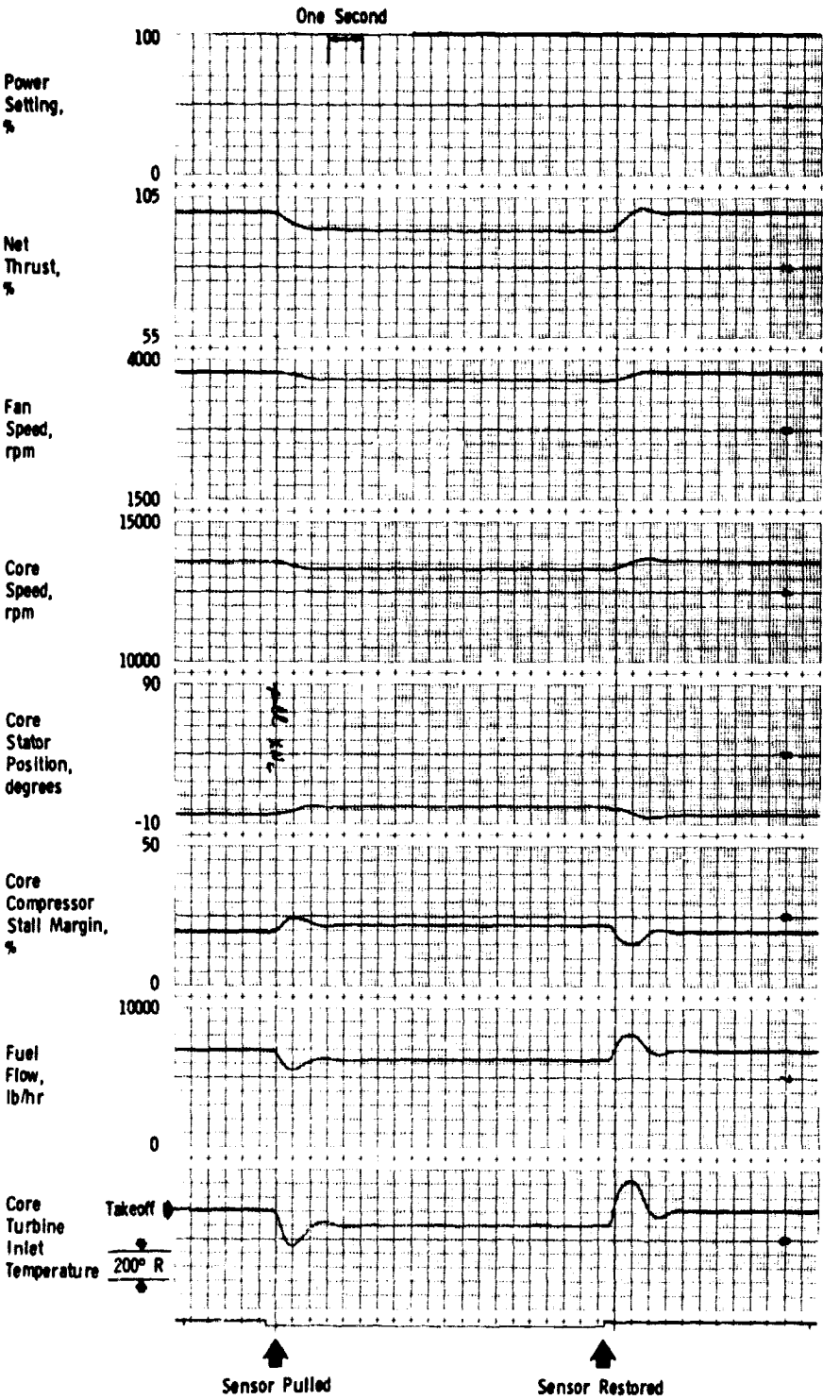

Figure 35. Computer Trace with XNL Sensor Pulled and with 16-Bit Control Computer Simulated.

7.0 SUMMARY OF RESULTS

A hybrid simulation of the OTW experimental engine has been constructed and used to develop the control system dynamic design. The engine simulation was based on the digital cycle deck used to generate the QCSEE preliminary technical requirements. Simulation results for throttle bursts from 62 to 100% takeoff thrust predict that the experimental engine will meet the dynamic requirement of 62 to 95% takeoff thrust in one second. Results for transient stall margins, temperature, and inlet Mach number indicate that safe engine operation will be maintained during this engine transient. Transient results also predict safe deceleration capability during throttle chops. Throttle chops with core stator reset are much slower than without reset to ensure safe operation of the fan.

Simulation results indicate that operation of the digital control with the fail-fixed servovalve can be designed to meet the accuracy and fast-response objectives for the OTW experimental engine.

Simulation of the Failure Identification and Corrective Action (FICA) strategy has demonstrated that the strategy built around an extended Kalman filter should meet the objectives. Based on the simulation results, the FICA will track sea level bursts and chops without giving a false indication of sensor failure. Also, based on the simulation results, the FICA will maintain good engine control for sea level bursts and chops with the single failure of an engine sensor.

APPENDIX A

DETAILED BLOCK DIAGRAMS AND SCHEDULE/DYNAMIC SPECIFICATIONS FOR OTW DIGITAL FUEL CONTROL

Included in this appendix are the block diagrams (Figures 36, 37 and 38) and the specifications for gains, time constants, schedules, and limits for the digital fuel control which is to be used on the first build of the OTW experimental engine (Tables II through VII).

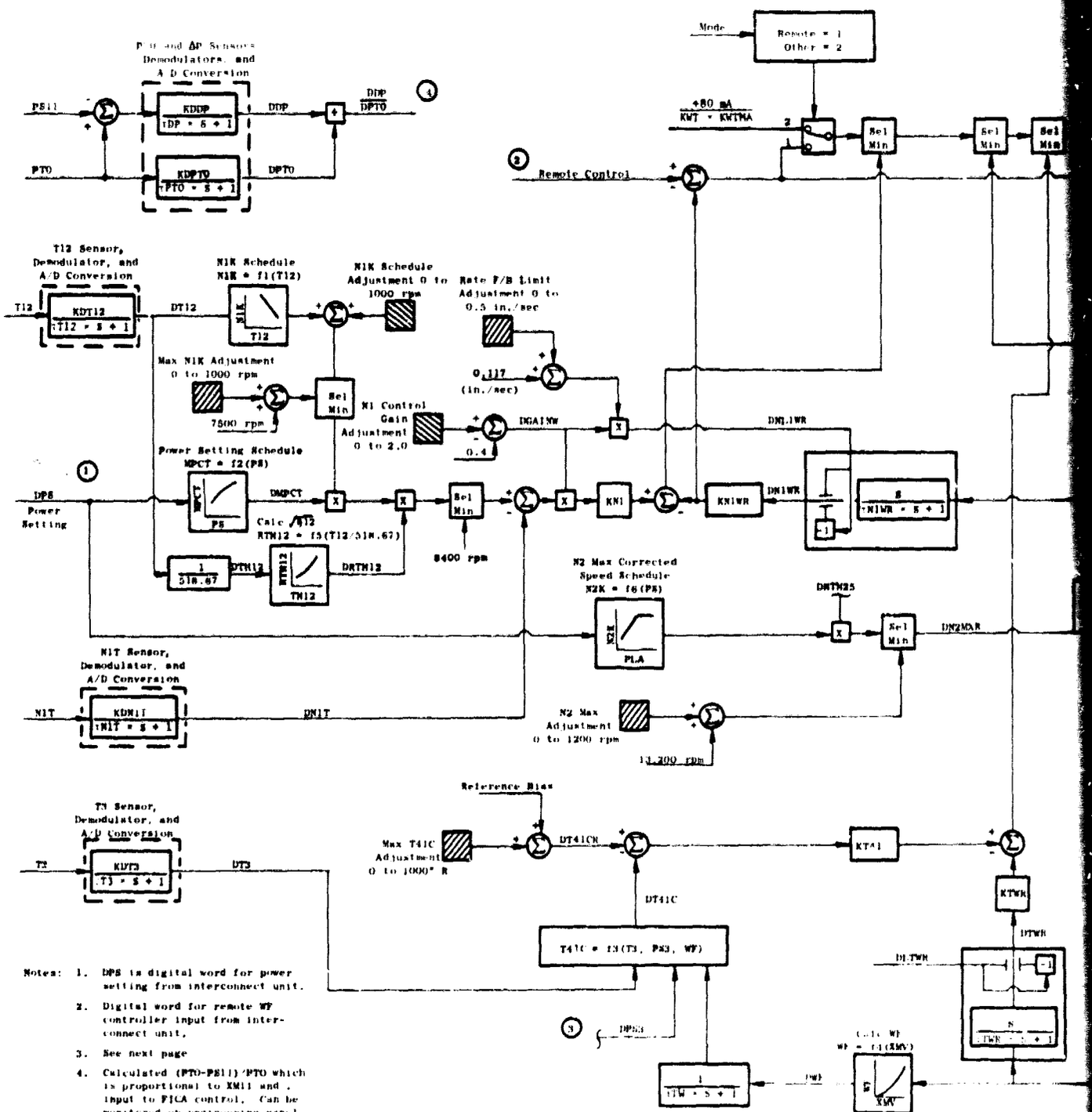

Figure 36. QCSEE OTW Digital Fuel Control Block Dia

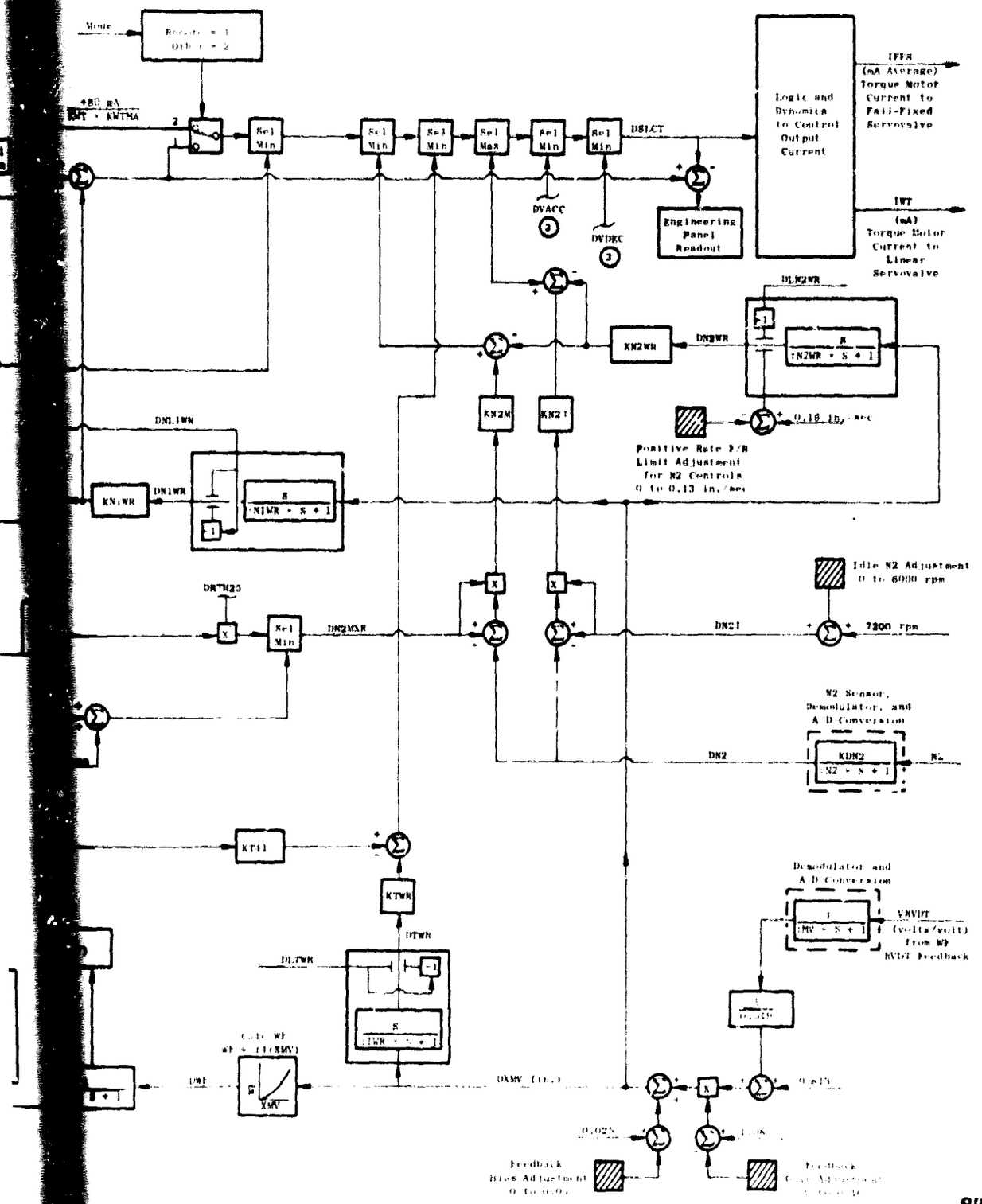

Digital Fuel Control Block Diagram.

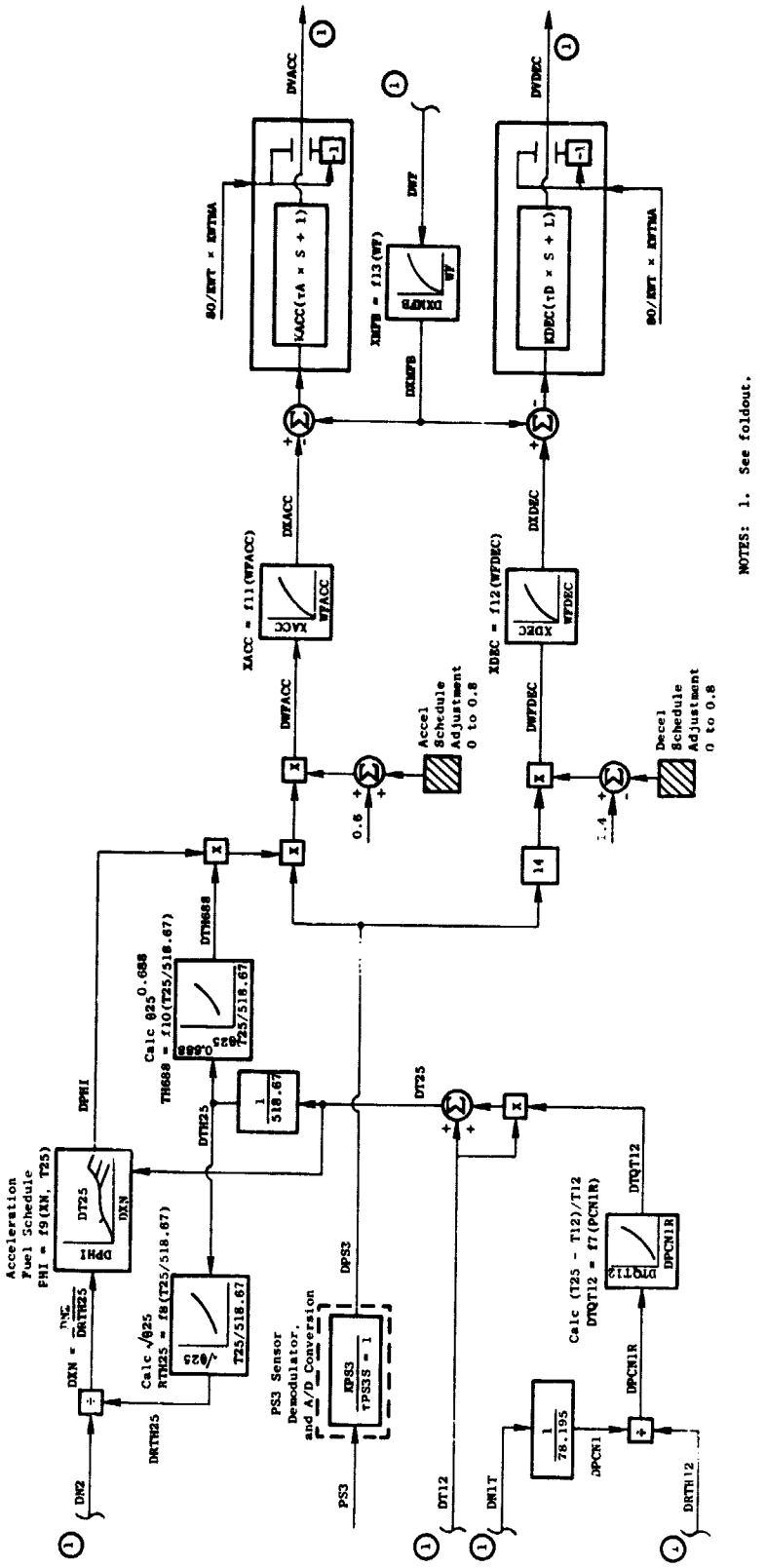

NOTES: 1. See foldout.

Figure 36. QCSEE OTW Digital Fuel Control Block Diagram (Continued).

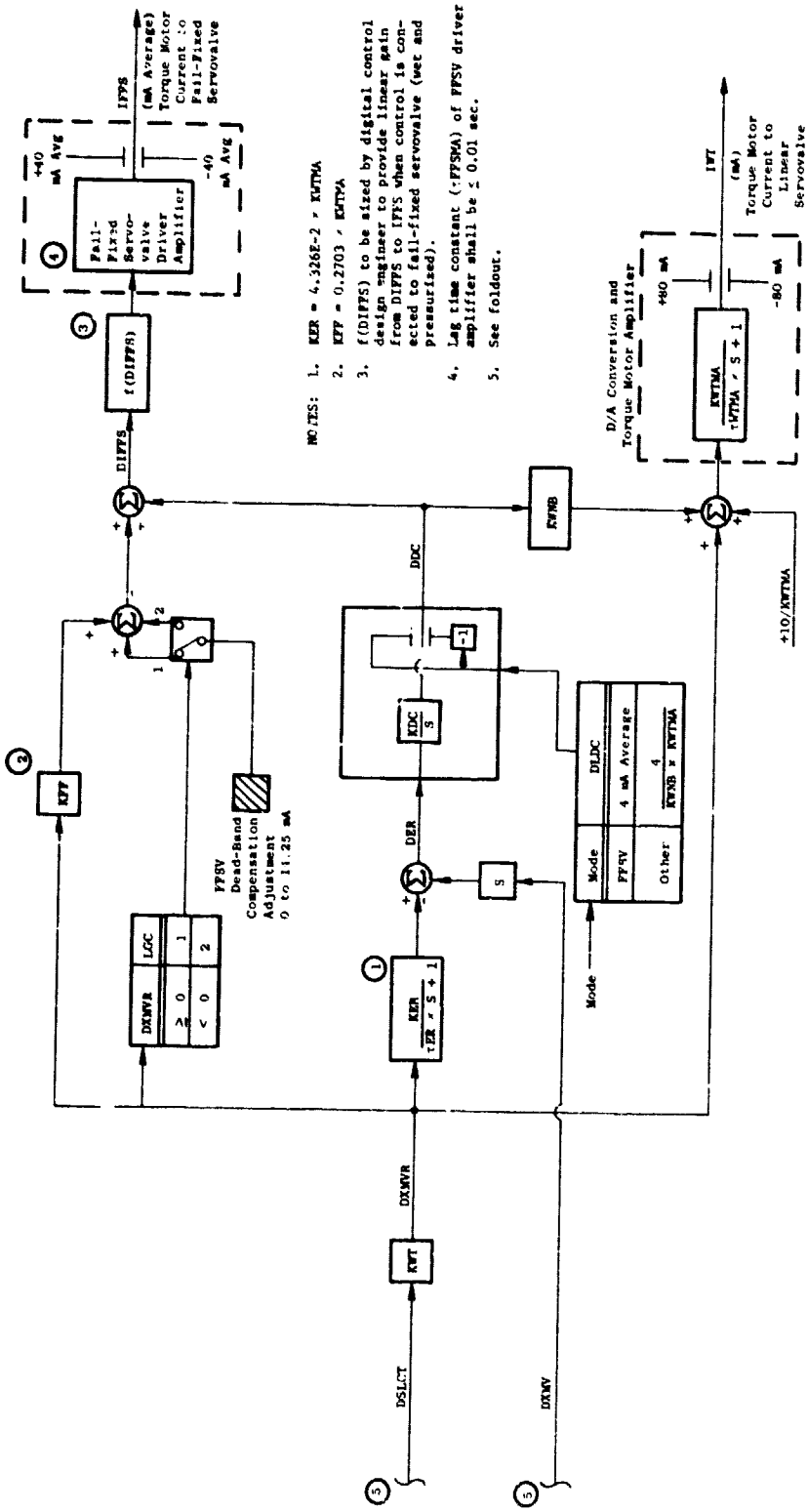

Figure 36. QCSEE OTW Digital Fuel Control Block Diagram (Concluded).

ORIGINAL PAGE IS
OF POOR QUALITY

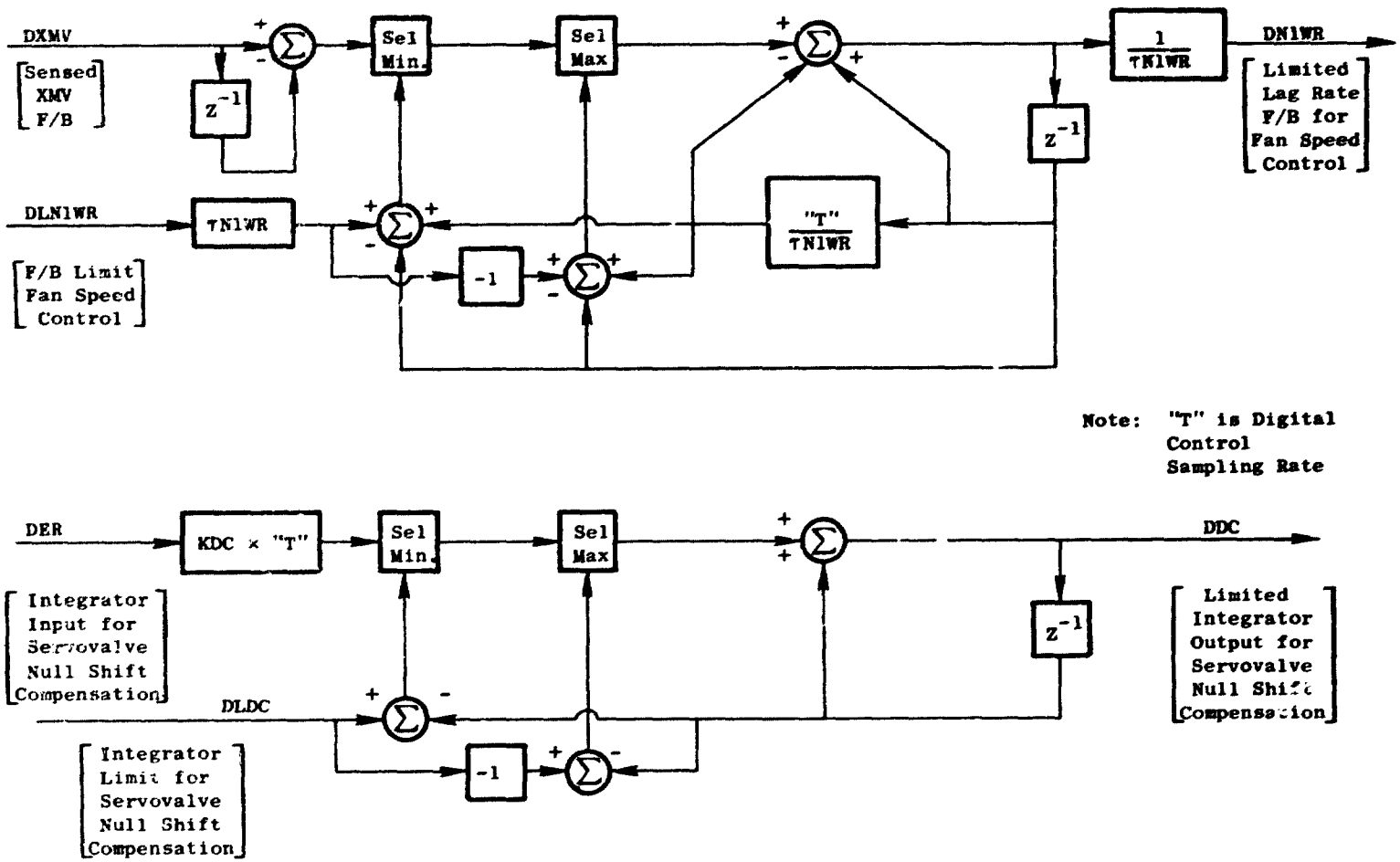

Figure 37. QCSEE OTW Digital Fuel Control Block Diagram for Lag-Rate Feedback with Rate Limit in N1 Control and Integrator with Limit for Servovalve Null-Shift Compensation.

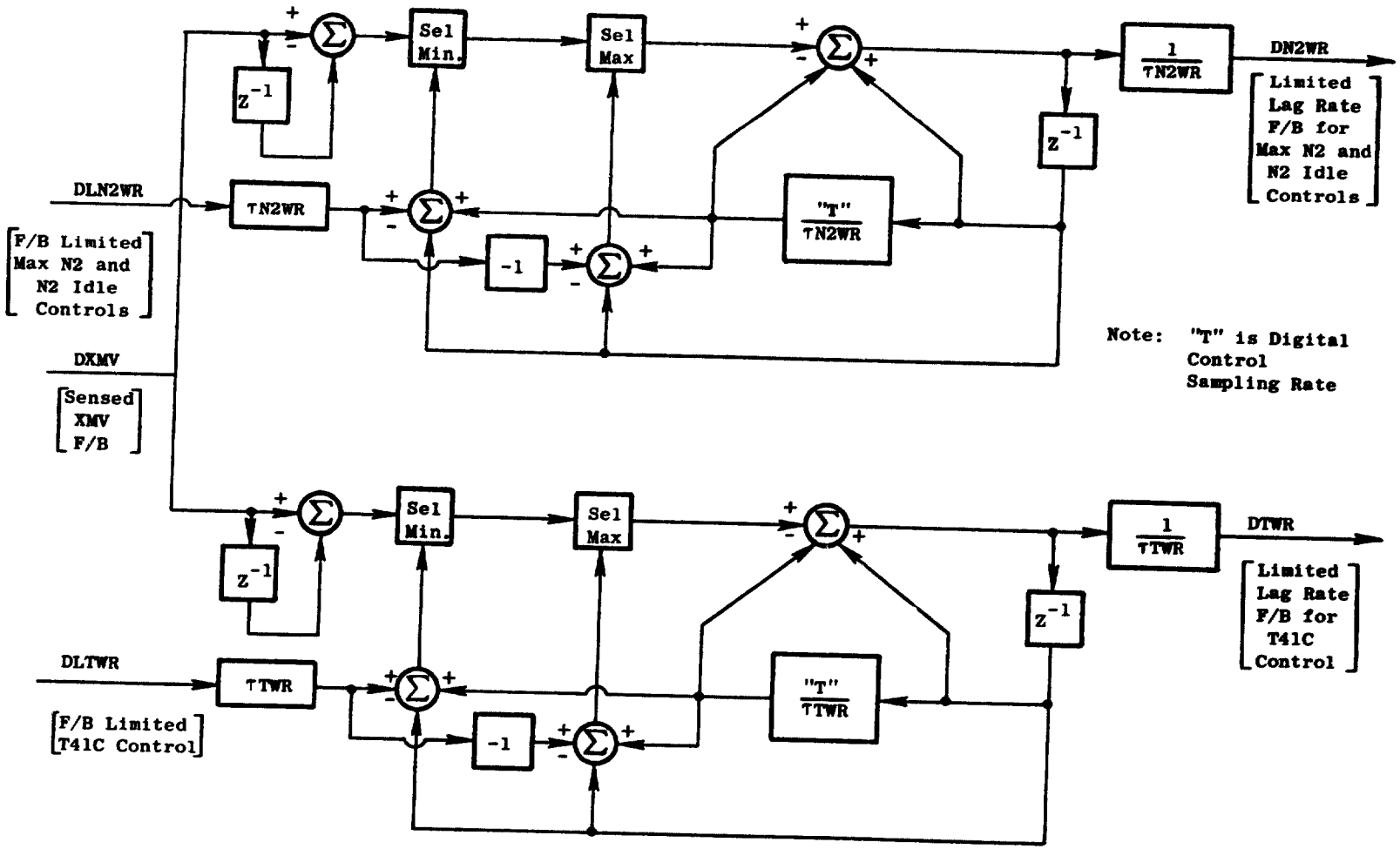

Figure 38. QCSEE OTW Digital Fuel Control Block Diagram for Lag-Rate Feedback with Rate Limits in N2 Max, N2 Idle, and T41C.

Table II. QCSEE OTW Digital Fuel Control Digital Gains.

	Gain	Per
KDN1T × KN1 × KWT × KWTMA	0.1225 mA	rpm
KN1WR × KWT × KWTMA	4.173 mA	m/sec
	164.3 mA	in./sec
KT41 × KWT × KWTMA	0.2919 μA	K
	0.5254 μA	°R
KTWR × KWT × KWTMA	0.8344 mA	m/sec
	32.85 mA	in./sec
KDN2 × KN2M × KWT × KWTMA	0.2967 μA (at DN2MXR = 13,200 rpm)	rpm
KDN2 × KN2I × KWT × KWTMA	0.1618 μA (at DN2I = 7200 rpm)	rpm
KN2WR × KWT × KWTMA	4.173 mA	m/sec
	164.3 mA	in./sec
KACC × KWT × KWTMA	10.3 mA	m
	405.7 mA	in.
KDEC × KWT × KWTMA	10.3 mA	m
	405.7 mA	in.
KDC × KWNB × KWTMA	9.86 mA	cm/sec
	3.881 mA	in./sec
KDC (Average)	2.66 mA	cm/sec
	1.049 mA	in./sec

Table III. QCSEE OTW Digital Fuel Control Digital Gain Distribution.

KWT × KWTMA	7.566
KDN1T × KN1	1.619×10^{-2}
KN1WR	21.709
KT41	6.9437×10^{-3}
KTWR	4.3417
KDN2 × KN2M	3.9215×10^{-3} at DN2MXR = 13200 rpm
KDN2 × KN2I	2.1384×10^{-3} at DN2I = 7200 rpm
KN2WR	21.709
KACC = KDEC	53.62

Note: The above digital-gain distribution is required for the lag-rate-feedback limits specified in table of digital constants.

Table IV. QCSEE OTW Digital Fuel Control Digital Scaling.

Symbol	Description	Range
DDP	Sensed [PTO - PS11]	0 to 82.7 kN/m^2 (0 to 12 psi)
DPTO	Sensed PTO	13.8 to 131.0 kN/m^2 (2 to 19 psia)
$\frac{DDP}{DPTO}$	Calculated [(PTO-PS11)/PTO]	0 to 0.6858
DT12	Sensed Fan Inlet Temperature	233 to 344 K (420 to 620° R)
DT3	Sensed Compressor Discharge Temperature	219 to 861 K (395 to 1550° R)
DT41C	Calculated HP Turbine Inlet Temperature	256 to 1922 K (460 to 3460° R)
DN1T	Sensed LP Turbine Speed	0 to 9595 rpm
DN2	Sensed Core Engine Speed	0 to 15492 rpm
DPS3	Sensed Compressor Discharge Pressure	0 to 2.07 MN/m^2 (0 to 300 psia)
DXMV	Sensed Metering Valve Position	0 to 2.065 cm (0 to 0.813 in.)

Table V. QCSEE OTW Digital Fuel Control Time Constants.

Frequency Range From 0.1 to 10.0 Hz

Symbol	Description	Value
τER	Inlet Lag in Servovalve Null-Shift Compenstation Circuit	0.075 sec
τN1WR	Rate-Feedback Lag in Fan Speed Control	0.50 sec
τN2WR	Rate-Feedback Lag in Max Core Speed and Idle Core Speed Controls	0.50 sec
τTWR	Rate-Feedback Lag in T41C Control	0.10 sec
τMV	WF RVDT Feedback Demodulator and A/D Converter Lag	$\leq$0.01 sec
τDP	(PTO-PS11) Sensor, Demodulator, and A/D Converter Lag	$\leq$0.02 sec
τPTO	PTO Sensor, Demodulator, and A/D Converter Lag	<0.50 sec
τT12	Fan Inlet Temperature Sensor, Demodulator, and A/D Converter	$\leq$6.00 sec at 48.83 kg/sec per m^2 (10 lb/sec per ft^2) Airflow Density
τN1T	LP Turbine Speed Sensor, Demodulator, and A/D Converter Lag	$\leq$0.01 sec
τN2	N2 Sensor, Demodulator, and A/D Converter Lag	$\leq$0.01 sec
τT3	T3 Thermocouple, Electrical Sensor Demodulator, and A/D Converter Lag	*
τPS3	PS3 Sensor, Demodulator, and A/D Converter Lag	$\leq$0.02 sec
τWTMA	D/A Converter and Torque Motor Driver Amplifier Lag	$\leq$0.01 sec
τFFSMA	Fail-Fixed Servovalue Driver Amplifier Lag	$\leq$0.01 sec

Table V. QCSEE OTW Digital Fuel Control Time Constants (Concluded).

Frequency Range From 0.1 to 10.0 Hz

Symbol	Description	Value
τA	Lead Time Constant in Accel Fuel-Flow Servoloop	0.05 sec
τD	Lead Time Constant in Decel Fuel-Flow Servoloop	0.05 sec
τTW	Lag Time Constant in Calculated WF Input to T41C Calculation	0.05 sec

* $\tau T3 = \tau(\text{Thermocouple}) + \tau(\text{Sensor, Demodulator, and A/D Converter Lag})$

$\tau(\text{Thermocouple}) = 0.952(W3/65.29)^{-1/2}$

$\tau(\text{Sensor, Demodulator, A/D}) \leq 0.02$ sec

Table VI. QCSEE OTW Digital Fuel Control Digital Constants.

Symbol	Description	Value
DLN2WR	WF Metering Valve Rate-Feedback Limit in Max and Idle N2 Speed Controls	0.3175 cm/sec (0.125 in./sec)
DLTWR	WF Metering Valve Rate-Feedback Limit in T41C Control	0.366 cm/sec (0.144 in./sec)

Table VII. QCSEE OTW Digital Fuel Control Schedules and Functions.

1. Corrected Fan Speed Schedule

$$N1K = 12125 - 9.3254 \times (T12)$$

2. Power Setting (PLA) Schedule

$$MPCT = 0.347138 + 0.834489\ E\text{-}2 \times (PLA) - 0.181628\ E\text{-}4 \times (PLA)^2$$

where

$$0 \leq (PLA) \leq 100\%$$

3. Calculated T41

$$T41C = K_{C0} + K_{C1} \times (T3) + K_{C2} \times \left(\frac{WF}{PS3C}\right)^{1.245}$$

Where

$$\left(\frac{WF}{PS3C}\right)^{1.245} = -2.77392 + 1.81672 \times \left(\frac{WF}{PS3C}\right) + 0.226184\ E\text{-}1 \times \left(\frac{WF}{PS3C}\right)^2 - 0.114039\ E\text{-}3 \times \left(\frac{WF}{PS3C}\right)^3$$

4. Calculated Engine Fuel Flow as a Function of Calculated Metering-Valve Position (XMV)

For $0 \leq (XMV) < 0.2809$

$$WF = 162.2 + 1653.33 \times (XMV) + 18277.8 \times (XMV)^2$$

For $0.2809 \leq (XMV) \leq 0.813$

$$WF = -348.68 + 4151.59 \times (XMV) + 15864.5 \times (XMV)^2$$

Note: These Equations are based on the average of test data from WGC Hydromechanical controls S/N 12359 and S/N 13082; the following equation defines the relation between metering-valve position (XMV) and RVDT feedback volts/volt

$$XMV = 0.813 + \frac{(V/V)}{0.519}$$

Table VII. QCSEE OTW Digital Fuel Control Schedules and Functions (Continued).

5. Calculated $\sqrt{\theta 12}$

For $244 \leq T12 \leq 322$ K ($440 \leq T12 \leq 580°$ R)

$$RTH12 = 0.383323 + 0.731799 \times (TH12) - 0.115215 (TH12)^2$$

6. Max Corrected Core Speed Schedule

For $0 \leq (PLA) \leq 46.57\%$

$$N2K = 7200 + 153.53 \times (PLA)$$

For $46.57 < (PLA) \leq 100\%$

$$N2K = 14350.$$

7. Calculated $\frac{T25-T12}{T12}$ as a Function of Percent Corrected Fan Speed

For $0 \leq PCN1R < 39.862$

$$DTQT12 = 0.358845\ E\text{-}2 + 0.195553\ E\text{-}3 \times (PCN1R) + 0.547267\ E\text{-}5 \times (PCN1R)^2$$

For $39.862 \leq PCN1R < 62.8$

$$DTQT12 = 0.895999\ E\text{-}2 - 0.518285\ E\text{-}3 \times (PCN1R) + 0.200000\ E\text{-}4 \times (PCN1R)^2$$

For $62.8 \leq PCN1R < 94.13$

$$DTQT12 = -0.249999\ E\text{-}2 + 0.559521\ E\text{-}4 \times (PCN1R) + 0.137619\ E\text{-}4 \times (PCN1R)^2$$

For $94.13 \leq PCN1R$

$$DTQT12 = 1.3351 - 0.273429\ E\text{-}1 \times (PCN1R) + 0.15387\ E\text{-}3 \times (PCN1R)^2$$

8. Calculated $\sqrt{\theta 25}$

For $244 \leq T25 \leq 379$ K ($440 \leq T25 \leq 683°$ R)

$$RTH25 = 0.383323 + 0.731799 \times (TH25) - 0.115215 \times (TH25)^2$$

Table VII. QCSEE OTW Digital Fuel Control Schedules and Functions (Continued).

9. Accel Fuel Schedule

If XN < 2600

PHI = 15.96

If XN $\geq$ 2600

$$PHIBDY = A_1\ XN\ [A_2 + XN \times (A_3 + A_4 \times XN)]$$

$$PHIT41 = 69.03 - 0.065 \times T25 - 0.0017 \times (XN - 12700)$$

PHI = AMIN1 (PHIBDY, PHIT41)

XN	A_1	A_2	A_3	A_4
2,600$\leq$XN<6,800	0.42118701E2	-0.25707655E-1	0.74804485E-5	-0.56754241E-9
6,800$\leq$XN<10,20	-0.19708559E3	0.86346402E-1	-0.10384008E-4	0.39665754E-9
10,200$\leq$XN	0.36912564E3	-0.80335893E-1	0.59159283E-5	-0.13263709E-9

XN = Core rpm/$\sqrt{T25/288.16}$ (rpm/$\sqrt{T25/518.69}$)

T25 = Core Inlet Temperature, K (° R)

$$PHI = WF/\left[PS3C \times (T25/518.69)^{0.688}\right]$$

10. Calculated $(\theta_{25})^{0.688}$

For 266 $\leq$ T25 $\leq$ 379 K

(478 $\leq$ T25 $\leq$ 683° R)

$$TH688 = 0.211270 + 0.888286 \times (TH25) - 0.996309\ E\text{-}1 \times (TH25)^2$$

11, 12, 13. Conversion of scheduled accel WF, decel WF, and sensed WF to equivalent WF metering valve position. These three functions Must Use the same polynomial-equation fit, which is:

$$XMV = 0.31297E\text{-}1 + 0.143045E\text{-}3 \times (WF) - 0.139539E\text{-}7 \times (WF)^2 + 0.613485E\text{-}12 \times (WF)^3$$

Table VII. QCSEE OTW Digital Fuel Control Schedules and Functions (Concluded).

Note: This equation is based on average of test data from WGC hydro-mechanical controls S/N 12359 and S/N 13082 and on the WGC equation defining the relation between metering valve position (XMV) RVDT feedback volts/volt, i.e:

$$(XMV) = 0.813 + \frac{(V/V)}{0.519}$$

APPENDIX B

DETAILED BLOCK DIAGRAM AND SCHEDULE/DYNAMIC SPECIFICATIONS FOR OTW DIGITAL CORE STATOR CONTROL

Included in this appendix are the block diagram (Figure 39) and the specifications for gains, time constants, schedules, and limits (Tables VIII through XII) for the digital core stator control which is to be used on the first build of the OTW experimental engine.

C-2

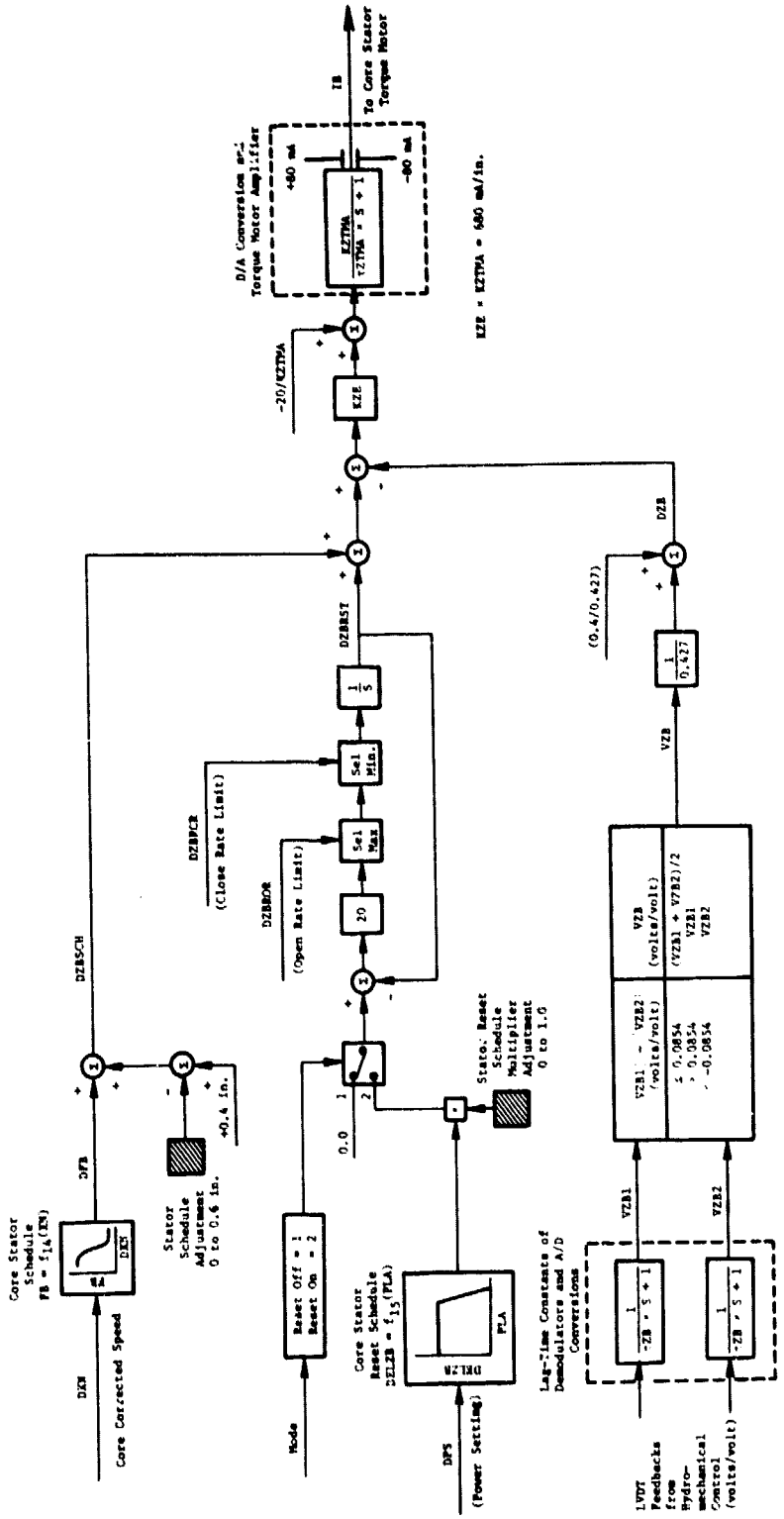

Figure 39. QCSEE OTW Core Stator Digital Control Block Diagram.

Table VIII. OTW Core Stator Digital Control Digital Scaling.

Symbol	Description	Range
DZB	Core Stator Position Feedback	-0.137 to +4.895 cm (-0.054 to +1.927 in.)

Table IX. OTW Core Stator Digital Control Time Constants.

Frequency Range From 0.1 to 10.0 Hz

Symbol	Description	Value
τZTMA	D/A Converter and Torque Motor Driver Amplifier Lag	$\leq$ 0.01 sec
τZB	LVDT Demodulator and A/D Converter Lag	$\leq$ 0.01 sec

Table X. OTW Core Stator Digital Control Digital Constants.

Symbol	Description	Value
DZBROR	Core Stator Reset Opening-Rate Limit	-2.79 cm/sec (-1.10 in./sec)
DZBRCR	Core Stator Reset Closing-Rate Limit	+0.19 cm/sec (+0.075 in./sec)

Table XI. QCSEE OTW Core Stator Schedule.

- FB = f_{14}(XN)

5 Second-Degree Equations

```
10 DIMENSION A(3,5)                                    Coefficients
20 DATA A
30&/2.2795249,-.013151068,.71650476E-4,    ◄ A(1,1),A(2,1),A(3,1)
40&.87748352,.032617459,-.30322192E-3,     ◄ A(1,2),A(2,2),A(3,2)
50&8.3086021,-.14282437,.72784862E-3,      ◄ A(1,3),A(2,3),A(3,3)
60&-5.7799969,.16498718,-.95213391E-3,     ◄ A(1,4),A(2,4),A(3,4)
70&16.450925,-.22620007,.76669457E-3       ◄ A(1,5),A(2,5),A(3,5)
80&/
90 900 FORMAT(V)
100 DO 100 J=1,66
110 READ(15,900)L,XN,FBACT
120 I=5
130 IF(117,-XN)10,10,1
140 L I=4
150 IF(94.-XN)10,10,2
160 2 I=3                                          } Coefficient Selection
170 IF(79.-XN)10,10,3                                  Log
180 3 I=2
190 IF(61.-XN)10,10,4
200 4 I=1
210 10 FB=A(1,I)+XN*(A(2,I)+A(3,I)*XN)     ◄ Feedback Equation
220 FB=AMAXI(0.,AMINI(FB,1.8688))          ◄ Min & Max Schedule Flats
230 FBERR=FBACT-FB
240 100 WRITE(14,900)XN,FB,FBERR
250 STOP;END
```

NOMENCLATURE

FB = Feedback Position in inches

$$XN = \frac{\text{Core rpm}}{\sqrt{\frac{T25\ ^\circ R}{418.69}}} \times 10^{-2}$$

◄ Note

Table XII. QCSEE OTW Core Stator Reset Schedule.

$$DELZB = f_{15} \text{ (\% PLA)}$$

For $0 \leq PLA \leq 80\%$	$DELZB = 0.77$
For $80 < PLA \leq 90\%$	$DELZB = -0.77E\text{-}1 \times PLA + 6.93$
For $90 < PLA \leq 100\%$	$DELZB = 0.0$

APPENDIX C

NOMENCLATURE

A8	Exhaust nozzle throat actual area	m^2 ($in.^2$)
AE8	Exhaust nozzle throat effective area	m^2 ($in.^2$)
ALT	Altitude	m (ft)
BETA	HP compressor stator angle	degrees
C	Various subscripted constants	
CP13	Fan tip discharge specific heat	J/kg-K (Btu/lb-° R)
CP3	HP compressor discharge specific heat	J/kg-K (Btu/lb-° R)
DLBETA	HP compressor stator error	degrees
DTAMB	Adder on standard atmosphere temperature	K (° R)
FAR41	HP turbine rotor inlet fuel/air ratio	
FAR49	LP turbine rotor inlet fuel/air ratio	
FAR5	LP turbine discharge fuel/air ratio	
FAR6	Mixer discharge fuel/air ratio	
FN	Net thrust	N (lbf)
GAM6	Mixer discharge specific heat ratio	
H12	Fan tip inlet enthalpy	J/kg (Btu/lb)
H13	Fan tip discharge enthalpy	J/kg (Btu/lb)
H3	HP compressor discharge enthalpy	J/kg (Btu/lb)
H36	Combustor inlet enthalpy	J/kg (Btu/lb)
H41	HP turbine rotor inlet enthalpy	J/kg (Btu/lb)
H49	LP turbine rotor inlet enthalpy	J/kg (Btu/lb)
H5	LP turbine discharge enthalpy	J/kg (Btu/lb)
H6	Mixer discharge enthalpy	J/kg (Btu/lb)
HCL42	Enthalpy of WACL42	J/kg (Btu/lb)
HCL48	Enthalpy of WACL48	J/kg (Btu/lb)
HCL49	Enthalpy of WACL49	J/kg (Btu/lb)
HCL5	Enthalpy of WACL5	J/kg (Btu/lb)
HCL55	Enthalpy of WCL55	J/kg (Btu/lb)
IB, Iβ	Torque motor current from digital stator control	mA
IWF, IWT	Torque motor current from digital fuel control	mA
K	Gain	
KC	Gain proportional to reciprocal of core rotor moment of inertia	rpm/sec/kg-m (rpm/sec/lb-ft)
KF	Gain proportional to reciprocal of total rotor moment of inertia for fan, gearbox, and fan turbine	rpm/sec/kg-m (rpm/sec/lb-ft)
N2, NH	HP compressor rotor physical speed	rpm
NL	Fan physical speed	rpm
NHPLA	Core speed demand from H/M PLA cam	rpm
PO	Free-stream pressure	N/m^2 (psia)
P11	Inlet throat total pressure	N/m^2 (psia)
P12	Fan tip inlet total pressure	N/m^2 (psia)
P13	Fan tip discharge total pressure	N/m^2 (psia)
P15	Bypass duct inlet total pressure	N/m^2 (psia)

P16	Bypass duct discharge total pressure	N/m^2 (psia)
P2	Fan hub inlet total pressure	N/m^2 (psia)
P21	Fan hub discharge total pressure	N/m^2 (psia)
P23Q2	Fan hub pressure ratio	
P25	HP compressor inlet total pressure	N/m^2 (psia)
P3	HP compressor discharge total pressure	N/m^2 (psia)
P4	Combustor discharge total pressure	N/m^2 (psia)
P42	HP turbine discharge total pressure	N/m^2 (psia)
P48	LP turbine vane inlet total pressure	N/m^2 (psia)
P5	LP turbine discharge total pressure	N/m^2 (psia)
P56	Core duct discharge total pressure	N/m^2 (psia)
P6	Mixer discharge total pressure	N/m^2 (psia)
P8	Exhaust nozzle throat total pressure	N/m^2 (psia)
PCN4	Percent HP compressor physical speed	
PCNLR	Percent fan corrected speed	
PHI12	Fan tip inlet entropy function	J/kg-K (Btu/lb-° R)
PHI41	HP turbine rotor inlet entropy function	J/kg-K (Btu/lb-° R)
PHI49	LP turbine rotor inlet entropy function	J/kg-K (Btu/lb-° R)
PLA	Power lever angle (power setting)	
PS11	Inlet throat static pressure	N/m^2 (psia)
PS16	Bypass duct discharge static pressure	N/m^2 (psia)
PS3	HP compressor discharge static pressure	N/m^2 (psia)
PS3MC	Control-sensed PS3	N/m^2 (psia)
PS3MEC	Control PS3 after FICA logic	N/m^2 (psia)
PS56	Core duct discharge static pressure	N/m^2 (psia)
PS8	Exhaust nozzle throat static pressure	N/m^2 (psia)
PW1	PW12 + PW2	W (hp)
PW12	Fan tip power	W (hp)
PW2	Fan hub power	W (hp)
PW25	HP compressor power	W (hp)
PW4, PW41	HP turbine power	W (hp)
PW48, PW49	LP turbine power	W (hp)
PWPXH	HP rotor power loss	W (hp)
PWPXL	LP rotor power loss	W (hp)
R12	Fan tip inlet gas constant	m/K (ft/° R)
S	Laplace variable	sec^{-1}
SLS	Sea level, static condition	
SM12	Percent fan tip stall margin % constant flow	
SM2	Percent fan hub stall margin % constant flow	
SM25	Percent HP compressor stall margin % constant flow	
T0	Free-stream temperature	K (° R)
T11	Inlet throat total temperature	K (° R)
T12	Fan tip inlet total temperature	K (° R)
T13	Fan tip discharge total temperature	K (° R)
T15	Bypass duct inlet total temperature	K (° R)
T2	Fan hub inlet total temperature	K (° R)
T21	Fan hub discharge total temperature	K (° R)
T25	HP compressor inlet total temperature	K (° R)
T3	HP compressor discharge total temperture	K (° R)
T36	Combustor inlet total temperature	K (° R)

T35	Control-sensed T3	K (° R)
T4	Combustor discharge total temperature	K (° R)
T41	HP turbine rotor inlet total temperature	K (° R)
T41C	Control-calculated T41	K (° R)
T42	HP turbine discharge total temperature	K (° R)
T48	LP turbine vane inlet total temperature	K (° R)
T49	LP turbine rotor inlet total temperature	K (° R)
T55	LP turbine frame discharge total temperature	K (° R)
T56	Core duct discharge total temperature	K (° R)
T56S	Control-sensed T56	K (° R)
T6	Mixer discharge total temperature	K (° R)
T8	Exhaust nozzle throat total temperature	K (° R)
W12	Fan tip inlet airflow	kg/sec (lb/sec)
W15	Bypass duct inlet airflow	kg/sec (lb/sec)
W2	Fan hub inlet airflow	kg/sec (lb/sec)
W21	Fan hub discharge airflow	kg/sec (lb/sec)
W25	HP compressor inlet airflow	kg/sec (lb/sec)
W2A	Fan front-face total flow	kg/sec (lb/sec)
W3	HP compressor discharge flow	kg/sec (lb/sec)
W36	Combustor inlet gas flow	kg/sec (lb/sec)
W4	Combustor discharge gas flow	kg/sec (lb/sec)
W41	HP turbine rotor inlet gas flow	kg/sec (lb/sec)
W48	LP turbine vane inlet gas flow	kg/sec (lb/sec)
W49	LP turbine rotor inlet gas flow	kg/sec (lb/sec)
W5	LP turbine discharge gas flow	kg/sec (lb/sec)
W56	Core duct discharge gas flow	kg/sec (lb/sec)
W6	Mixer discharge gas flow	kg/sec (lb/sec)
W8	Exhaust nozzle throat gas flow	kg/sec (lb/sec)
WA41	HP turbine rotor inlet airflow	kg/sec (lb/sec)
WA49	LP turbine rotor inlet airflow	kg/sec (lb/sec)
WA5	LP turbine discharge airflow	kg/sec (lb/sec)
WACL42	HP turbine discharge cooling flow	kg/sec (lb/sec)
WACL48	LP turbine vane inlet cooling flow	kg/sec (lb/sec)
WACL49	LP turbine rotor inlet cooling flow	kg/sec (lb/sec)
WACL5	LP turbine discharge cooling flow	kg/sec (lb/sec)
WCL55	LP turbine frame discharge cooling flow	kg/sec (lb/sec)
WF, WFM	Engine fuel flow	kg/hr (lb/hr)
XM	Flight Mach number	
XM11	Inlet throat Mach number	
XMV, Z_{WF}	Fuel metering valve power piston stroke	cm (in.)
XNH	HP compressor physical speed	rpm
XNL	Fan physical speed	rpm
ZBETA, $Z\beta$	HP compressor stator actuator stroke	cm (in.)
Z^{-1}	Z transform	
τ	Time constant	sec

REFERENCES

1. Advanced Engineering and Technology Programs Department, Group Engineering Division, "Quiet Clean Short-Haul Experimental Engine (QCSEE) Over-the-Wing Digital Control Systems Design Report," National Aeronautics and Space Administration, CR 135337, Section 4.2.

2. Kuo, B.C., Automatic Control Systems, Prentice-Hall, Inc., NJ, 1962, pp 419-422.

3. Astrom, K., Introduction to Stochastic Control Theory, Academic Press, NY, 1970.

4. Anderson, T.W., An Introduction to Multivariable Statistical Analysis, J. Wiley and Sons, Inc., NY.